Model Development For Micro–Channel Cooling Technology

by

D'Arcy McGlynn

A thesis
presented to the University of Waterloo
in fulfillment of the
thesis requirement for the degree of
Master of Applied Science
in
Chemical Engineering and Mechanical Engineering

Waterloo, Ontario, Canada, 2013

AUTHOR'S DECLARATION

I hereby declare that I am the sole author of this thesis. This is the true copy of the thesis, including any required final revisions, as accepted by my examiners.

I understand that my thesis may be made electronically available to the public.

ABSTRACT

The micro–channel research literature presents a clear need to provide accurate models that can predict pressure drop and heat transfer coefficients for a greater number of experimental data sets while capturing the physical phenomena of various flow patterns associated with the onset of nucleate boiling in the two–phase region. The model approach developed have been evaluated for the purpose of facilitating an efficient design instrument for micro–channels to predict the pressure drop related to heat input for the single phase through to the boiling [two–phase] region as well as heat transfer coefficient calculations for a single micro–channel. The simplified homogeneous model provides a lower bound for pressure drop estimates and the weighted annular–homogeneous model produces an upper bound value. Input parameters include the micro–channel dimensions, fluid flow rate, inlet temperature, thermo–physical properties of the respected fluid, and outlet pressure. Polynomial correlations for water are obtained from curve–fitting data available from the 1997 Ashrae Handbook over the temperature range of 0.01 to 200 ^{0}C for the thermodynamic properties that include liquid density, viscosity, thermal conductivity, specific heat capacity and change of enthalpy [latent heat of vapourization].

The model results are evaluated over four independent experimental data sets that are available in the literature to demonstrate the sufficient accuracy for channel dimensions ranging from 50 μm to 713 μm. The independent data sets were numerically reproduced from figures presented in the research literature. The boiling front, pressure drop, heat transfer coefficient, wall temperature profile and vapour quality characteristics are evaluated. Heat transfer coefficient calculations were made via the Kandlikar correlation and the Kandlikar enhancement factor method that is corrected for vapour quality. The model produced pressure drop results that were within about a 30% error to the experimental data sets evaluated for heat fluxes in the range of 50 W/cm^2 to values exceeding 150 W/cm^2. Heat transfer coefficient values calculated between the two correlations of Kandlikar were within an estimated error of 30% to experimental measurements and demonstrated results in the two–phase region that exceeded 110 000 W/cm^2 K.

ACKNOWLEDGEMENTS

I would like to acknowledge Dr. Ioannis Chatzis, Dr. Richard Culham, Dr. Ali Elkamel and Dr. John Medley for reviewing the MASc thesis.

DEDICATION

I dedicate my MASc thesis to my incredible mother [Mary] & brother [Daniel].

TABLE OF CONTENTS

LIST OF FIGURES

LIST OF TABLES

NOMENCLATURE

a	=	Acceleration Term
a'	=	Net Seebeck Coefficient $\left[\frac{\mathrm{V}}{\mathrm{K}}\right]$
A, A_{CH}	=	Cross–Sectional Channel Area $[m^2]$
A_{Dh}	=	Cross–Sectional Channel Area Based on Hydraulic Diameter $[m^2]$
A_{TZ}	=	Cross–Sectional Trapezoid Channel Area $[m^2]$
A1, B, C	=	Antoine Equation Constant
Bo	=	Boiling Number $\equiv \left[\frac{\mathrm{q}}{\mathrm{Gh_{LG}}}\right]$
c_p	=	Heat Capacity of Fluid $\left[\frac{\mathrm{J}}{\mathrm{kg\ K}}\right]$
Co	=	Convection Number $= \left[\frac{1-\mathrm{x_v}}{\mathrm{x_v}}\right]^{0.8}\left[\frac{\rho_\mathrm{G}}{\rho_\mathrm{L}}\right]^{0.5}$
$C_1 – C_5$	=	Kandlikar Heat Transfer Coefficient Correlation Constants [See Table 3.1]
d	=	Depth $[m]$
D_h	=	Hydraulic Equivalent Diameter $[m]$
e	=	Liquid Effluent Fraction
E	=	Clausius–Clapeyron Equation Constant
f	=	Darcy Friction Factor $\equiv \left[\frac{64}{Re}\right]$
f_F	=	Fanning Friction Factor $\equiv \left[\frac{\tau_\mathrm{w}}{\frac{1}{2}\rho u^2}\right]$
f_{TP}	=	Two–Phase Friction Factor $[-]$
F	=	Force $\left[\frac{N}{m^2}\right]$
$\hat{F}$	=	Friction Loss
F_{fl}	=	Fluid Dependent Parameters [See Table 4]
Fr_{lo}	=	Froude Number $\equiv \left[\frac{\mathrm{G}^2}{\rho_\mathrm{L}\mathrm{g\ D_h}}\right]$
g	=	Acceleration of Gravity $\left[\frac{\mathrm{m}}{s^2}\right]$
G	=	Mass Flux $\left[\frac{\mathrm{kg}}{\mathrm{m^2\ s}}\right]$
h	=	Heat Transfer Coefficient $\left[\frac{\mathrm{W}}{\mathrm{m^2\ K}}\right]$
h_{TP}	=	Two–Phase Heat Transfer Coefficient $\left[\frac{\mathrm{W}}{\mathrm{m^2\ K}}\right]$

h_{LG}	=	Latent Heat of Vapourization $\left[\frac{\mathrm{J}}{\mathrm{kg}}\right]$
H	=	Height $[m]$
k	=	Thermal Conductivity of Fluid $\left[\frac{\mathrm{W}}{\mathrm{m\ K}}\right]$
k_W	=	Heat Sink Material Thermal Conductivity $\left[\frac{\mathrm{W}}{\mathrm{m\ K}}\right]$
K	=	Friction Loss Coefficient $[-]$
L	=	Channel Length $[m]$
$\dot{m}$	=	Fluid Mass Flow Rate $\left[\frac{\mathrm{kg}}{\mathrm{s}}\right]$
MAE	=	Mean Absolute Error $[-]$
N	=	Number of Data Points $[-]$
Nu	=	Nusselt Number $\equiv \left[\frac{hD_h}{k_L}\right]$
p	=	Pressure $\left[\frac{N}{m^2}\right]$
Pr	=	Prandtl Number $\equiv \left[\frac{\mu C_p}{k_L}\right]$
P_{CH}	=	Perimeter of Channel $[m]$
P_{SAT}	=	Saturation Pressure $\left[\frac{N}{m^2}\right]$
q	=	Heat Supply $[W]$
q"	=	Heat Flux $\left[\frac{W}{m^2}\right]$
$\dot{Q}$	=	Fluid Flow Rate $\left[\frac{mL}{min}\right]$
r	=	Radius $[m]$
R	=	Gas Constant $\equiv \left[\frac{8.3145 \cdot J}{mol \cdot K}\right]$
Re	=	Reynolds Number $\left[\frac{\rho D_h u}{\mu}\right]$
S	=	Surface Perimeter $[m]$
t	=	Time $[s]$
tk	=	Fin Thickness
T	=	Temperature $[°C]$
T_{IN}	=	Coolant Inlet Temperature $[°C]$
T_{OUT}	=	Coolant Outlet Temperature $[°C]$
T_W	=	Wall Conduction Temperature $[°C]$

u	=	Fluid Velocity $\left[\frac{m}{s}\right]$
u_{LL}	=	Liquid Film Velocity $\left[\frac{m}{s}\right]$
U	=	Overall Heat Transfer Coefficient $\left[\frac{W}{m^2 °C}\right]$
v	=	Specific Volume $\left[\frac{m^3}{kg}\right]$
w	=	Channel Width $[m]$
W_s	=	Shaft Work $\left[\frac{N \cdot m}{s}\right]$
x_e	=	Exit Vapour Quality $[-]$
x_v	=	Vapour Quality $[-]$
x	=	x – direction
y	=	y – direction
z	=	z – direction
z_L	=	Length of Single Phase Flow $[m]$
Z_0	=	Figure of Merit $\left[\frac{1}{K}\right]$

Greek

α	=	Void Fraction $[-]$
β	=	Aspect Ratio $[-]$
Γ_{LG}	=	Mass Flow Rate Gradient of Vapour $\left[\frac{kg}{m^3}\right]$
δ	=	Film Thickness $[m]$
k'	=	Net Thermal Conductivity $\left[\frac{W}{m \cdot K}\right]$
ΔP	=	Pressure drop $[Pa]$
μ	=	Viscosity of Fluid $\left[\frac{kg}{m \cdot s}\right]$
ν	=	Kinematic Viscosity $\left[\frac{m^2}{s}\right]$
π	=	3.14159
P_H	=	Homogeneous Fluid Density $\left[\frac{kg}{m^3}\right]$
ρ, ρ_L	=	Fluid Density $\left[\frac{kg}{m^3}\right]$
ρ_G	=	Vapour Density $\left[\frac{kg}{m^3}\right]$
ρ'	=	Net Electrical Resistivity $[Ohm - m]$
η	=	Fin Efficiency $= \frac{\tanh\left[\left[\frac{2h}{k_W tk}\right]^{1/2} H\right]}{\left[\left[\frac{2h}{k_W tk}\right]^{1/2} H\right]}$
ω	=	Frequency $[\mathrm{Hz}]$
τ_i	=	Interfacial Shear Stress $\left[\frac{N}{m^2}\right]$
τ, τ_W	=	Wall Shear Stress $\left[\frac{N}{m^2}\right]$
θ	=	Angle to Horizontal Plane $[°]$

Subscripts

AN	=	Annular Flow
Bottom	=	Bottom
B	=	Bubble
C	=	Vapour Core

CBD	=	Convective Boiling
CH	=	Channel
Conv	=	Convection
e	=	Exit
eff	=	Planform Area
F/B	=	Film Bubble
F–Slug–Tran	=	Fluid Flow between Film and Slug Flow Region
k	=	Phase
G	=	Vapour
H	=	Homogeneous
i	=	Interface
L	=	Liquid
LG	=	Property Difference between Liquid and Vapour
LL	=	Liquid Film
IN	=	Inlet
One–Tran	=	One–Transition between Film and Slug Flow Region
OUT	=	Outlet
P	=	Perimeter
PRED	=	Prediction Value
Sat	=	Saturation
Slant	=	Slant
Slug	=	Slug Flow
Supp	=	Supplied
SP	=	Single Phase
Top	=	Top
T	=	Total
TP	=	Two–Phase
UC	=	Unit Cell
W	=	Wall
x	=	x – direction
y	=	y – direction
z	=	z – direction

CHAPTER 1
INTRODUCTION

The following MASc thesis is intended to provide a model that can be implemented into design initiatives to predict a number of operating parameters for flow boiling behavior in micro–channels for high heat flux applications. Such parameters include pressure drop, heat transfer coefficient values and other thermo–physical properties for liquids over the single phase through to the boiling [two–phase] region.

In the flow boiling [two–phase] micro–channel research literature there is much confounded information regarding the comparisons of experimental results to theoretical model predictions. It suggests that research is needed in a number of different areas such as channel geometries, expected heat transfer coefficient correlations, flow patterns, surface roughness effects, and contemplation over the validity of conventional equations for larger [macro] channels being applied to smaller [micro] channels. Thus, in the present thesis the literature is carefully reviewed to select the most productive research areas to pursue.

Initially interest was in thermal management applications for heat fluxes of 100 W/cm^2 but now the challenge is to achieve heat fluxes up to 300 W/cm^2 and higher in the future [Thome – 2006]. A need to identify technology that could meet and exceed high heat flux applications over the range of 100 – 300 W/cm^2 was required. The findings could then be incorporated into a number of applications such as electronic cooling, fuel cells, laser diodes, telecom, and opto–electronic packaging. Other relevant applications include radar as well as aerospace avionics components and micro–chemical reactors [Bhide et al. – 2009].

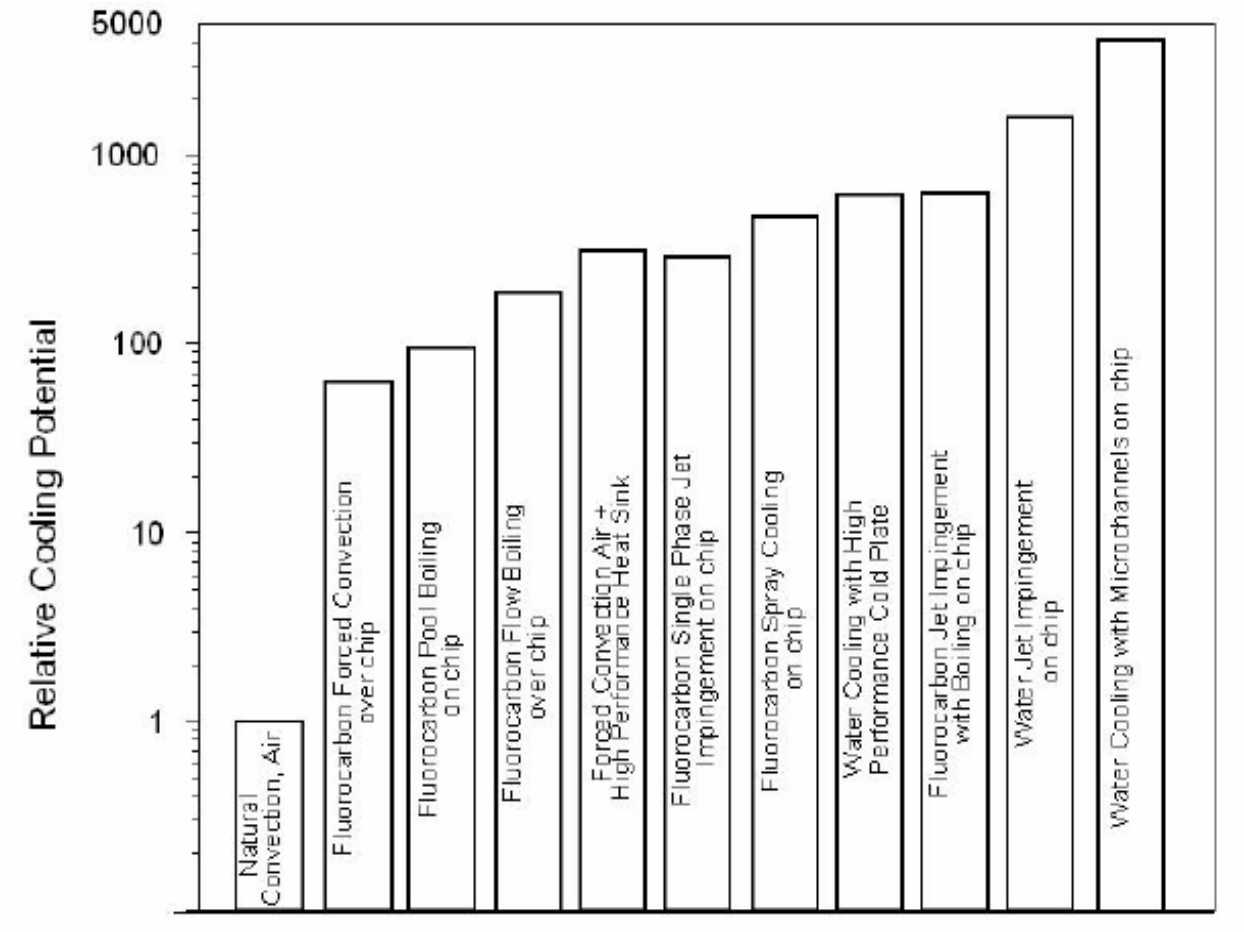

Figure 1.1 – Cooling Potential of Various Heat Transfer Technologies [Adapted From: Ohadi – 2007]

The technological approaches that provide cooling solutions for such high heat flux are outlined in Figure 1.1. Micro–channel cooling is identified to hold the most potential to address high heat flux beyond 100 W/cm^2. In Figure 1.1 the relative cooling potential of, "water cooling with micro–channels on chip," was estimated to provide about twice the cooling capability of, "water jet impingement on chip." Figure 1.1 also illustrates that there is about a 10 fold difference in cooling potential from, "fluorocarbon forced convection over chip," compared with, "water cooling with micro–channel on chip."

The aforementioned results suggest that large cooling potential can be achieved by incorporating the correct technology. Additionally, the large difference between, “natural air convection,” to that of, “water cooling with micro–channel on chip,” provides a rationale for shifting from air to liquids for higher cooling capacities. This illustrates the effect of different coolants regarding improved cooling capability.

Review of the available heat transfer coefficients in Figure 1.2 for different coolants and conditions demonstrates the need to focus on the boiling region to achieve better cooling results. Figure 1.2 also illustrates that water has superior thermal conductivity properties to that of the dielectric fluoro–chemical liquids. Furthermore boiling conditions for water produce an estimated 10 fold increase in the heat transfer coefficient values compared with single phase forced convection results of water as well as boiling conditions for fluoro–chemical liquids.

Therefore from Figure 1.1 it can be concluded that micro–channels are presented to have the highest relative cooling potential to meet high heat flux application demands. In addition to the cooling potential of micro–channels, the boiling conditions for water exhibit the largest heat transfer coefficient values as outlined in Figure 1.2.

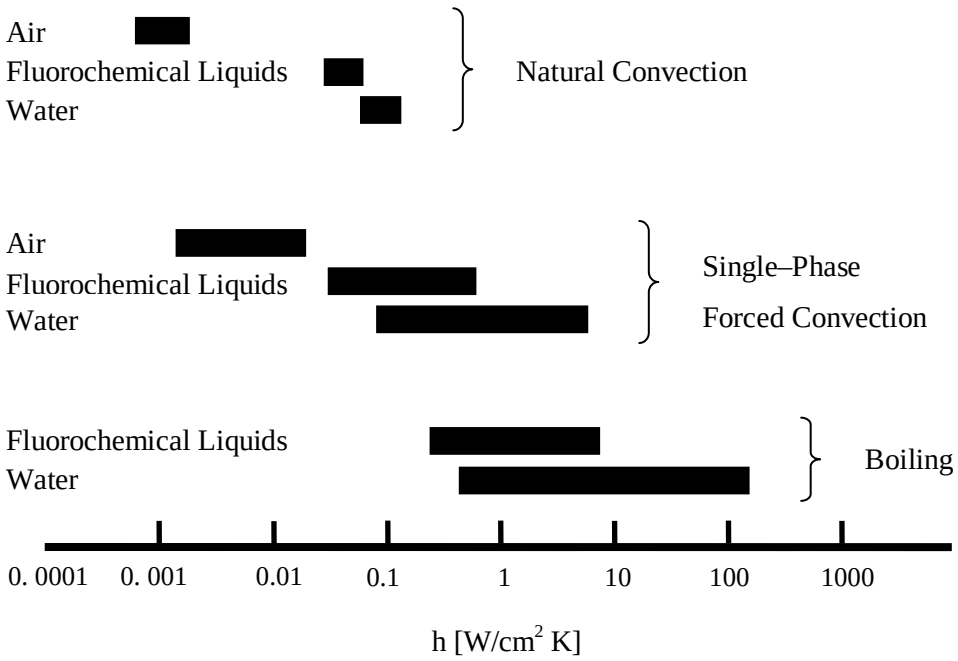

Figure 1.2 – Heat Transfer Coefficients for Different Coolants [Adapted From: Yarin et al. – 2009]

Table 1.1 is employed to provide an effective overview of the work completed and where further research can be conducted. Table 1.1 illustrates that adequate work has been completed for the single phase regions except for the transition area which requires more research effort. Although two–phase flow will be a much more demanding effort, work should continue in this area to better comprehend the physical phenomena.

Table 1.1 – Research Area Classification for Transport Phenomena Understanding [Adapted From: Qu and Mudawar – 2003]

Fluid State	Topic	Isolated Micro – Channel	Parallel Micro – Channels
Single – Phase Liquid	Laminar: Pressure drop	Adequate	Adequate
	Laminar: Heat Transfer	Adequate	Adequate
	Transition	Limited	Limited
	Turbulent: Pressure drop	Adequate	Adequate
	Turbulent: Heat transfer	Adequate	Adequate
Two – Phase	Incipient boiling	Limited	Limited
	Flow patterns	Limited	Limited
	Hydrodynamic Instabilities	Very Limited	Very Limited
	Pressure drop	Limited	Very Limited
	Heat transfer	Limited	Very Limited
	Critical heat flux	Limited	Very Limited

A review of the current literature indicates that heat transfer research related to flow boiling in micro–channels is a very popular topic [Thome – 2006]. However, experimental findings on flow boiling and flow regimes have shown that the top–rated macro–scale flow boiling models and maps do not extrapolate well to micro–channels [Thome – 2006].

The necessity for modeling efforts is further supported by Bertsch et al., 2008 in their review paper that outlines there to be a clear need for physical models to reflect flow boiling in micro–channels. The paper goes on to mention that such models should be validated against large sets of experimental measurements covering a wide range of parameters. Moreover few correlations in the current literature are based on the prevalent flow regimes in micro–channels and even those that are developed

in this manner have usually considered only a single flow regime [Bertsch et al. – 2008]. Bertsch et al., 2008 also recommends careful characterization of flow regimes through high speed visualization along with local heat transfer and pressure drop measurements. Such procedures would enhance the validation of models that are developed for the various flow regimes.

Therefore the present thesis addresses the cooling technology with the capability for high heat flux applications in the range of 100 to greater than 300 W/ cm^2. This is particularly relevant to the electronics industry where fans are reaching their limit of acceptable noise levels regarding their current heat dissipation performance. As has been explained the cooling techniques have now begun to shift from air to that of liquids. Liquid cooling is the preferred near term solution however cooling through means of flow boiling of refrigerants is suggested as the best long term solution [Wolverine Tube Inc – 2010]. Thus it is essential to develop physical models for the relevant flow regimes to predict both heat transfer coefficient and pressure drop in micro–channel flow boiling to enable effective thermal design applications [Harirchian and Garimella – 2012]. Such physics based models are expected to be applicable to a wider range of parameters and not just relevant to specific data sets [Harirchian and Garimella – 2012].

A news article from Purdue University states that micro–channel technology is expected to be employed within the near future and is anticipated to remain in the market for an estimated 20 years thereafter [Venere – 2005]. To see micro–channel technology being incorporated into industrial applications such as the MSI N280GTX OC HydroGen graphics card further supports the relevance of these cooling techniques. Details are provided at Micro–Star International Co., Ltd [www.msi.com] via the following webpage link – www.msi.com/product/vga/N280GTX-OC-HydroGen.html#!mm=product [Accessed: October 29, 2012].

1.1 Trends in Micro–Processors

To present some background regarding the proponents for the identification of new cooling technologies to address high heat flux demands an outlook of the microelectronics industrial efforts toward improving device performance through higher operating frequencies associated with increasing the number of transistors in a central processing unit chip are illustrated. Microelectronics trends are expected to produce larger power densities, denser circuit integrations and additional stringent temperature constraints [Phillips – 1988].

Increasing circuit integration is driven by the need for greater processing speed which is dependent upon the signal delay times. The signal delay times are directly proportional to the physical length of the interconnections between the circuit components [Phillips – 1988]. This situation can be compared with the nerve synapses found in the human body that exchange information. The aforementioned material is interconnected through the fact that processing speed can be measured by how many millions of instructions per second are executed. The total power dissipation requirements per chip are directly proportional to the rate of instructions executed.

Figure 1.3 illustrates the number of transistors [semi–conductor materials that allow for the control of electronic current] on an Intel CPU [Central Processing Unit] chip. The number of transistors increased from 2 300 in 1971 to 55 x 10^6 for a Pentium IV processor [3.06 GHz core frequency] introduced in November 2002 [Zhang et al. – 2004]. The current trend in the electronics systems has brought the validity of Moore's Law which states the number of transistors on an integrated circuit would double every 18 months into the forefront since it is becoming difficult to maintain such a trend.

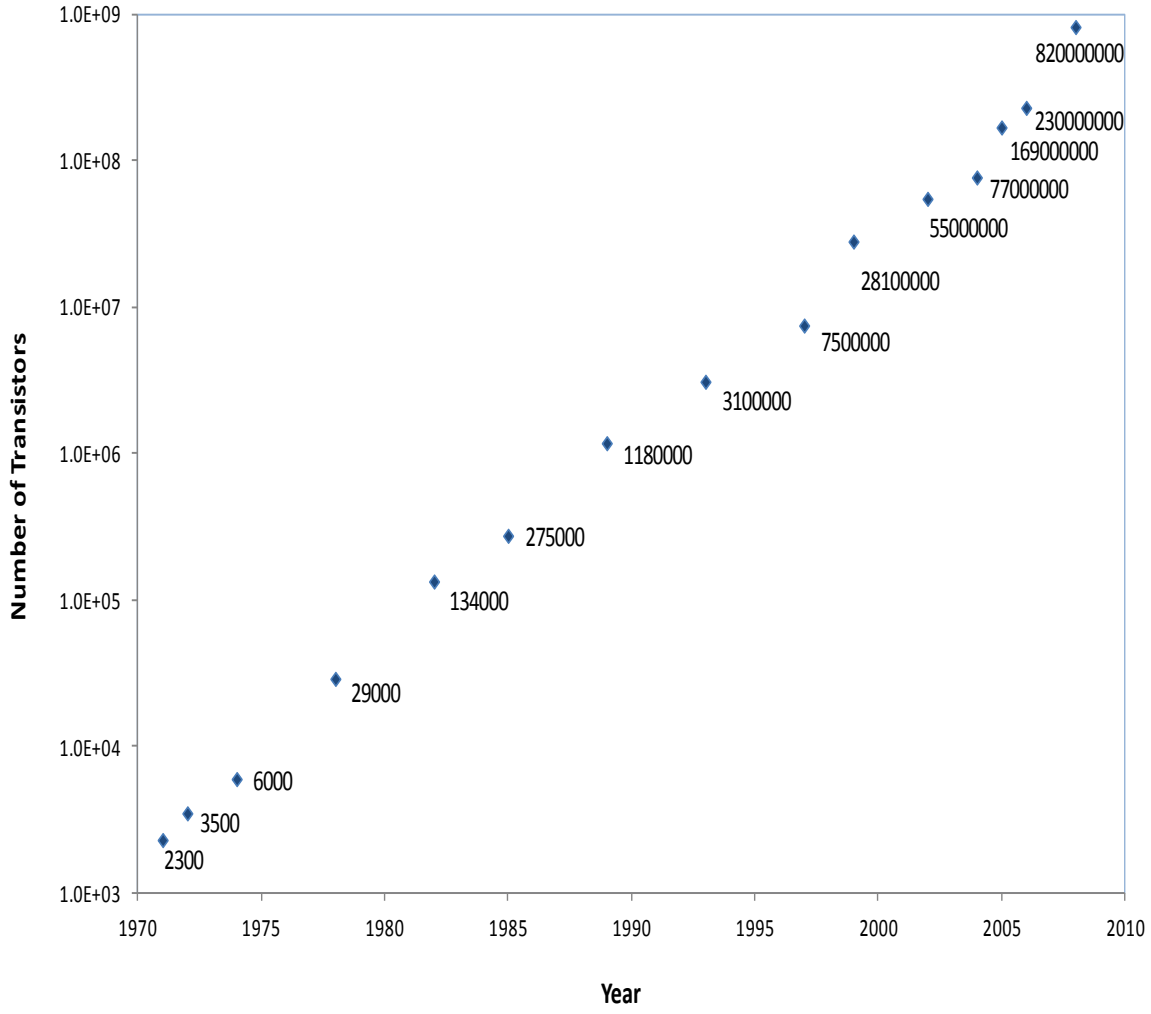

Figure 1.3 – Number of Transistors Integrated in Single Intel CPU Chip for Moore's Law [Adapted From: Zhang et al. – 2004]

The following data covers Intel processors from the model Intel 4004 in 1971 through to the Pentium IV of 2002. An updated figure had been seen appropriate to illustrate how the transistor count has evolved from the year of 1970 to 2008 and onward. Figure 1.4 illustrates the number of transistors for the Intel Wolfdale Core Xeon L5215 of 2008 to the SandyBridge EP Core Xeon E5 – 4603 model of 2012 that was provided from data available at Tech ARP, 2012.

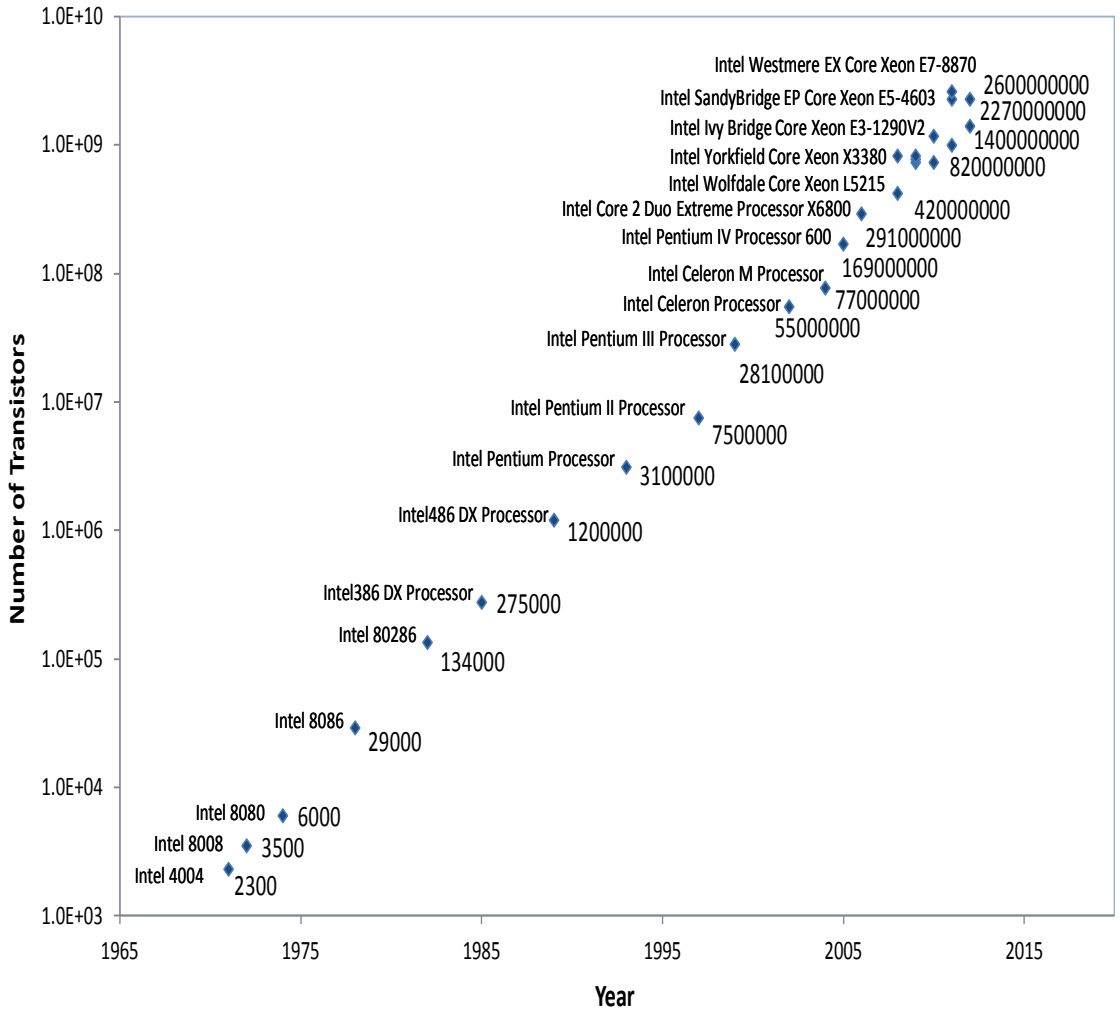

Figure 1.4 – Number of Transistors Integrated for Intel CPU [Adapted From: Data Available at Tech ARP – 2012]

Figure 1.4 includes the transistor count data for different processors from 2008 to illustrate various CPU versions produced in a given year. It is clearly illustrated that the number of transistors continues to increase for Intel processing units with now 2.6 billion transistors being incorporated in the Westmere EX Core Xeon E7 – 8870 for 2011 [Tech ARP – 2012]. However it is important to note that the numbers of transistors appear not to be increasing at the same pace as they had in Figure 1.3 from Zhang et al., 2004.

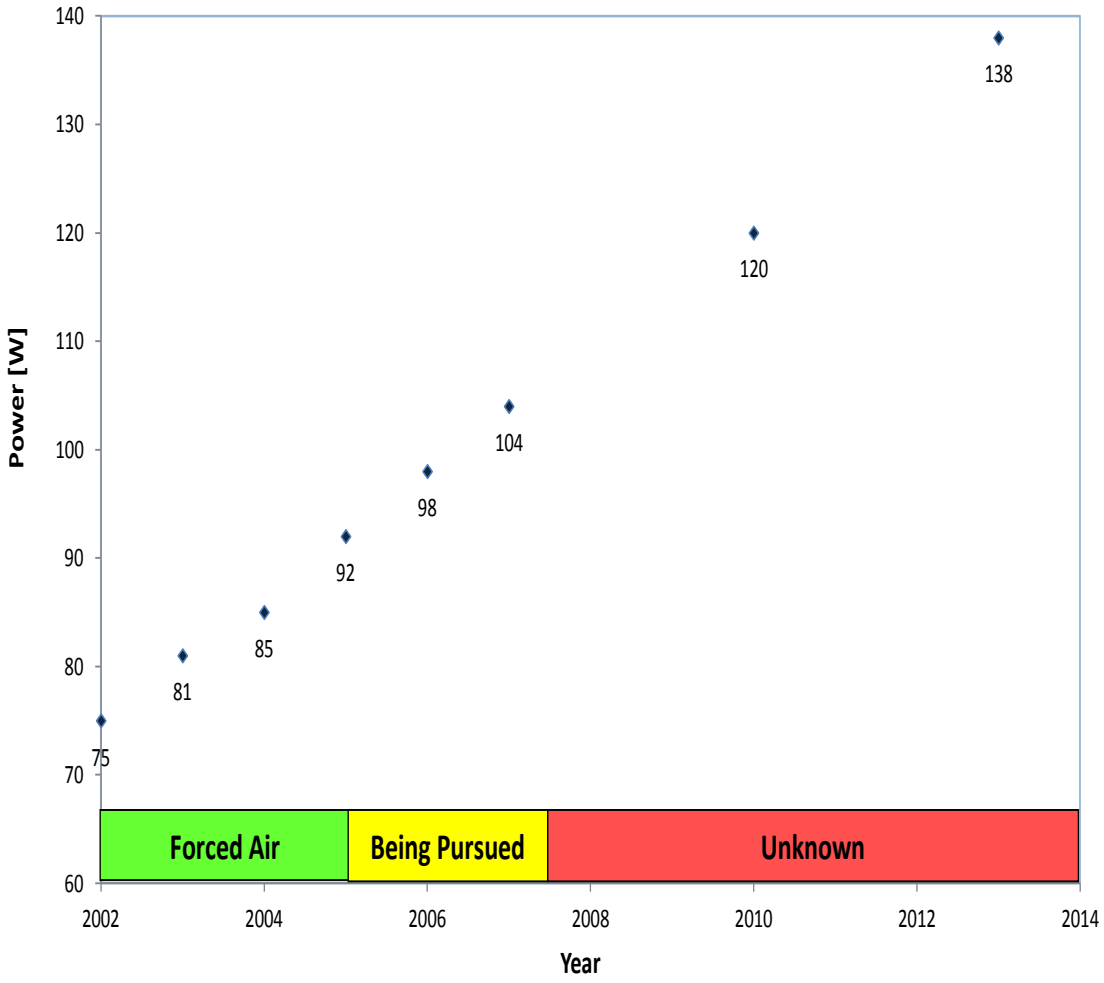

Figure 1.5 – IRTS Expectations for Packaging and Assembly Requirements for Single Cost Performance IC Chips [Adapted From: Zhang et al. – 2004]

Through the implementation of increased integrated circuits the desktop computer micro–processor is expected to exceed over 130 W in the near future which is illustrated in Figure 1.5. This could result in an unprecedented increase in heat flux at the package level [term used to define the component that encapsulates the square of silicon containing the integrated circuit]. It is noted that the increase in chip power dissipation has greatly complicated the thermal management of microelectronics [Phillips – 1988]. Methods for cooling such as fans and traditional heat sinks are considered to no longer be viable due to increased heat flux expectations along with considerations to acceptable noise levels produced from their use.

The trend for increasing the number of transistors integrated into the central processing chip to meet the needs for greater processing speed is having a profound effect on the heat flux or dissipation at the product level [Phillips – 1988]. Figures 1.3 to 1.5 provide support for this expectation of increased heat dissipation requirements along with the higher integration of circuit densities with more packed transistors per central processing unit. In comparison with other sources that illustrate heat dissipations rates to have risen from about 30 W/cm^2 from a few years ago to over 100 W/cm^2 today [Thome – 2006]. It is mentioned that the challenge is now to arrive at 300 W/cm^2 and higher in the near future [Thome – 2006]. There is interest to acquire industrial applications for heat fluxes of 1 000 W/cm^2 or more.

To provide perspective to the reader about the current heat flux challenges some examples will be outlined to enable a conceptual framework of comprehension. At 10 cm from a 100 W light bulb a heat flux of 0.6 W/cm^2 is produced [Vatell Corporation – 2002]. A propane torch will provide a heat flux of 10 W/cm^2 at the flame tip and an oxy–acetylene torch produces a heat flux of 100 W/cm^2 at the flame tip [Vatell Corporation – 2002]. To put such heat flux as 1 000 W/cm^2 into perspective the heat flux at the surface of the sun is estimated to be 6 500 W/cm^2 from radiation effects alone [Vatell Corporation – 2002]. Therefore the expected heat flux of future applications is around 60 times less than the heat flux calculated for the surface of the sun from radiation effects for anticipated applications of 100 to 300 W/ cm^2.

Heat transfer performance is viewed as a vital aspect of technological development for the future. The subsequent impact on current heat transfer applications where improvements are required will be of great significance thereby expanding the scope of its use and ultimately leading to new innovative functions. Thus novel cooling technologies are required to meet these heat flux challenges. Such cooling technologies currently investigated include: cold plates, fans, heat pipes, immersion cooling, jet impingement, liquid metal cooling, micro–channel heat sinks, micro–heat exchangers, spray cooling and solid state technologies. Some of these cooling technologies are touched upon to provide background into other methods and illustrate further clarity to the chosen area of research.

Thermal management has emerged as a challenge to electronic packaging at the chip, module, and system levels. One reason for this trend is the alarming increase in component concentration in the chip itself through integration technologies [Mudawar – 1992]. Thermal management has also been

compounded by the increased signal speed requiring shorter distances between the chips in multichip modules and a closer packaging of the modules [Mudawar – 1992]. Since a key measure of technological advances in the electronics industry for device performances are considered to be related to the ability to integrate the largest number of electronic components in a given surface area, these advances have produced an unprecedented increase in device heat dissipation [Lee and Mudawar – 2005]. Such high performance computers are rapidly outpacing the capabilities of the best commercial heat sinks including those with integrated heat pipes [Upadhya – 2006]. The problems are seen to be augmented by three compounding trends that include a higher total chip power, higher local heat flux and smaller system enclosures [Upadhya – 2006]. Liquid cooling systems are viewed to be the leading solution for the high power density requirements of future processors [Upadhya – 2006].

1.2 Technology Overview

The overview of other cooling technology applications will begin with air cooling since it has been widely implemented into electronics, servers and other heat flux areas that are need to improve heat transfer performance.

1.2 – 1 Air Cooling

It is generally acknowledged that traditional air–cooling techniques are about to reach their limit for the cooling of high–power applications. Figure 1.6 illustrates the general concept for air cooling of electronics. Transport properties of air require forced circulation at speeds which approach near the upper accepted limits for noise and vibration [Mudawar – 1992]. With standard fans, a maximum heat transfer coefficient of maybe 150 W/m^2K can be reached with acceptable noise levels, which is equivalent to 1 W/cm^2 for a 60°C temperature difference [Lasance and Simons – 2005].

Non–standard fans or dedicated heat sink combinations for central processing unit cooling are expected to have a maximum of about 50 W/cm^2, which is a factor of 10 times higher than expected 15 years ago. It is noted that incorporation of new initiatives could extend the use of fan cooling technology [Lasance and Simons – 2005].

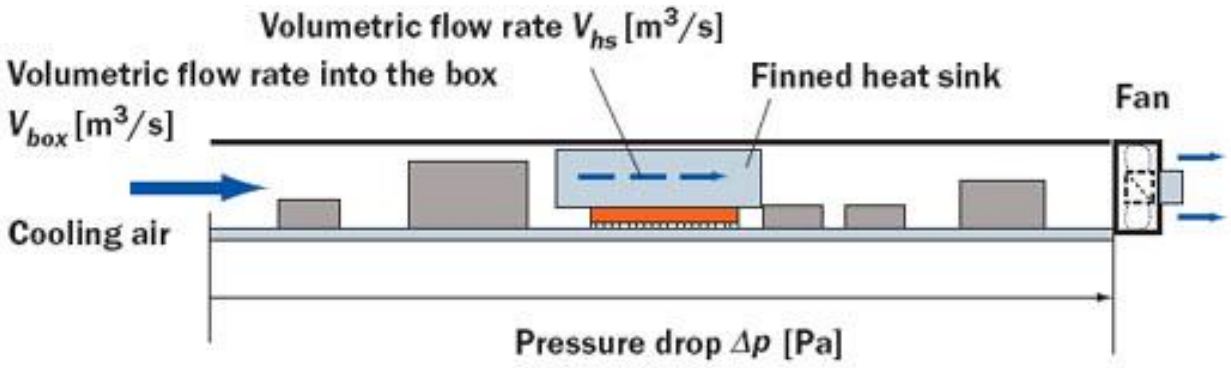

Figure 1.6 – Air Cooling for Electronics [Adapted From: Nakayama – 2006]

1.2 – 2 Spray Cooling

Spray cooling involves injecting a heat transfer liquid in a dispersed manner over a desired cooling region. The mist resulting from the dispersion process provides cooling to the surface through the combination of thermal conduction from the liquid – surface interface as well as the evaporation of the liquid to vapour contact. Spray cooling with Fluorinert™ for been incorporated in the CRAY SV2 system to dissipate heat fluxes from 15 to 55 W/cm^2 [Lasance and Simons – 2005]. Heat fluxes of 160 W/cm^2 have been cooled for RF power amplifier applications and implementations of other technologies could hold promise for 270 W/cm^2 [Lasance and Simons – 2005].

1.2 – 3 Heat Pipes

Heat pipes are another technology that has been employed in electronic cooling applications and are generally known to be highly efficient and relatively low weighted systems. The heat transfer capacity of an average water copper heat pipe is estimated to be 100 W/cm^2 [Lasance and Simons – 2005]. Heat pipes are passive devices [capillary driven] that transport heat from a heat source [evaporator] to a heat sink [condenser] and are effective over larger distances through the working fluids latent heat of vapourization. A heat pipe generally has the following aspects that include an evaporator section, an adiabatic [transport] section and a condenser section [Bejan and Kraus – 2003]. The major components of the heat pipe include the sealed container, wick structure and working fluid. The net pressure difference in the liquid saturated wick component between the capillary radii in the evaporator and condenser ends of the wick structure enables the flow of the liquid from the condenser through the wick structure to the evaporator region [Bejan and Kraus – 2003]. This capillary driven process produces a continuous fluid flow without the need for an external pump and can be employed over a wide range of operating conditions due to various choices of working fluids. Heat pipes are viewed as attractive options for a wide range of heat transfer applications [Bejan and Kraus – 2003].

1.2 – 4 Solid–State Thermoelectric Technology

A thermoelectric Peltier cooler is characterized as a small electronic cooling product that has the advantage of no moving parts and quiet operation. Thermoelectric technology enables cooling below ambient temperature where the devices operates on direct current that may be used for heating or cooling through reversing the direction of current flow.

Figure 1.7 illustrates the Peltier cooler that outlines when a positive DC voltage is applied to the n–type thermo–element the electrons pass from the p– to the n–type thermo–element and the cold side temperature decreases as heat is absorbed [Lasance and Simons – 2005].

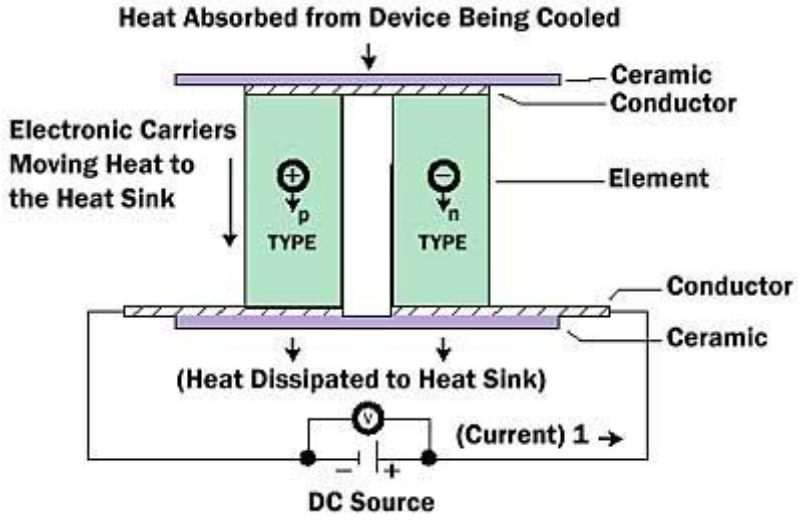

Figure 1.7 – Peltier Technology [Adapted From: Lasance and Simons – 2005]

The heat absorption [cooling] is proportional to the current and the number of thermoelectric couples. The disadvantage includes that more energy is required to be put into the Peltier cooler than is generally carried from the element that is to be cooled.

Thermoelectric materials are usually characterized by their figure of merit [Z_0] defined in Equation [1.1]. It is has been noted that for about 40 years the maximum figure of merit values for these materials has been 1, however in the past few years nano–structured thin–film growth have resulted in values greater than 2 [Mayer and Ram – 2006].

$$Z_0 = \frac{a'^2}{\rho' k'} \qquad [1.1]$$

It is desirable to incorporate good thermoelectric materials to acquire high figure of merit values. Currently the best thermoelectric materials noted are alloys of Bi_2Te_3 with Sb_2Te_3 and Bi_2Te_3 with Bi_2Se_3 [Lasance and Simons – 2005]. New innovative technology will be on the forefront of increased thermoelectric applications where thin–film thermoelectric devices of thicknesses 1–2 micrometers could achieve heat dissipation rates over 100 W/cm^2 [Lasance and Simons – 2005].

Localized areas of high heat flux will create hot spots on the surface of the die [die is a formal term for the square of silicon containing an integrated circuit]. These localized areas of high heat flux limit chip performance, decrease reliability and reduce yield. Increasing the heat dissipation from hot spots alone will result in computer speed gains of 30 – 200% in CMOS processors [Nextreme Thermal Solutions Inc – 2006]. In accordance with rapid increases of integration density the thermal management solutions must be well designed to ensure proper functionality. Moreover research on the thin–film thermoelectric applications could support the direction to incorporate the technology towards protective clothing, as well as specific medical applications that include certain laboratory equipment.

1.2 – 5 Micro–Channels

Micro–channel work began in the 1980s at Stanford University by Tuckerman and Pease who are accredited with the development of the research initiative [Tuckerman and Pease – 1981]. Tuckerman's initial work illustrated that micro–channel heat sinks pumping water could dissipate heat up to 790 W/cm^2 which promoted a great deal of interest for further development in this area.

Figure 1.8 illustrates a general micro–channel design where it is important to state that such applications are becoming the new frontier in terms of heat transfer capability. More research is being conducted to master the art of heat transfer and push it to the next level for higher heat flux applications. Cold plates that integrate micro–channels are now being incorporated in various applications to evaluate the technologies effectiveness.

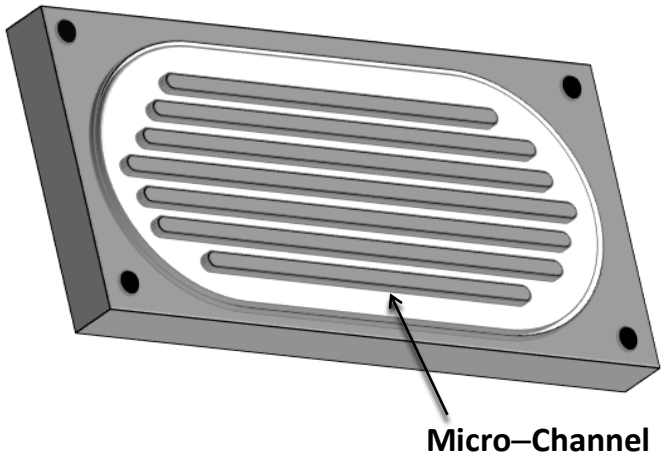

Figure 1.8 – Illustration of Micro–Channel Technology [Adapted From: Steinke et al. – 2006]

The practical implementation of micro–channels depend largely on the availability of reliable predictive tools structured upon the fundamental understanding of the fluid flow and heat transfer behavior as well as the utilization of effective thermal design methodology [Lee and Qu – 2006]. Micro–channels are generally defined as having hydraulic diameters approximately around ten to two–hundred micrometers. Such heat sinks are prime contenders for the next generation of high performance cooling systems [Qu and Mudawar – 2002]. Micro–channel heat exchangers using two–phase convective boiling are one of the most promising future technologies for the cooling of micro processors [Prasher et al. – 2005]. However, the research on two–phase boiling in micro–channels is still limited [Zhang and Pinjala – 2005]. The expected advantages for convective two–phase boiling include increased heat dissipation capability, less volume of liquid coolant required, minimized flow, lower pressure drop, more uniform device temperature and reduced thermal resistance due to latent heat of vapourization [Zhang and Pinjala – 2005].

In many practical cases the small flow rate within micro–channels produces laminar flow resulting in a heat transfer coefficient inversely proportional to the hydraulic diameter. In other words, the smaller the channel, the higher the heat transfer coefficient. Boiling curves have been obtained to display that the critical heat flux at a flow rate of 64 mL/min to be 200 W/cm^2 with the pressure drop around 0.3 bar for larger channels [Zhang and Pinjala – 2005]. Unfortunately, the pressure drop increases with decreased channel width when flow rate and other variables are constant. However, micro–channels are stated to hold the capability to cool heat fluxes up to 1 000 W/cm^2 [Lasance and Simons – 2005]. Industry has been using fluid cooling methods in the gaming markets and now the server sector is closely noting the progression of such technology [Wolverine Tube Inc – 2010].

An overview of the literature articulates a good comprehension of the single phase research component for micro–channels, where conventional correlations for larger [macro] channels were supported to provide suitable results to investigations using smaller [micro] channels. An identified need has been established for two–phase flow investigations to continue for micro–channel research. The need to develop a clear model that could be validated against larger datasets of experiments to better reflect the various facets involved in the two–phase flow region is presented [Bertsch et al. – 2008]. The model developed should incorporate flow pattern maps to better capture the physical phenomena visualized and not to limit such efforts to a single flow regime view.

To approach the problem through a fresh outlook as well as attend to the aforementioned concerns the model development will cover the areas of concern through implementing a different approach of already proven assumptions. The homogeneous and annular flow models for the two–phase region have been incorporated in literature and demonstrated reasonable results. However the homogeneous model has often been applied indiscriminately to problems in which other flow patterns would be expected [Collier and Thome – 1994]. Moreover the annular flow model considers only one single flow regime that could be improved upon as it is documented that oscillations of flow patterns do occur.

Therefore by combining the two models it is postulated that such an effort would enable greater flexibility to cover larger experimental datasets. A review of the literature reveals few studies that have covered modeling of flow boiling based on the existing flow regimes and taken into account the interfacial structure between the liquid and vapour phases [Harirchian and Garimella – 2012]. Even such studies have assumed the existence of a single regime in the channels where it has been illustrated in the literature however that different flow regimes can be present in micro–channels under operational and geometric conditions or even in a single micro–channel along its length [Harirchian and Garimella – 2012]. Augmenting a weighted approach to the models to more effectively reflect the flow regions captured by each model will be pursued. The homogeneous model is stated to be well–suited for the bubbly, misty, slug, and wavy annular regions. The annular model has been developed to provide good representation of the wavy annular as well as the annular flow regions. With the prediction of flow boiling in micro–channels complicated by the simultaneous existence of single phase flow, sub–cooling as well as saturated flow boiling [Zhang and Pinjala – 2005]. The rapid oscillations noted in the [flow boiling] two–phase region where both the homogeneous and annular flow patterns are assumed to simultaneously occur are to be incorporated. The aforementioned assumption would provide the means to weight each the homogeneous and annular model for the flow boiling [two–phase] region. The effectiveness of such an approach will be the valuable endeavor of the following MASc thesis.

1.3 Summary

Micro–channels are viewed as the most likely technology capable of meeting the future demands for high heat flux applications. Flow boiling applications have greater heat transfer coefficient values to that of air for thermal management technologies to contribute to research efforts underway to handle heat fluxes in the area of 100 to 300 W/ cm^2. The trend for increasing the number of transistors integrated into the central processing chip is expected to produce greater heat flux demands [Phillips – 1988]. The number of transistors has been illustrated to have steadily increased to 2.6 billion in 2011. It is acknowledged that there are other methods of cooling such as immersion cooling not mentioned that could also be implemented into appropriate applications. However, a brief introduction into some of the cooling options available has been presented.

Support is illustrated for physics based flow boiling models that could capture a more complete picture of the prevalent flow pattern behavior observed in micro–channels. The model developed will need to be validated against more than one experimental data set to illustrate effectiveness towards predicting a number of parameters such as pressure drop. Therefore the deliverables of the MASc thesis project includes the identification as well as evaluation of novel cooling technologies along with model development as means to provide an effective design instrument. The development of the model approach will take steps towards providing a more complete picture for the flow boiling behavior noted in the literature. The approach of the two–phase model will include both the single phase and two–phase flow regime to evaluate pressure drop corresponding to heat input as well as to provide validity to results for more than one set of experimental data from available sources in the research literature.

Micro–channel technology has been implemented into industrial applications such as the MSI N280GTX OC HydroGen graphics card. These applications demonstrate the relevance of such cooling methods where a news article from Purdue University states that micro–channel technology is expected to be employed within the near future and is anticipated to remain in the market for an estimated 20 years thereafter [Venere – 2005]. Hence a significant research effort has begun around the world to develop the necessary methods for designing and optimizing multi–micro–channel heat spreaders for cooling of computer chips [Thome – 2006].

CHAPTER 2
LITERATURE REVIEW

It is the intent of the literature review to provide an overview the research work accompanying the development of micro–channel cooling technology. The research literature has focused on different areas over the past 30 years or more of investigation from the initiation of such work in 1982. Efforts have been employed to integrate previous works to provide a clear outline of information from early design considerations, through single and then two–phase flow developments.

Micro–channels are viewed as networks of small channels that allow the flow of either liquid and/or vapour. Micro–channel research developed from discussions about fabrication method challenges, experimental set up, model equations to now more information into the understanding of particular heat transfer and fluid mechanics at the micro scale level. Micro–channels are generally defined as presented in Table 2.1.

Table 2.1 – Channel Classification for Conventional to Nano–Channels [Adapted From: Kandlikar and Grande – 2003]

Channel Classification	
Conventional Channels	$D_h > 3mm$
Mini–Channels	$200\mu m \le D_h \le 3mm$
Micro–Channels	$10\mu m \le D_h \le 200\mu m$
Transitional Channels	$0.1\mu m \le D_h \le 10\mu m$
Molecular Nano–Channels	$D_h \le 0.1\mu m$

2.1 Design of Micro–Channel Heat Sinks

Micro–channel research has focused on the following areas that include: 1) Evaluation of effectiveness of various design features regarding pressure drop and heat transfer aspects, 2) Single phase flow, 3) Two–phase flow, 4) Two–phase flow patterns, and 5) Model development.

From the design perspective important factors to consider include the heat transfer mechanism, hydraulic diameter, non–circular channel effects, bubble frequency, channel material, surface roughness, flow pattern effects, cyclical dry out, rewetting, instability effects and local hot spots [Thome – 2006]. In the case of two–phase flow the latent heat of vapourization progresses downstream to cool a desired region from a heat source in contact with the micro–channel heat sink. The channel shape, network design and dimensions all impact the overall heat transfer effectiveness. The most basic micro–channel heat sinks originated from the straight channel configuration which is illustrated in Figure 2.1.

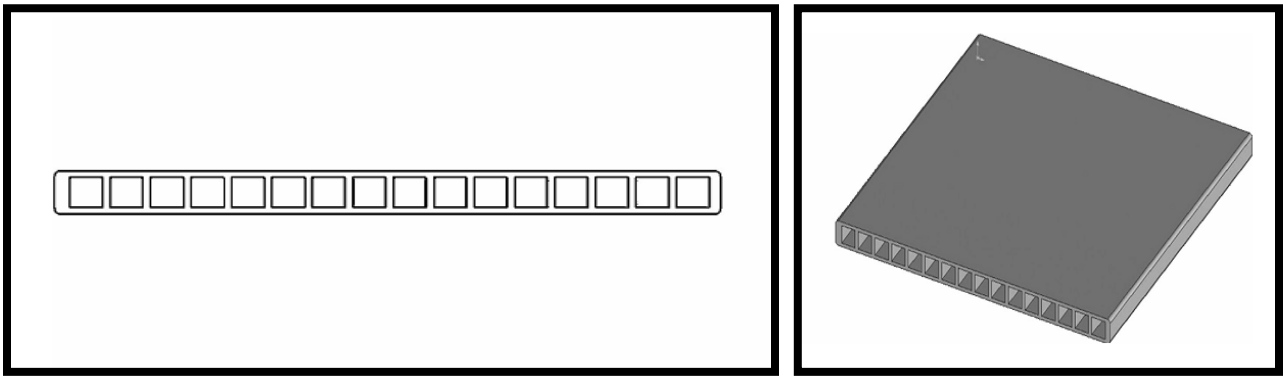

Figure 2.1 – Traditional Micro–Channel Heat Sinks [Adapted From: Thome – 2006]

Advances in micro–channel heat sink construction equipment enable precise designs as the channels illustrated in Figure 2.2. It can be demonstrated that machining has reached the level to produce such channels that incorporate bends while maintaining material integrity. The construction of such networks rival traditional and conventional fabrication methods earlier employed.

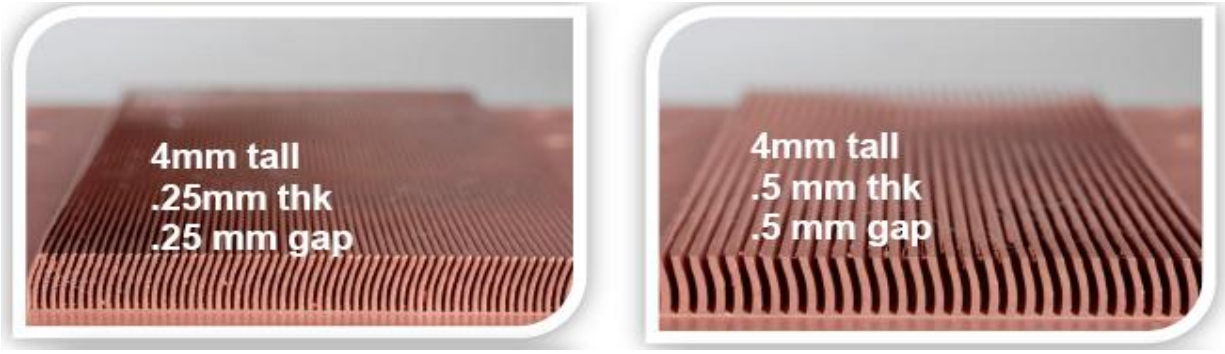

Figure 2.2 – Industrial Micro–Channel Heat Sink [Adapted From: Wolverine Tube Inc – 2010]

Tree–shaped networks have also been suggested in the literature similar to that illustrated in Figure 2.4 to address the need to minimize pressure drop while increasing heat transfer performance lacking in the straight channel networks illustrated in Figure 2.3 – a.

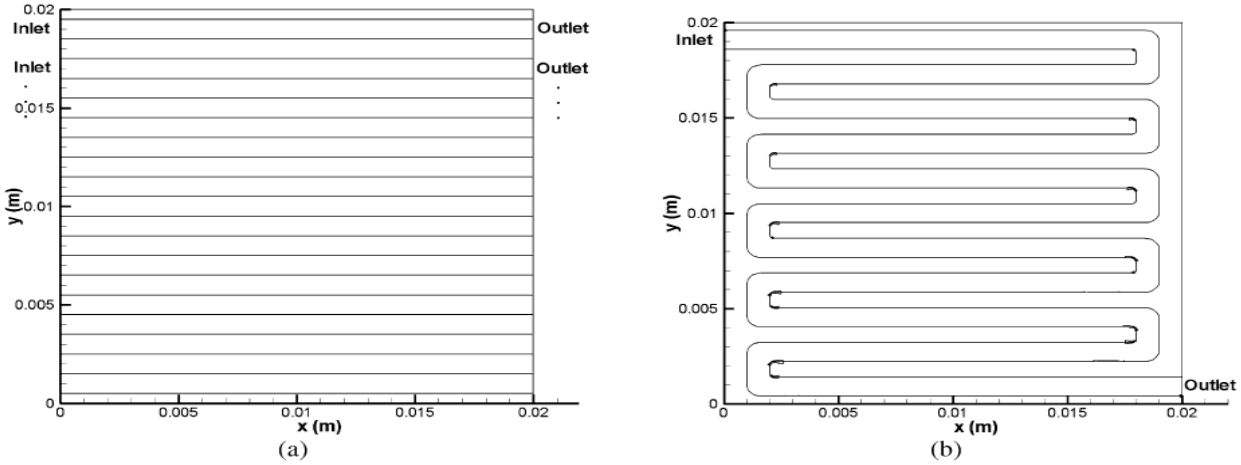

Figure 2.3 – Straight [a] and Serpentine [b] Channel Networks [Adapted From: Wang et al. – 2006]

Figure 2.4 illustrates a three–dimensional construction of a tree–like network. It has been noted that the tree network design produces about half the pressure drop and possesses a larger heat transfer capability than the corresponding serpentine flow pattern illustrated in Figure 2.3 – b while having the same surface area and inlet Reynolds numbers. The tree–like network allows for distribution of heat transfer among the levels of micro–channels that result from each bifurcation stage [split point] [Wang et al. – 2006].

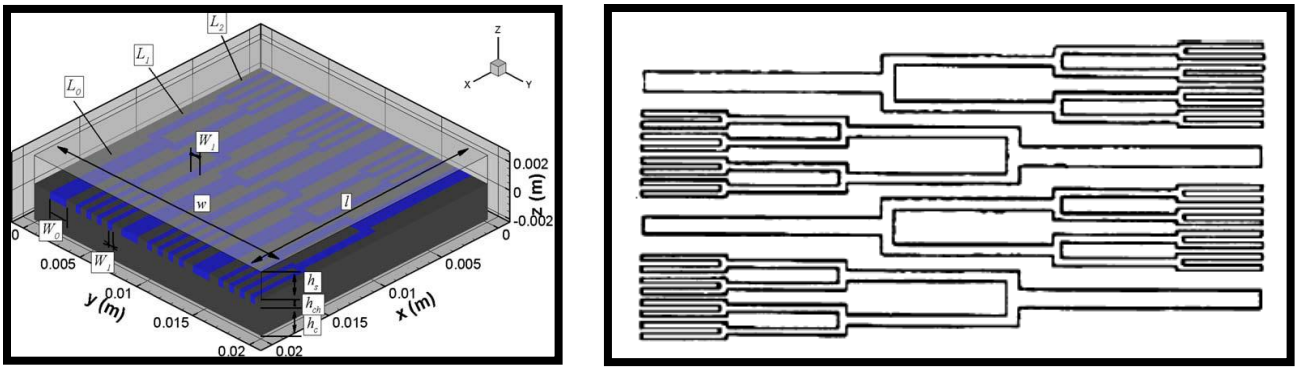

Figure 2.4 – Tree–Shaped Micro–Channel Heat Sink Network [Adapted From: Wang et al. – 2006]

The results of the above research illustrate that changing the design configuration can greatly impact the effectiveness of both the pressure drop and heat transfer characteristics in the micro–channel. The proposed designs such as serpentine flow paths have been ruled out in practicality due to an increased pressure drop that translates to higher pumping costs [Wang et al. – 2006]. It is important to note that the fabrication of micro–channels generally incorporates materials such as aluminum, copper or silicon [Liu and Garimella – 2003]. Fabrication is achieved through etching or micro–precision machining where some of the cooling fluids used include water, liquid nitrogen and various refrigerants such as R134a. Furthermore the recent progress of the surface micromachining technology has the capability to expand the frontier of engineering applications [Fushinobu et al. – 2004]. Figure 2.2 demonstrates the Wolverine Tube Inc advanced manufacturing capabilities that could extend new initiatives in the near future.

2.2 Single–Phase Flow

Early research work on single phase flow regarding pressure drop and heat transfer effects for micro–channels has often provided conflicting results. The ability to accurately account for the surface roughness has led to the general misunderstandings in this particular field of study [Webb – 2003]. A fundamental question in the micro–channel research area has been to determine whether the heat transfer and friction laws for macro–size channels can also be applied to micro–channels [Webb – 2003]. Contradictory conclusions have been drawn for various parameters and conventional correlations such as the Nusselt and Reynolds number regarding their accuracy when applied to micro–scale systems [Steinke et al. – 2006]. It had been suggested that such discrepancies could have resulted from errors in measurement of the micro–channel dimensions rather than any micro–scale effects [Steinke et al. – 2006].

The main difference between micro–systems and macro–systems is the considerable surface–to–area ratio exhibited at the micro level. The resulting scaling effects of macro to micro are noted through reduced Reynolds number as well as a non–negligible axial temperature gradient. These scaling effects in combination with variable rather than constant property solutions to the analytical equations have resulted in higher values of Nusselt numbers [Herwig and Mahulikar – 2006]. Although variable property analysis is relatively unimportant at the macro level, it should not to be overlooked at the micro level.

The previous arguments outline the concerns encountered in the literature in this area of research. Single phase micro–channel heat sinks have been studied extensively during the last two decades [Qu and Mudawar – 2002]. The research literature has illustrated that fluid flow characteristics in single micro–channels agree well with macro–channels [Webb – 2003]. It has been stated that if any non Navier–Stokes flow phenomena existed, their influence may have been masked by experimental uncertainty [Lee et al. – 2005]. However, reviews of the literature demonstrate that the conventional continuum model of the conservation of mass, momentum [Navier–Stokes] and energy provides adequate accuracy in representing the micro–channel flow and heat transfer characteristics [Liu et al. – 2007]. The flow of coolant in these heat sinks is usually considered to be laminar due to the small hydraulic diameter of the micro–channels. In addition the flow inside the micro–channels is considered to operate under fully developed hydrodynamic and thermal conditions. The flow and thermal analysis

of individual micro–channel heat sinks is for the most part straight forward [Radmehr and Patankar – 2004]. Single phase micro–channel heat sinks have been effectively attended to as well as modeled [Qu and Mudawar – 2002]. Therefore single phase micro–channel research can be viewed from the perspective of fluid flow through a pipe [macro–channel] where sufficient analytical and practical data values can be referred to resolve any encountered challenges.

Much research effort in the both areas of single phase and two–phase heat sinks has focused on experimental work of micro–channels [Lee and Qu – 2006]. The majority of the single phase studies demonstrated that conventional macro–channel predictive tools are fairly accurate at providing the pressure drop and heat transfer characteristics [Lee and Qu – 2006]. There have been a few studies covering optimization of heat sink geometry to minimize the overall thermal resistance through the design variable of constant pressure drop or constant pumping power [Lee and Qu – 2006]. However considerable deviations have been experienced with two–phase flow which has spurred the effort to develop new predictive tools [Lee and Qu – 2006].

2.3 Two–Phase Flow

Two–phase flow applications typically require knowledge of single–phase flow characteristics for analytical development [Webb – 2003]. Hence the analysis of single phase fluid flow in micro–channels is the first step for design [Webb – 2003]. Through increasing interest and a better understanding of two–phase flow in micro–channels it is evident that such applications will become the standard for electronic cooling in the near future [Cabral and Lam – 2003]. Flow boiling would enable the advantage of the latent heat to be liberated from heat transfer fluids to operate at lower mass flow rates which reduces the pumping power requirements resulting in a more energy efficient system [Wolverine Tube Inc – 2010]. Liquid cooling is the preferred near term solution while it is acknowledged that cooling through means of flow boiling of refrigerants seems to be the best long term solution [Wolverine Tube Inc – 2010]. The aforementioned arguments provide justification for the micro–channel research direction towards the understanding of flow boiling.

The area and reach of two–phase flow are covered thoroughly in the introductory paragraph from the book, "Convective Boiling and Condensation – 3rd Edition," by Collier and Thome, 1994 that outlines the subject of boiling and condensation corresponding to conditions of natural or forced convection as extremely important. Such knowledge of the fluid dynamics as well as the heat transfer processes occurring during convective boiling and condensation is incorporated into the design of water tubes, air conditioning equipment, heat pumps, pipe stills, surface condensers, water cooled nuclear reactors, refrigeration equipment, heat pumps, petrochemical plant reboilers, along with other items of chemical and power plant industries [Collier and Thome – 1994].

Two–phase flow or flow boiling through micro–channels was investigated by various researchers because of their ability to achieve high heat transfer coefficients [Prasher et al. – 2005]. It has been demonstrated that flows in mini and micro–channel heat sinks are capable of removing heat fluxes generated by high density packages in excess of 200 W/cm^2. Thus the flow boiling approach could meet and exceed high heat flux applications over the range of 100 – 300 W/cm^2. However the major disadvantages associated with the use of such cooling methods include the need for the system to avoid instability when operating close to the critical heat flux as well as to minimize surface temperature gradients between the channel and the upper surface of the heat sink [Dickey and Lam – 2003]. Though there have been investigations of two–phase flow for micro–channel heat sinks the fundamental

understanding of these devices is quite limited [Qu and Mudawar – 2002]. It would seem that every aspect of two–phase flow and heat transfer in micro–channels exhibits significant departure from macro–channel depictions [Qu and Mudawar – 2002]. Research work on two–phase flow or flow boiling in micro–channel is still considered limited [Zhang and Pinjala – 2005].

A significant motivation for moving in the flow boiling direction is associated with the enhanced heat transfer capability experienced in the two–phase region [Qu and Mudawar – 2002]. Several correlations were examined and deemed unsuitable for predicting the heat transfer coefficient in the saturated boiling region. The noted deviations between the predictions and experimental data were attributed to the use of turbulent flow assumptions employed in all the correlations. Additionally the deviations were attributed to the unique features of two–phase micro–channel heat sinks such as the abrupt transition to slug flow, hydrodynamic instability and the large number of liquid droplets entrained in the annular flow regime [Qu and Mudawar – 2002]. Such results support the need to further study boiling behavior in micro–channel heat sinks and the need to acquire new predictive tools specifically tailored to micro–channel flow [Qu and Mudawar – 2002].

A review of two–phase flow by Thome, 2006 was closely studied since the paper provided the up to date developments in the field and identified many areas yet to be improved. The paper noted that macro–scale flow pattern maps are typically unable to predict the transitions observed in micro–channels. Without delving too far into details, two–phase flow regimes in micro–channels at very low mass velocities provided capillary flow and laminar flow conditions as a natural limit [Thome – 2006]. The variations between macro–scale and micro–scale characteristics show slug flows that have length to diameter ratios on the order of 2 to 3, while in micro–channels ratios can exceed 50 to 1 [Thome – 2006]. The need for more development in the two–phase area are echoed in other literature where it is mentioned that there is a shortage of reliable experimental databases and comprehensive modeling tools that can tackle the diversity of coolants, geometries, and operating conditions of micro–channel heat sinks [Qu and Mudawar – 2002]. Literature reveals a need to put effort into modeling of flow boiling based on the existing flow regimes and to consider the contact layer relationships between the liquid and vapour phases [Harirchian and Garimella – 2012]. Further studies of flow patterns and parametric study of the cooling performances are beneficial to the modeling and design of high efficient micro–channel apparatus operated in the two–phase regimes [Zhang and Pinjala – 2005].

2.4 Two–Phase Flow Patterns

Two–phase flow patterns are recommended for the prediction of flow boiling heat transfer in micro–channels. Figure 2.5 illustrates the general flow regimes encountered for refrigerant R 245a in larger micro–channels. In these cases macro–scale flow pattern maps are typically unable to predict the transitions observed in micro–channels. The predominance of surface tension over gravity forces causes a reduction in the tubes' orientation influence for micro–channel two–phase flow patterns [Thome – 2006].

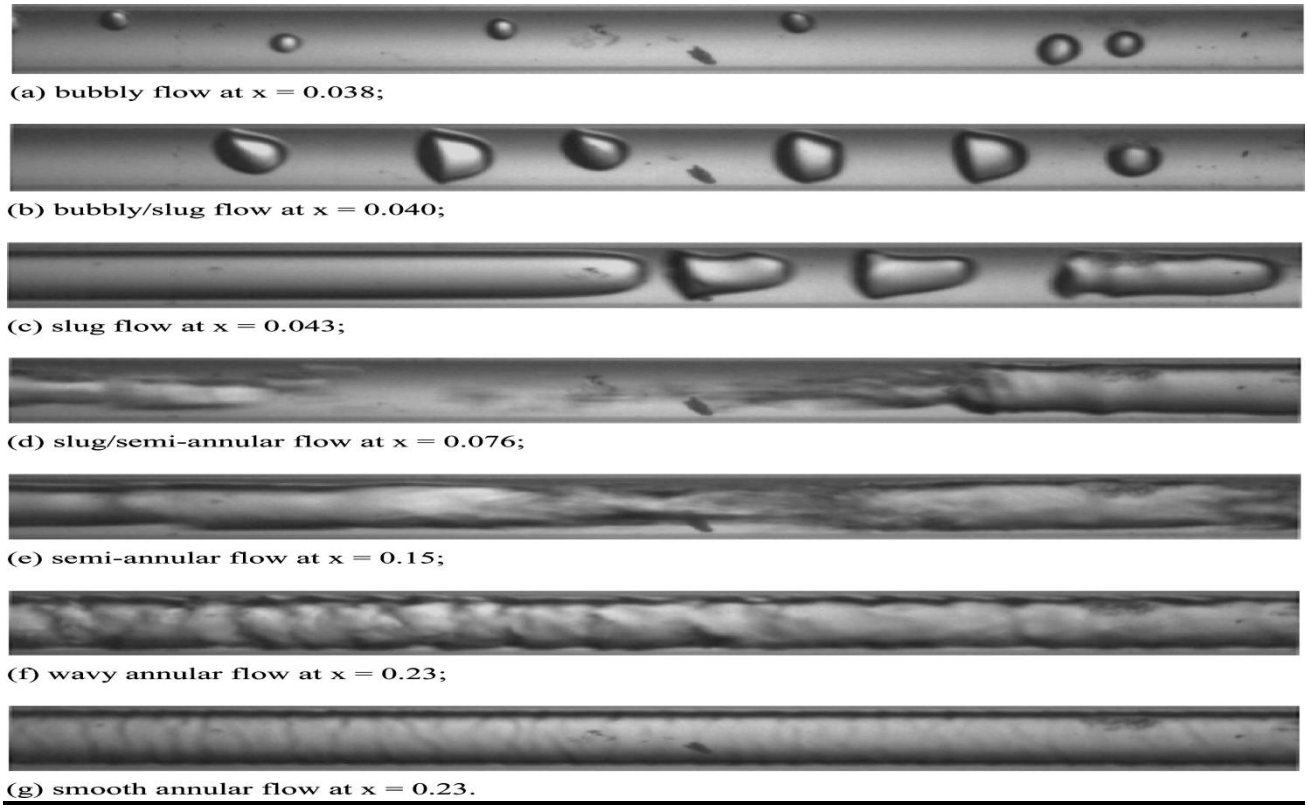

Figure 2.5 – Flow Patterns in 0.509 mm Micro–Channel for R245a at 35^{o}C and 500 kg/m^{2}s [Adapted From: Thome – 2006]

Figure 2.6 illustrates the flow patterns for water acquired through visual imaging with the actual images located on the left and an enhanced version using MatLab image processing located on the right [Galvis and Culham – 2012]. The corresponding letters from a to f, are used to designate the different flow patterns of water under diabatic conditions for the various vapour quality values [x_v] identified as follows: a) bubbly flow at x_v = 0.0037, b) slug flow at x_v = 0.12, c) churn flow at x_v = 0.19, d) annular flow at x_v = 0.24, e) wavy annular flow at x_v = 0.31, and f) inverted annular flow at x_v = 0.47 [Galvis and Culham – 2012].

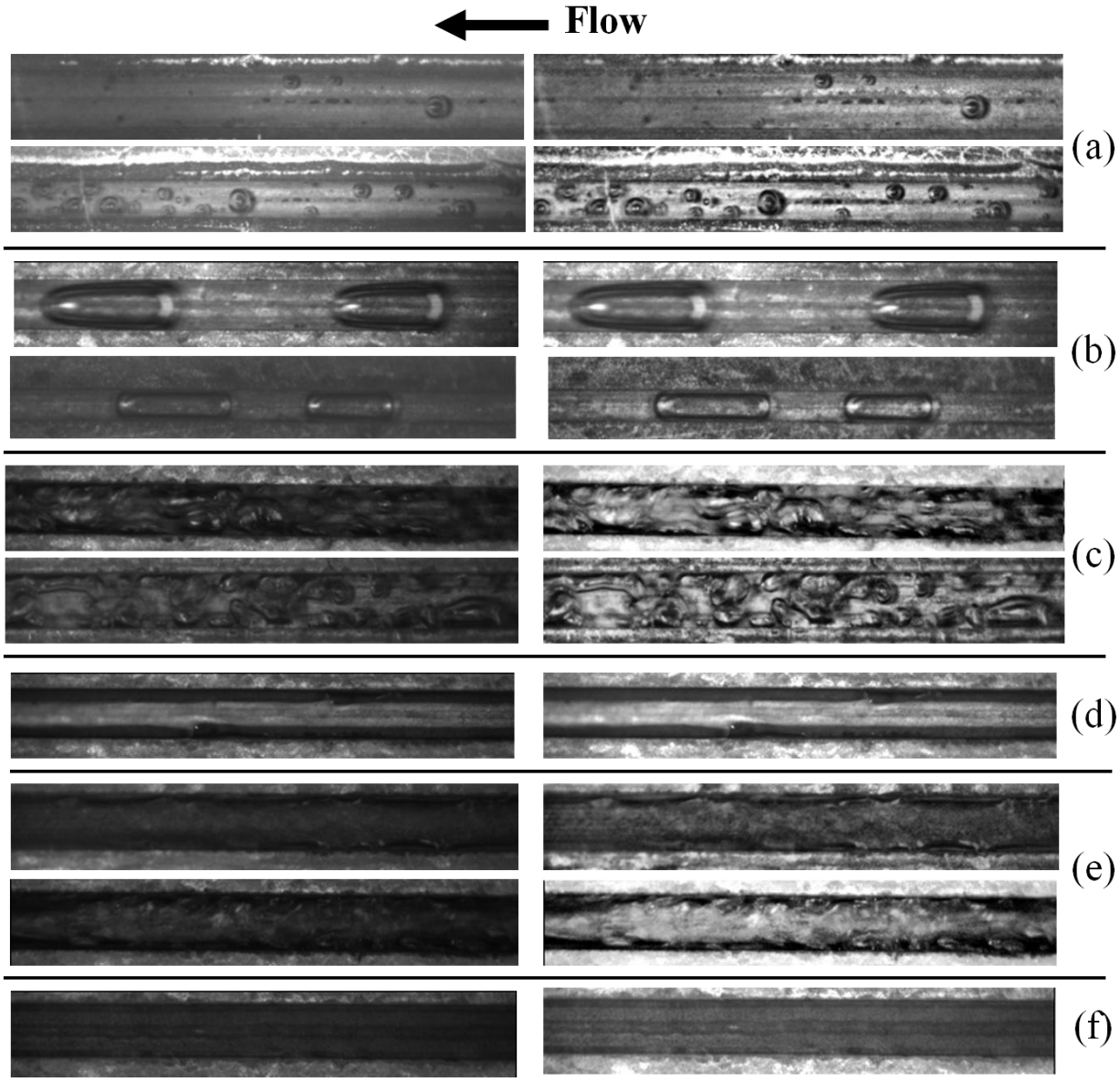

Figure 2.6 – Flow Patterns in Micro–Channel for Water [Adapted From: Galvis and Culham – 2012]

High speed visualizations illustrate that the flow patterns depend on the mass flux, heat flux and channel size. The images also show the main flow patterns observed after the onset of nucleation boiling include bubbly, slug, churn, wavy annular, annular, and inverted annular flow [Galvis and Culham – 2011]. Furthermore it has been noted that more accurate models for the heat transfer coefficient will be obtained if the model efforts are applied to each particular flow regime [Galvis and Culham – 2011]. The full range of flow patterns seen in conventional sized channels include: nucleate boiling flow, bubbly flow, slug flow, annular flow, as well as annular flow with nucleation occurring in the thin film, churn flow and dry out have been observed in micro–channels [Bertsch et al. – 2008]. Additionally flow reversal and flow instabilities have been noted under certain conditions [Bertsch et al. – 2008].

Intermittent dry out in both single and multi micro–channels have been observed with water in a 0.150 mm channel which is due to the very rapid vapourization at high heat fluxes. This rapid evaporation in micro–channels exhibits flow expansion in both directions that in turn disrupts the flow regime [Thome – 2006]. Research was also carried out to model clearly the flow of elongated bubbles as depicted in Figure 2.7. The interfacial phenomena observed to occur in two–phase flow is described as following certain stages from an initial liquid slug, nucleation of small vapour bubbles and then lastly an erupt departure of the small bubbles from the liquid slug which leave behind a small thin layer of liquid [Thome – 2006].

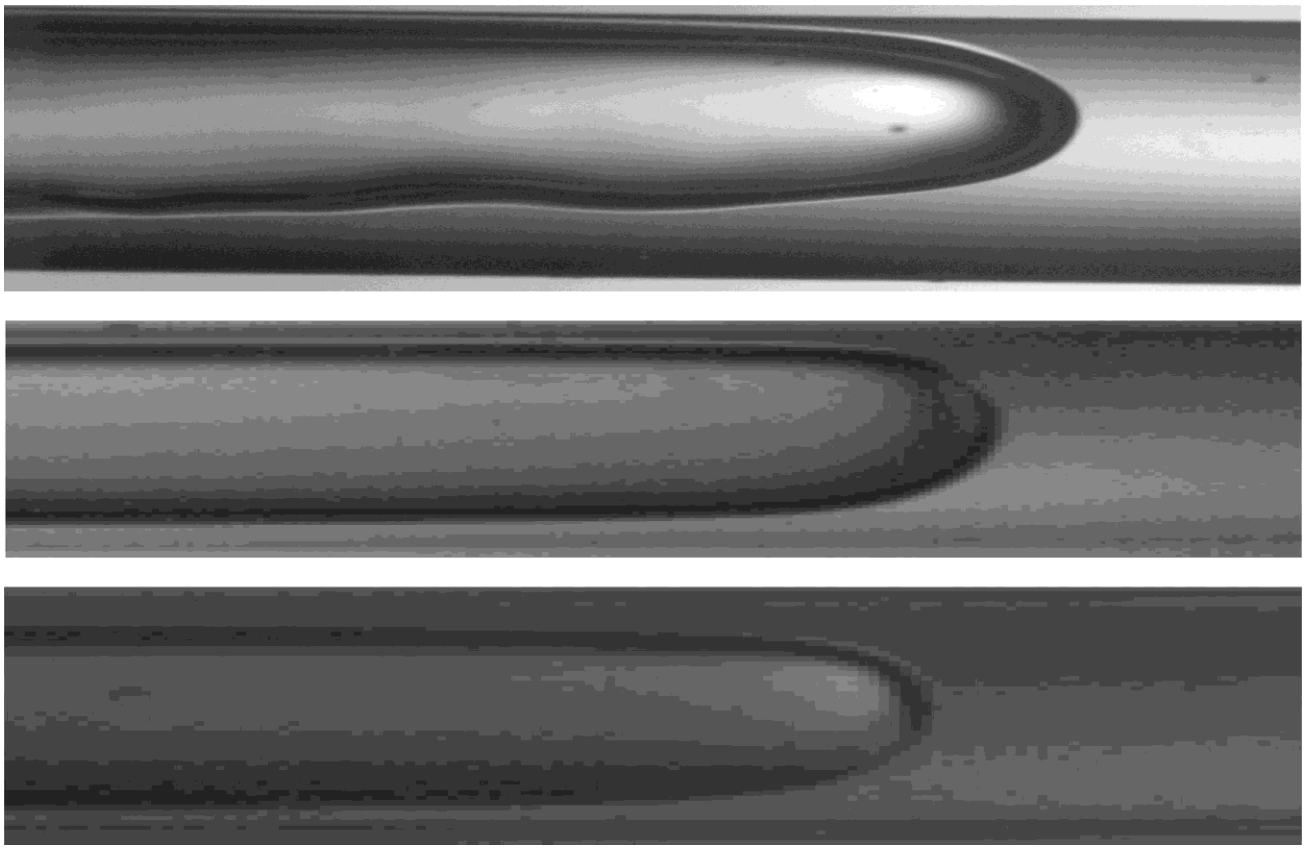

Figure 2.7 – Images of Elongated Bubbles in Three Sizes of Small Horizontal Channels [Adapted From: Thome – 2006]

The importance of understanding elongated slug flow, relates ultimately to flow patterns and thus the heat transfer capabilities of micro–channels under particular operating conditions. An accurate prediction of flow boiling heat transfer in micro–channels that accounts for the numerous trends in the published work seems to be impossible without taking into account the influence of flow patterns [Thome – 2006]. The macro–scale and micro–scale are not well correlated when the boiling incipience in micro–channels is examined. This is illustrated by deviations from the predictions of classical correlations intended for macro–scale systems [Thome – 2006]. Other factors could also be involved in the aforementioned behavior such as the nucleation and growth of bubbles that were influenced by other two–phase events occurring elsewhere along the length of the channel [Qu and Mudawar – 2002].

Following the onset of boiling, bubbles quickly coalesced into oblong bubbles typical of slug flow and high fluxes produced mostly annular flow. Parallel channel instability caused the flow in an individual channel to oscillate between different flow pattern regimes even at constant operating conditions [Qu and Mudawar – 2002]. It is noted that future studies should explore these issues more thoroughly in pursuit of a better fundamental understanding of boiling in micro–channel heat sinks. Such efforts are a necessary step towards developing more reliable predictive tools for micro–channel heat sink design [Thome – 2006]. It would be encouraged that the resulting flow pattern be integrated into the development of heat transfer prediction models and not remain an independent tool [Thome – 2006].

Future fundamental work needs to more carefully resolve the two–phase flow regimes outlined through microscopy and localized pressure distribution measurements. This will be critical for interpreting and modeling the transient nature of two–phase flow and the onset of dry out [Koo et al. – 2001]. Additional research into the mechanisms of flow boiling in small channels is necessary [Bertsch et al. – 2008]. Models based on the physics of the boiling process and the appropriate flow patterns, flow regime maps are likely to yield better extrapolation beyond the boundaries of the operating ranges [mass flux, heat flux, vapour quality, and hydraulic diameter] relative to purely empirical curve fits. There are a few such models based on the flow regimes that have been presented [Bertsch et al. – 2008]. There is a clear need for the development of physics based models of micro–channel flow boiling. Such model predictions should be compared with large databases of experimental measurements covering a wide range of parameters [Bertsch et al. – 2008]. Few correlations in the current literature are based on the prevalent flow regimes in micro–channels; even those that are usually consider only a single flow regime [Bertsch et al. – 2008]. It is important that the flow regime maps be first developed based on simultaneous high speed visualization and local heat transfer and pressure drop measurements in carefully characterized experimental setups. Such a broad database would then allow the development and validation of models that include the flow regimes to be expected for a given set of parameters [Bertsch et al. – 2008].

2.5 Two–Phase Flow Models

The methods used to analyze two–phase flow are extensions of those already well tried for single–phase flows [Collier and Thome – 1994]. Two–phase flow in micro–channel heat sinks offer the same attributes as their single–phase counterparts while providing the added benefits of higher convective heat transfer coefficients, better temperature uniformity, and smaller coolant flow rates [Qu and Mudawar – 2002]. Through simulating, experimenting, as well as theorizing a better understanding of certain limitations and the impact of assumptions is achieved [Pang et al. – 2004]. Such efforts aid future studies by cautioning the researchers on making inaccurate or unrealistic assumptions when developing a model for micro–channel applications [Pang et al. – 2004]. It has been expressed that the best agreement between predictions and experimental results were achieved with numerical simulation, however a few of the fin models are found to provide fairly accurate predictions [Qu and Mudawar – 2002].

There has been much effort to establish a suitable two–phase flow model to capture the necessary physical phenomena. Three techniques in modeling the two–phase region pressure drop include the homogeneous equilibrium model, Martinelli–Nelson correlation and the Lockhart–Martinelli correlation which provided better agreement to experimental results [Qu and Mudawar – 2002]. Most two–phase research studies are experimental and very few are dedicated to modeling [Qu and Mudawar – 2002]. An important objective of such work is to develop heat transfer modeling tools that are essential to the design and optimization of heat sink geometry [Qu and Mudawar – 2002].

The model presented by Qu and Mudawar, 2002 considered only the annular flow regime [Bertsch et al. – 2008]. The three zone model by Thome has been investigated with minimal success as it predicted 45% of the experimental data with a mean absolute error of 50%, and thus this was good justification for further work [Thome – 2006]. In any case, the diverse trends existing for micro–channel flow boiling data cannot for now be captured by any other method [Thome – 2006]. The need for further study of boiling behavior in micro–channel heat sinks, and for new predictive tools specifically tailored to such phenomena is expressed in the literature [Qu and Mudawar – 2002]. Therefore the following section intends to cover some of the methodology that has been used to date to estimate two–phase flow behavior.

Few regime based models exist in the literature for the prediction of heat transfer coefficient and pressure drop values regarding flow boiling in micro–channel [Harirchian and Garimella – 2012]. A review of the literature reveals only a few studies that have put effort into the modeling of flow boiling based on the existing flow regimes and taken into account the interfacial structure between the liquid and vapour phases [Harirchian and Garimella – 2012]. Research studies have assumed the existence of a single regime in the channels while it has been shown in the literature that different flow regimes can be present in micro–channels under certain operational and geometric conditions or in a single micro–channel along its length [Harirchian and Garimella – 2012].

2.5 – 1 Homogeneous Flow Model

The homogeneous model has been generally applied in literature over various two–phase flow patterns and demonstrated reasonably accurate predictions regarding pressure drop values compared to experimental data under diabatic and adiabatic conditions [Thome – 2006]. Under the assumptions of the homogeneous model the momentum equation can be outlined as expression [2.1] as presented in the works of Kelkar et al., 2005 and Sarangi et al., 2009. Figure 2.8 is provided to illustrate a conceptual representation of the homogeneous flow regime that includes small bubbles, larger bubbles leading close to slug like behavior and a few other vapour formations that could be defined as the start of churn or wispy like annular flow.

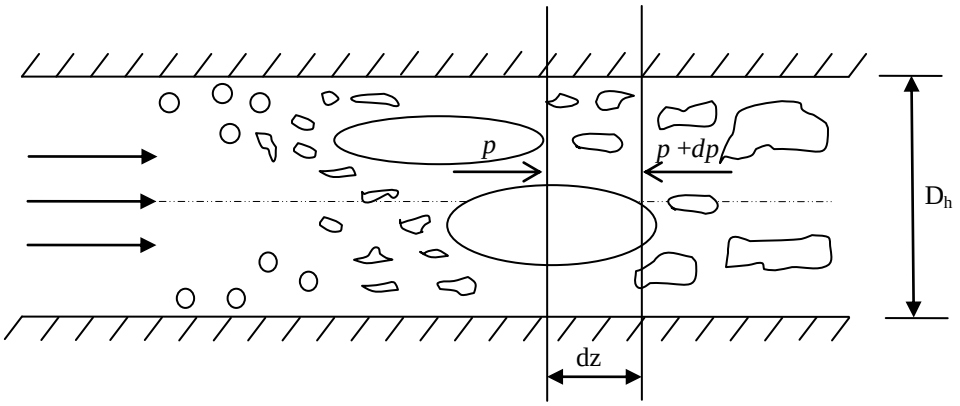

Figure 2.8 – Conceptual Illustration of Homogeneous Flow Pattern

$$-\frac{\partial p}{\partial z} = \frac{f_{TP} G^2}{2\rho_H D_h} + \frac{1}{A_{CH}} \frac{\partial}{\partial z}\left(\frac{G^2 A_{CH}}{\rho_H}\right) \qquad [2.1]$$

Some of the attributes of the homogeneous model include the assumption that both liquid as well as vapour are a single mixture of fluid [Hewitt and Hall–Taylor – 1970]. Moreover the velocity and density of the mixture are considered to be constant across the channel.

The homogeneous density is calculated between the liquid and the vapour components of the fluid through incorporating the vapour quality as outlined in Equation [2.2].

$$\frac{1}{\rho_H} = \frac{x_v}{\rho_G} + \frac{\left[1 - x_v\right]}{\rho_L} \qquad [2.2]$$

The homogeneous approach has been implemented to represent the pressure drop of the two–phase region by many authors that include Koo et al., 2002, Kelkar et al., 2005, Qu and Mudawar, 2002, Bhide et al., 2009 as well as Sarangi et al., 2009. Two–phase empirical friction factors in the range of 0.0029 to 0.005 have been incorporated in the homogeneous model where the values were acquired from the experimental data of steam provided in Collier and Thome, 1994. Calculations of the two–phase friction factors can be completed for the homogeneous model. Such calculations often include the viscosity relationship developed by Cicchitti et al. outlined in Equation [2.3] from Collier and Thome, 1994.

$$\mu_H = x_v \mu_G + \left[1 - x_v\right]\mu_L \qquad [2.3]$$

Initially the homogeneous flow assumption had been stated to be only accurate for low surface tension coolants such as methanol, isobutane and HFC's [Kelkar et al. – 2005]. The work of Kelkar et al., 2005 modeled the fluid isobutane employing the homogeneous flow approach for the two–phase region in a micro–channel via a one–dimensional representation of the momentum and energy equations. The model provided a three–dimensional heat conduction solution for the solid region and incorporated a one–dimensional representation for two–phase flow within the micro–channel. The Kandlikar enhancement factor heat transfer coefficient correlation had been employed to calculate the heat transfer characteristics for the two–phase region. The dimensions of the micro–channel were 0.3 mm [thickness], 0.5 cm [width] by 1.5 cm [length]. The model was later updated to capture heat transfer and two–phase flow for multiple micro–channels [Kelkar et al. – 2006].

The recent work by Sarangi et al., 2009 has demonstrated that the homogeneous flow model for pressure drop calculations could be extended to include water that is of a higher surface tension with good accuracy. Zhang et al., 2002 modeled two–phase flow for water through the homogeneous approach for a single micro–channel of 40–50 µm wide 50–100 µm deep and for multiple micro–channels as well. The model of Zhang et al., 2002 considered a one–dimensional analysis for the micro–

channel via the finite volume method for both single and two–phase flow. Results demonstrated that pressure drop predictions achieved relatively good agreement with experimental data. The homogeneous model is largely implemented for its simplicity and ability to provide a basis for comparison to other methods. The published literature demonstrates that the homogeneous approach has achieved reasonable results for pressure drop calculations from a number of researchers.

2.5 – 2 Annular Flow Model

The annular flow model is another representation that has been more frequently used in the micro–channel research literature. The annular flow is a particularly important flow pattern as it occurs over the major part of mass volatility for a wide range of pressure and flow conditions [Collier and Thome – 1994]. Figure 2.9 illustrates annular flow regime where the liquid phase is viewed to pass along the outer wall while the vapour core travels through the centre of the channel.

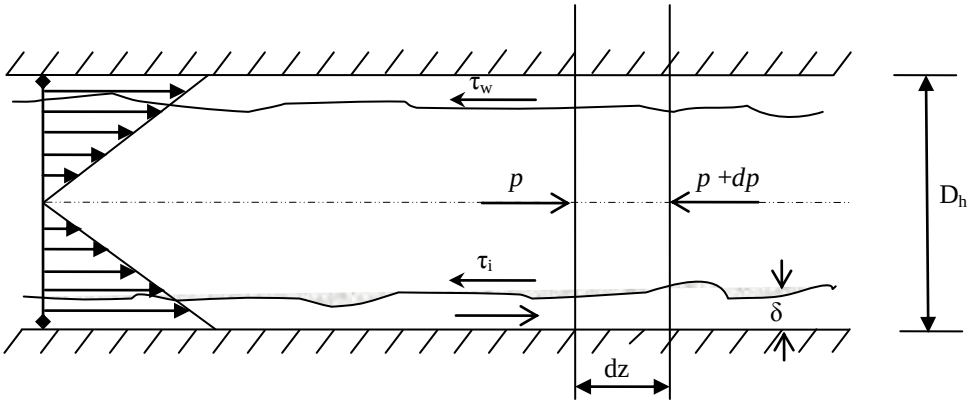

Figure 2.9 – Horizontal Annular Flow Schematic [Adapted From: Collier and Thome – 1994]

Thorough analysis of the annular flow pattern enables thermal methods of single phase flow to be applied. The liquid mass flow rate is contained as a symmetrical film on the channel wall with a small smooth interface between the liquid film and vapour phase. The shear force of the laminar film can be expressed as that of Equation [2.4] outlined from Sarangi et al., 2009.

$$\tau = \mu_L \frac{\partial u_{LL}}{\partial y} \qquad [2.4]$$

Moreover another fundamental feature of the annular flow is that the method by which such flow is formed greatly influences subsequent behavior of the system downstream [Collier and Thome – 1994]. The new momentum equation of the liquid film via the control volume approach can be expressed as Equation [2.5] which is outlined by Sarangi et al., 2009. The expression for the pressure drop in the annular flow region provided in Sarangi et al., 2009 is represented in Equation [2.6].

$$p(\delta - y)P_{CH} - \left(p + \frac{\partial p}{\partial z}\Delta z \right)(\delta - y)P_{CH} - \tau P_{CH}\Delta z + \tau_i P_{CH}\Delta z \qquad [2.5]$$

$$\left(-\frac{\partial p}{\partial z} \right) = \frac{3\mu_L}{P_{CH}\rho_L \delta^3}\dot{m}_{LL} - \frac{3}{2\delta}\tau_i + \frac{3}{2\delta P_{CH}}\Gamma_{LG}u_i \qquad [2.6]$$

The work of Qu and Mudawar, 2002 as well as Sarangi et al., 2009 have incorporated the annular flow model approach and included the single phase region that has been omitted by the majority of the authors. This provided a more complete representation for the flow regimes occurring in the micro–channel. Analysis of the model by Qu and Mudawar, 2002 as well as Sarangi et al., 2009 capture the effects of fluid flow rate, power input and channel geometry on the pressure drop and heat transfer coefficient. The model presented by Sarangi et al., 2009 predicted the boiling front that outlines the location along the length of the channel where two–phase flow is expected to start as well as pressure drop values and thermal resistance as a function of the micro–channel operating conditions that include the fluid flow rate, heat input and outlet pressure.

The temperature difference across the liquid film is governed by the rate of heat transfer and conductivity of the liquid phase [Hewitt and Taylor – 1970]. The temperature of liquid is changing axially and the film temperature distribution is effected by the velocity profile of the liquid although it is usually ignored [Hewitt and Taylor – 1970]. The heat transfer coefficient is largely dictated by local fluid dynamic conditions and is able to be represented by Equation [2.7] as provided in Sarangi et al., 2009.

$$h = \frac{k_L}{\delta} \qquad [2.7]$$

Qu and Mudawar, 2002 employed the assumption of a homogeneous mixture to represent the vapour core in the development of their annular flow model. The work of Sarangi et al., 2009 considers a thin liquid film and pure vapour core region for their annular flow model.

However, a unique unsteady annular flow with periodic destabilization of the liquid– gas interface has been observed [Herescu and Allen – 2006]. It has been noted that at high heat fluxes there are quasi periodic rewetting and refilling of the channels observed as well as a reversal of flow and explosive vapourization [Agostini et al. – 2007]. It has been proposed that this behaviour could explain why the heat transfer coefficient decreases with vapour quality as observed in many studies [Agostini et al. – 2007].

Actually this cyclical dry out is not an unstable phenomenon because it leads to constant wall temperature [Agostini et al. – 2007]. The dry out of the liquid film initiated at the center of the inner walls in an annular flow pattern demonstrates that through increased evaporation the contact line retreats to the corners of the micro–channel [Singh et al. – 2008]. Over time the film thickness in this stratified region gradually reduces until eventually there is a dry out period where only vapour flows through the channel [David et al. – 2011]. In this cyclical process there is a liquid only period followed by an annular flow with thinning films proceeded by a dry region [David et al. – 2011]. The behavior described is noted to exhibit similar characteristics for the nucleate boiling phenomena [Kandlikar – 2004]. Corner wedge flow has been identified between two–phase transition regimes for adiabatic air–water flow [David et al. – 2011]. Such findings are similar in nature to studies illustrating that the presence of liquid in the corners of the channel significantly reduces viscous dissipation so that the introduction of even a thin film of fluid is sufficient to induce motion [Dong and Chatzis – 2004]. The aforementioned result illustrates that corner flow augments the flow ability of the fluid along the length of the channel. The most commonly observed flow pattern was an annular slug regime which is defined where a bubble expands to fill the channel and extends into the channel causing a vapour core and wetting thin film [Steinke and Kandlikar – 2004].

2.5 – 3 Multiple Flow Models

The multiple flow model that included slug flow regime has been another approach adopted by Agarwal and Garimella, 2006 to capture the flow patterns observed for two–phase flow in their experiments involving fluid R134a. In the intermittent regime, visualization studies illustrated that the vapour phase travels as long solitary bubbles surrounded by an annular film which is separated by liquid slugs [Agarwal and Garimella – 2006]. Figure 2.10 illustrates this flow behavior that would provide the basis to develop a model to predict such phenomena [Agarwal and Garimella – 2006]. Slug flow has been illustrated to be the most observed pattern to occur in the two–phase flow region [Galvis and Culham – 2012].

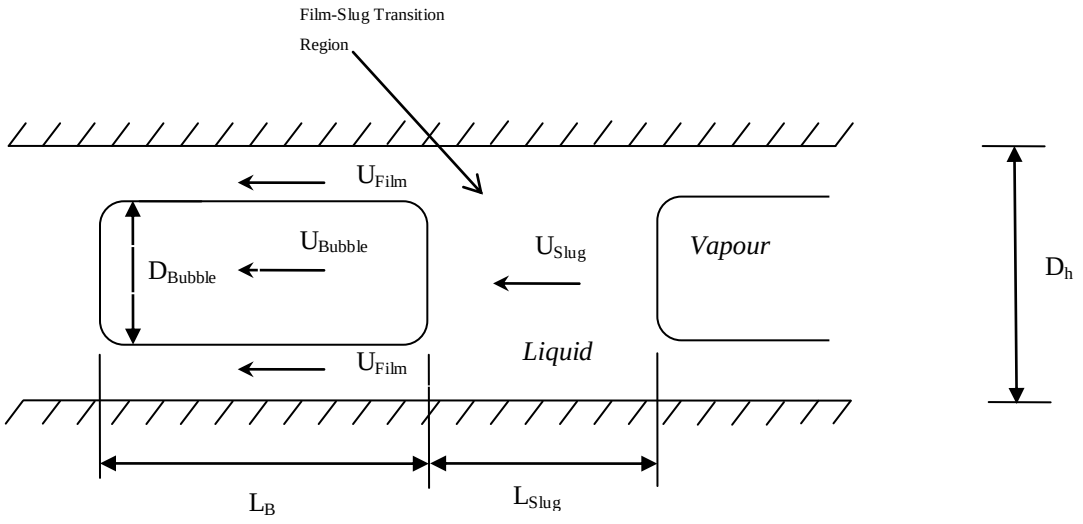

Figure 2.10 – Schematic of Intermittent Flow [Adapted From: Agarwal and Garimella – 2006]

It was proposed that the bubble traveled faster than the liquid slug implying that there would be continual uptake of the liquid from the film into the front of the slug which had been taken into account in the model developed by Agarwal and Garimella, 2006. Moreover through recorded flow patterns it had been assumed that the bubble is cylindrical with no entrainment of vapour in slug pattern or liquid in the bubble. Such assumptions would enable the total pressure drop for the flow patterns to be described from contributions of the liquid slug, the vapour bubble as well as the flow of liquid between the film and slug as outlined in the following Equation [2.8].

$$\Delta p_T = \Delta p_{Slug} + \Delta p_{F/B} + \Delta p_{\substack{F-Slug- \\ Tran}} \qquad [2.8]$$

This combined model accurately predicts pressure drops in the annular, disperse wave, mist, discrete wave, and intermittent flow regimes for both circular as well as non–circular micro–channels of similar hydraulic diameters for the experimental conditions reviewed in the paper by Agarwal and Garimella, 2006.

$$\frac{\Delta p}{L} = \left(\frac{\partial p}{\partial x}\right)_{F/B}\left(\frac{L_B}{L_{UC}}\right) + \left(\frac{\partial p}{\partial x}\right)_{Slug}\left(\frac{L_{Slug}}{L_{UC}}\right) + \Delta p_{\substack{One- \\ Tran}}\left(\frac{N_{UC}}{L}\right) \qquad [2.9]$$

Agarwal and Garimella, 2006, illustrated that the annular flow pressure drop model could apply to neighbor regimes that include disperse wave and mist flows. The model incorporated appropriate interpolation techniques to address the regions of overlap and transition between the different flow regimes [Agarwal and Garimella – 2006].

2.5 – 4 Other Model Design Considerations

The complex nature of flow boiling and two–phase flow in micro–channels is still not well understood and has impeded the practical implementation the technology [Liu and Garimella – 2007]. Among the unresolved issues of particular importance is the quantitative prediction of the boiling heat transfer coefficient in micro–channels over a wide range of conditions that include subcooling to saturated boiling [Liu and Garimella – 2007]. A limited number of studies in the literature revealed a lack of consensus on the understanding and prediction of boiling heat transfer and two–phase flow in micro–channels [Liu and Garimella – 2007]. In particular flow pattern based models have been proposed to correlate boiling data however these models are typically applicable over a narrow range of experimental conditions. Thus a clear need is presented for additional systematic studies which carefully address the experimental characterization and modeling of boiling heat transfer in micro–channels [Liu and Garimella – 2007].

With water becoming the coolant of choice for many high heat flux cooling applications such as lasers and fusion reactor blankets due to its superior thermal transport properties to those of all other known refrigerants. It is widely accepted that saturated flow boiling in channels is governed by two mechanisms: nucleate boiling and forced convection boiling [Qu and Mudawar – 2003]. Good agreement between the exact and approximate methods indicate that with carefully chosen assumptions such analytical results can lead to adequate descriptions of the thermal performance, while allowing easier manipulation of micro–channel geometries for the purpose of optimization [Liu and Garimella – 2003]. In spite of the simplicity, the one–dimensional resistance analysis approach appears to adequately represent the physics of the heat transfer problem, and is recommended for use in the design and optimization of practical micro–channel heat sinks [Liu and Garimella – 2003]. Simplified model approaches are sought where the goal is to account for the important physics of the problem even if some of the details may need to be sacrificed [Liu and Garimella – 2003].

2.6 Two–Phase Flow Experimental Data

Experimental research investigations have provided valuable insight into the characterization and performance assessment of two–phase micro–channel heat sinks, however the fundamental understanding of such technology remains quite limited [Qu and Mudawar – 2002]. Virtually every aspect of two–phase fluid flow and heat transfer in a micro–channel seems to exhibit significant departure from macro–channel depictions [Qu and Mudawar – 2002]. There are also vast differences in boiling behavior in micro–channels between experiments [Qu and Mudawar – 2002].

Table 2.2 – Onset of Nucleate Boiling Characteristics of Experiments [Adapted From: Liu and Garimella – 2007]

Author	Channel Geometry	Hydraulic Diameter [mm]	Mass Flux [kg/m^2s]	Fluid	Heat Flux [kW/m^2]	Pressure [MPa]
Bergles and Rohsenow [1964]	Cylindrical Tube	2.387	2.1–19.4 x 10^3	Distilled Water	1 890 – 18 900	0.261
Sato and Matsumara [1964]	Cylindrical Tube	–	–	Water	100 – 750	0.1
Unal [1975]	Cylindrical Tube	4 – 20	132 – 2 818	Water, R–22	20 – 1 920	0.1 – 15.8
Hino and Ueda [1985]	Cylindrical Tube	7.0	158 – 1 600	FC – R–113	11.78 – 46.90	0.147
Kennedy et al. [2000]	Cylindrical Tube	1.17, 1.45	800 – 4 500	De–ionized and De–gassed Water	0 – 4 000	0.344 – 1.034
Hapke et al. [2000]	Cylindrical Tube	1.5	100 – 500	De–ionized Water	50 – 200	0.1
Hetsroni et al.	Cylindrical Tube	1.07	49 – 146	Distilled Water	62 – 162	0.1
Stoddard et al. [2002]	Annular Channel	0.724 – 1.0	85 – 1 428	Fully De–gassed Water	124 – 1 000	0.344 – 1.034
Suetal [2001]	Annular Channel	1.0, 1.5	45 – 180	Pure Water	40 – 210	0.2 – 3.5
Qu and Mudawar [2002]	Rectangular Channel	0.231 x 0.713	130 – 1 440	De–ionized Water	200 – 2 000	0.12
Liu et al. [2005]	Rectangular Channel	0.275 x 0.636	309 – 883	De–ionized Water	100 – 730	0.1
Lee et al. [2004]	Trapezoidal Channel	0.413	170 – 899	De–ionized Water	1.49 – 500	0.161

Table 2.2 illustrates a general overview for operating conditions of various geometries as well as performances experienced for past experiments that experienced nucleate boiling. The geometries of in the experiments included a cylindrical tube, annular channel, rectangular channel and a trapezoidal channel. The hydraulic diameters of the geometries investigated ranged approximately between 0.4 to 20 mm with water as the fluid employed in all experiments.

A clearer understanding of the underlying physics of flow boiling in micro–channels obtained from well designed experiments and simulations is necessary to achieve better predictions through these models [Bertsch et al. – 2008]. Experimental studies in the literature have focused on characterizing the heat transfer performance and pressure drop, flow patterns, flow instabilities, and critical heat flux, a variety of predictive correlations for heat transfer and pressure drop [Harirchian and Garimella – 2012].

Two–phase experimentation is not without its challenges and is carefully presented in the following paragraph from the literature concerning commercial thermocouples that have a thickness of several hundred micrometers. Thermocouples have two disadvantages: one is that it is impossible to attach thermocouples to exact locations at the surface of a micro–scale structure, and the other is the difficulty to measure the surface temperature distribution when using several thermocouples [Jang and Kim – 2003]. It is also stated that certain sensors have complex manufacturing processes and difficult calibration procedures that should also be considered in experimental assessments [Jang and Kim – 2003].

Experimental data show that the average heat transfer coefficient is much larger in the two–phase region than in the single–phase region [Qu and Mudawar – 2002]. Such experimental data further demonstrates the higher expected cooling performance of two–phase micro–channel heat sinks over their single–phase counterparts [Qu and Mudawar – 2002]. Empirical correlations in the literature have been developed by fitting curves to specific experimental data considered in the studies, and although they may precisely predict the original experimental data based on which they are developed, the accuracy of predictions is limited to the range of operating conditions and fluids considered [Harirchian and Garimella – 2012]. The regime based models on the other hand are expected to extrapolate to a wider range of parameters with better accuracy [Harirchian and Garimella – 2012].

2.6 – 1 Experimental Data of Zhang et al. – 2002

The experimental data set of Zhang et al., 2002 that outlines the pressure drop values compared to heat input is presented in Figure 2.11 for a single micro–channel with dimensions that include a width of 50 µm and depth of 70 µm. The micro–channel was fabricated through the DRIE etching process where further details are disclosed in their paper. Additional attributes include that a 600 µm by 250 µm deep reservoir is defined at the inlet with a 2 cm long entrance region.

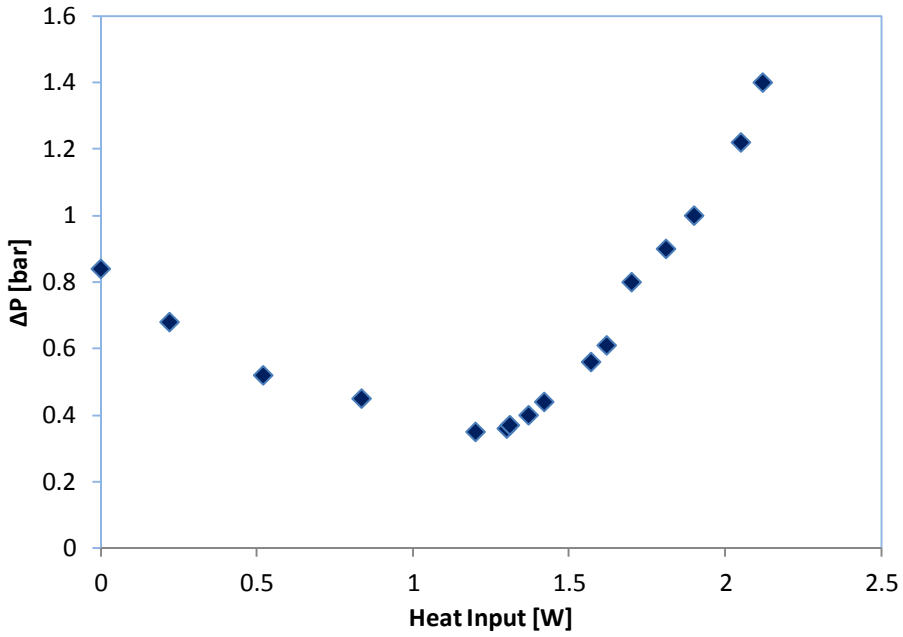

Figure 2.11 – Experimental Data: L = 1.6 cm, w = 50 µm, d = 70 µm, D_h = 58.3 µm, T_{IN} = 20^0C, P_{OUT} = 1.17 bar, $\dot{Q}$ = 0.1 mL/min [Adapted From: Zhang et al. – 2002]

A syringe pump provided a constant flow rate of water to the micro–channel system. The pressure transducer was located at the flow entrance of the fixture where it was noted that the internal flow channels were much larger than the micro–channels. Thus it was stated that the pressure drop within the fixture could be neglected for their experiment.

The resistor formed on the back side of the micro–channel provided both the function of a heater and thermometer. The length of the heater was 1.6 cm which does not cover the entire 2 cm length of the micro–channel. The thermometers enabled the current and voltage difference to be measured to facilitate the calculation of temperature values for each of the nine segments installed. The thermometers were calibrated by placing the silicon chip in a convection oven with a reference thermocouple [Zhang et al. – 2002]. Current and voltage signals at every measurement point began to fluctuate in time after the onset of boiling [Zhang et al. – 2002]. The single micro–channel experiment presented an estimated heat loss of 26% from the system with a 12% loss attributed to preheating conditions [Zhang et al. – 2002].

2.6 – 2 Experimental Data of Bhide et al. – 2009

Experiments were conducted by Bhide et al., 2009 for two–phase flow in a single micro–channel with dimensions less than one hundred microns. The micro–channel dimensions as well as the operating conditions employed are comparable to the work completed by Zhang et al., 2002.

Figure 2.12 oultines the corresponding pressure drop results for the flow rates 0.1 and 0.14 mL/min regarding the 65 µm hydraulic micro–channel. The micro–channel heat sink was open to the atmosphere and therefore the outlet pressure is considered to be 1 bar.

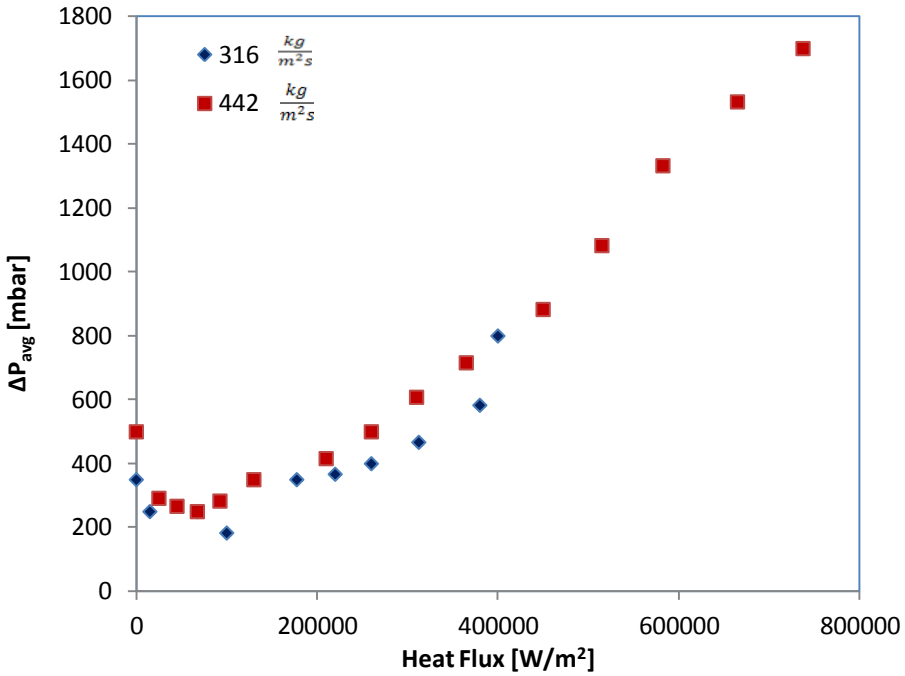

Figure 2.12 – Experimental Data: L = 2 cm, w_{TOP} = 137 µm, w_{BOTTOM} = 62 µm, z = 53 µm, D_h = 65 µm, T_{IN} = 30^{0}C, P_{OUT} = 1 bar, $\dot{Q}$ = 0.1 mL/min & 0.14 mL/min [Adapted From: Bhide et al. – 2009]

The single micro–channel experienced fluid flow rates of 0.1 to 0.6 mL/min and had power supplied that was in the range of 0 to 7 W [0 – 112 W/cm^2]. The maximum inlet subcooling temperature in these experiments is 30^{0}C. The trapezodial shaped channel was 2 cm in length and had deionized water pumped through a peristaltic pump [Masterflex Easy–flow II EW–77200–50]. The heat flux is calculated

based on the heated perimeter of the micro–channel multiplied by its respected length. It is important to state that the heat flux illustrated in Figure 2.12 has been corrected for the appropriate power supply and resistance losses.

Figure 2.13 outlines the heat transfer coefficient measurements completed by Bhide et al., 2009 for the 65 µm hydraulic diameter trapezoidal micro–channel for the corresponding mass flux of 448 kg/m^2 s. The heat transfer coefficient values were measured from the 1.65 cm location of the 2 cm in length single micro–channel at heat fluxes greater than 75 W/cm^2. Figure 2.13 outlines the decreasing trend of the heat transfer coefficient values ranging from 80 000 to 60 000 W/m^2 K over vapour qualities of 0.10 to 0.46 [Bhide et al. – 2009].

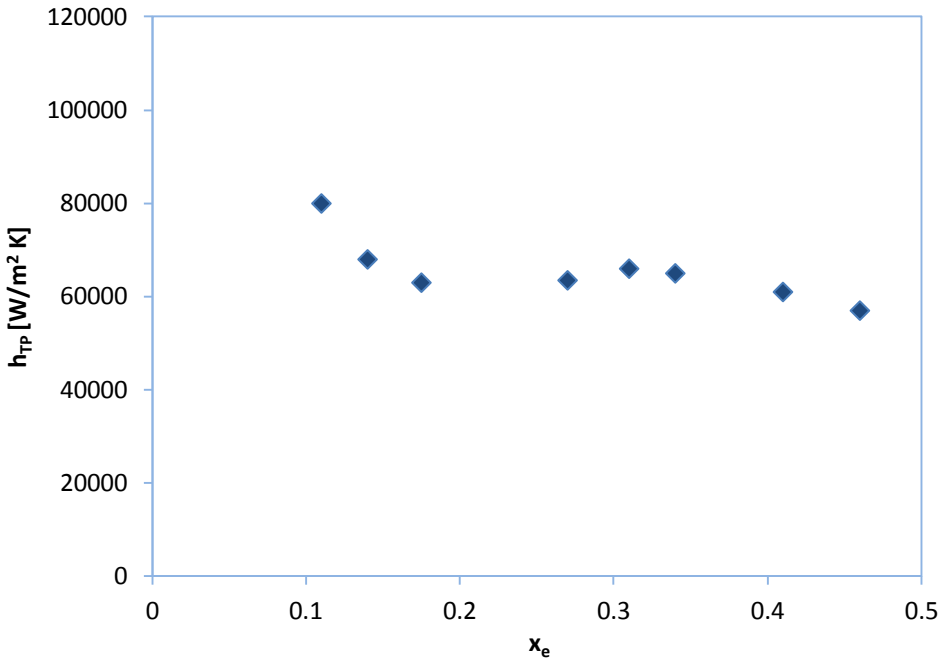

Figure 2.13 – Experimental Data: L = 2 cm, w_{TOP} = 137 µm, w_{BOTTOM} = 62 µm, z = 53 µm, D_h = 65 µm, T_{IN} = 30^{0}C, P_{OUT} = 1 bar, $\dot{Q}$ = 0.1424 mL/min [Adapted From: Bhide et al. – 2009]

2.6 – 3 Experimental Data of Qu and Mudawar – 2003

The experimental data from Qu and Mudawar, 2003 is provided in Figure 2.14. The operating conditions employed the use of water as the working fluid at an inlet temperature of 60^0C and outlet pressure of 1.17 bar. The dimensions of the single channel in the experiment by Qu and Mudawar, 2003 include a width of 231 µm a depth of 713 µm and a length of 4.48 cm. The hydraulic diameter is calcluated to be 349 µm and the mass flux employed had been 255 kg/m^2 s.

The single copper micro–channel had inserted four type K thermocouples along the centre plane to measure the temperature distribution. It is noted that after the test module had been assembled multiple layers of ceramic fibre were wrapped around the heat sink to reduce heat loss to the environment. It is important to state that the throttling value situated upstream of the test module maintained an exit pump pressure that had been elevated to 2.0 bars to prevent flow oscillations [Qu and Mudawar – 2003].

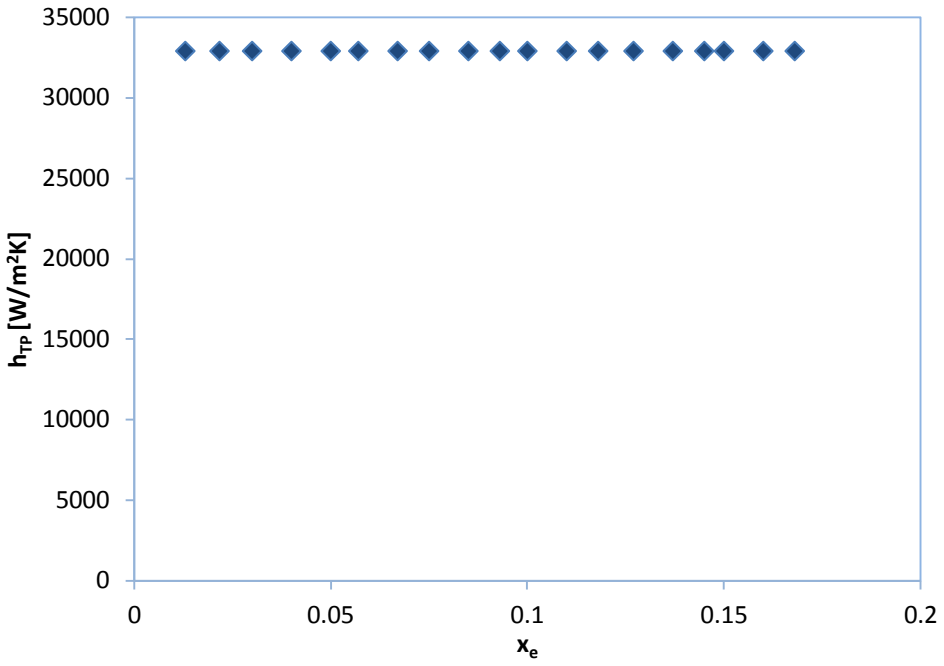

Figure 2.14 – Experimental Data: L = 4.48 cm, w = 231 µm, d = 713 µm, D_h = 349 µm, T_{IN} = 60^0C, P_{OUT} = 1.17 bar, $\dot{Q}$ = 2.56 mL/min [Adapted From: Qu and Mudawar – 2003]

2.6 – 4 Experimental Data of Galvis and Culham – 2012

The independent experiment conducted in the paper by Galvis and Culham, 2012 outlines additional details concerning the set up and operating conditions completed. The channel dimensions include a depth of 378 µm, width of 471 µm, a length of 2.19 cm that corresponds to an estimated hydraulic diameter of 419 µm. Mass fluxes of 364 kg/m^2 s and 730 kg/m^2 s for water were utilized during the experiment with an inlet temperature of 50^{0}C and outlet pressure of 1 bar. Figure 2.15 illustrates the experimental data for the heat transfer coefficient compared to the respected exit vapour quality for two different mass fluxes.

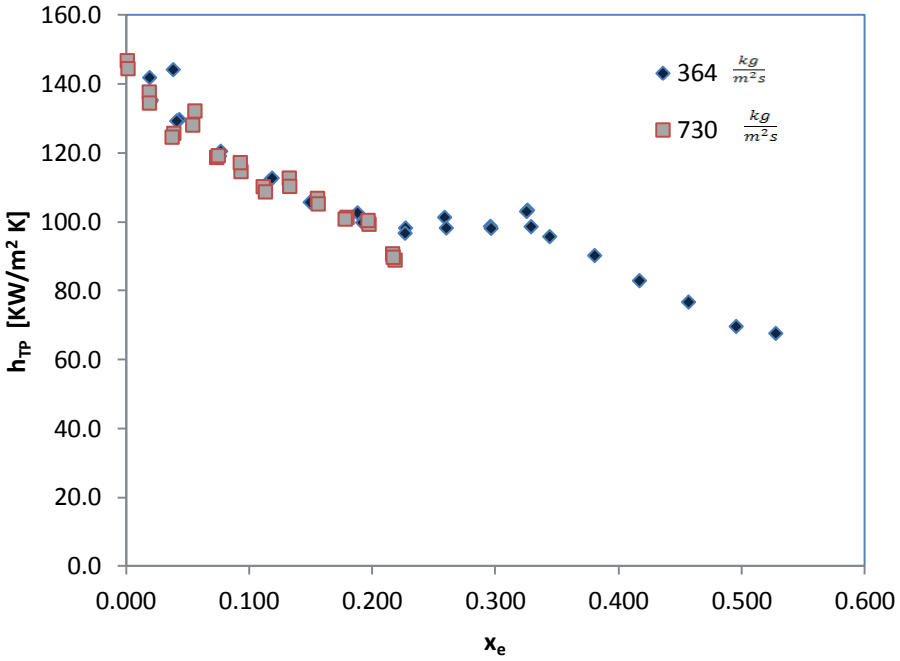

Figure 2.15 – Experimental Data: L = 2.19 cm, w = 471 µm, d = 378 µm, D_h = 4.19 µm, T_{IN} = 50^{0}C, P_{OUT} = 1 bar, $\dot{Q}$ = 4 & 8 mL/min [Adapted From: Galvis and Culham – 2012]

Ultra pure water was used as the working fluid with the flow rates to the test section provided by the display of the syringe pump and also from a Flo – sensor model. The micro–channel was cleaned with a test liquid and also through the incorporation of a high efficiency inline filter of a 25 micro rating to enable the removal of foreign particles [Galvis and Culham – 2012].

The test unit included an interchangeable micro–evaporator, heater block, cartridge heater, thermal insulation and top cover plate with sight glass window which enabled flow pattern visualization. The micro–evaporator was machined from a 44 x 10 x 13 mm block of oxygen free copper which consisted of a single straight channel with a square cross–sectional profile to negate the non–uniform flow distribution observed with multiple micro–evaporator channels.

The micro–evaporator was heated along its lower boundary through a 400 watt cartridge heater which was embedded in the oxygen free copper heater block. The heat flow provided to the channel was supplied until steady state conditions or the maximum temperature of 180^0C was reached [Galvis and Culham – 2012]. The heater block practically provided uniform heat input along the length of the channel. Heat was conducted from the heater along the heater block to the micro–evaporator where it was transferred to the fluid. The single channel evaporator and the heater block were completely enclosed in insulation to minimize heat loss to surroundings [Galvis and Culham – 2012].

An external reference junction was used to account for accurate temperature readings. Thermocouples were also embedded in the evaporator and heater block along the mid plane to determine the temperature gradient for the surface at five locations along the length of the channel. The aforementioned devices enabled the measurement of local fluid temperature, wall temperature and pressure drop along the length of the channel. A circulating bath was maintained at 24^0C at the outlet before having the fluid returned to the reservoir at atmospheric pressure.

2.7 Chapter 2 – Summary

In summary much research remains to be done to better understand two–phase flow boiling in mini and micro–channels. The literature has covered many areas that include fabrication measures, geometries, single phase flow, two–phase flow, two–phase flow patterns, employed assumptions, and heat transfer characteristics. There is an expressed need for a model that can facilitate the many different flow patterns experienced over the length of a channel for various operating conditions in the two–phase region to predict pressure drop, heat transfer coefficients as well as other parameters.

Two–phase micro–channel heat sinks offer additional attributes compared to their single–phase counterparts that include higher convective heat transfer coefficients, better temperature uniformity, and smaller coolant flow rates, however the disadvantage of a greater pressure drop are noted. Review of the literature demonstrate that the continuum model of conventional mass, momentum and energy equations are of adequate accuracy in representing the micro–channel flow and heat transfer characteristics for single phase flow and should be of reasonable accuracy for two–phase flow conditions.

The flow patterns of macro–channels that include bubbly, slug, churn, wavy annular and annular flow have been identified in micro–channels. Conventional relationships used for macro–channels are considered to be of reasonable accuracy for micro–channels. The homogeneous and annular flow model approaches are well documented in the literature where it is stated that fluid properties should be corrected for temperature variations along the length of the channel. In conclusion few models based on flow regimes have been published in the literature where it is expected that such effort would apply to boarder experimental conditions with greater accuracy. Models would need to be validated against larger data sets to demonstrate effective results for predicting various parameters under different operating conditions. Four independent experimental data sets from the literature that outline results for pressure drop and heat transfer coefficients for various operating conditions were presented and are to be compared to model results in Chapter 4.

CHAPTER 3
MODEL DEVELOPMENT

3.1 Background

In the development of the following model there are important notes to be brought forth to outline the design methodology. It is the intent of the work to construct a simple yet useful model to surpass some of the challenges encountered in the micro–channel research literature. Although the prediction of flow boiling in micro–channels is complicated by the simultaneous existence of single phase flow, sub–cooled flow boiling and saturated flow boiling that is noted to occur [Zhang and Pinjala – 2005]. This section will provide an overview of the principles and the structure employed in the model to estimate the two–phase flow behavior through the homogeneous, annular and weighted annular–homogeneous approaches. In spite of the progress thus far in micro–channel research, certain fundamental problems in flow and heat transfer are still unclear [Yarin et al. – 2009]. From the accumulation of literature there are a number of models that fit specific experimental data or correlations but lack less of a general capability to address larger data sets.

There are numerous aspects to consider for micro–channel research including the choice of best heat transfer fluid, surface roughness effects, channel geometry, aspect ratio effects, fin effects for conduction of the heat, local hot spot cooling, transient effects of start–up imposed heat flux, and avoidance of a damaging temperature [Thome – 2007]. Good agreement between the exact and approximate methods used in the literature illustrate that with carefully chosen assumptions, results can lead to adequate descriptions of the thermal performance [Liu and Garimella – 2003]. Such assumptions will enable the modification of various micro–channel geometries for the purposes of performance optimization [Liu and Garimella – 2003].

A general micro–channel heat sink containing several channels is illustrated in Figure 3.1 to demonstrate the conceptual application for the model. The micro–channel heat sink dimensions for the length, width and height are illustrated in Figure 3.1.

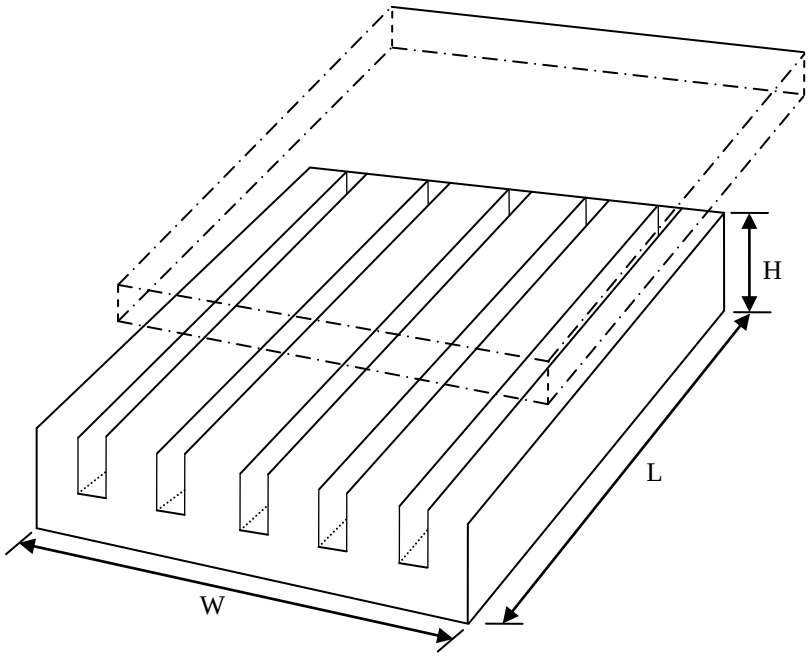

Figure 3.1 – Schematic of Multi–Micro–Channel Heat Sink [Adapted From: Jang and Kim – 2003]

The model is intended to be applied over dimensions ranging from a couple of micrometers to a few millimeters. When developed on sound fundamentals it is expected that the model can be further expanded when needed for future work. In the process of developing a model literature as well as mathematical resources from a range of applications such as pressure relief values was consulted. It is important to note that modeling challenges regarding two–phase flow have been investigated in the chemical processing and nuclear industries. The model will incorporate both single and two–phase flow calculations along the length of the channel to provide a more representative approach to the expected operating environment.

3.2 Model – [Assumptions and Logic]

Figure 3.2 illustrates a single channel with the necessary elements to begin developing equations for the fluid dynamics and heat transfer characteristics of an expected operating environment. Assumptions and logic pertaining to each the single and two–phase flow regime will be developed. References to past researchers that have employed similar model assumptions will be provided. Figure 3.2 illustrates the dimensions of the channel that includes the width [w], height [H], length [L] as well as heat supplied to the channel identified as [q].

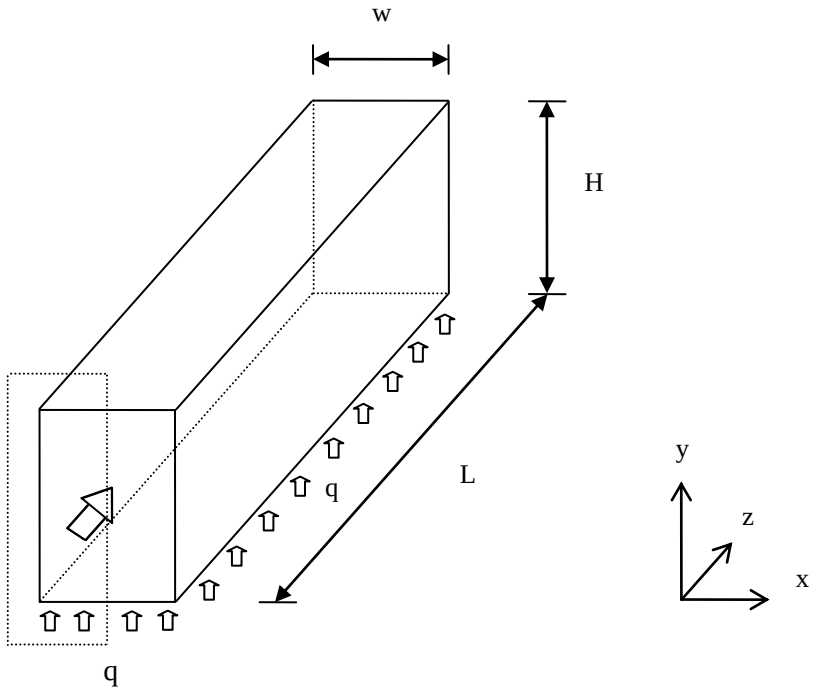

Figure 3.2 – Schematic of a Single Micro–Channel [Adapted From: Patterson et al. – 2004]

3.2 – 1 Single Phase Flow Model Assumptions

To cover some of the single phase assumptions it is noteworthy to mention that this particular area is well researched and better understood then the subsequent two–phase region.

Assumption 1: The physical characteristics for a single channel will be evaluated. One–dimensional analysis will be deemed of sufficient accuracy to capture the appropriate physical phenomena. One–dimensional representation of the conservation equations have been employed in the works of Kelkar et al., 2005, Koo et al., 2002, Qu and Mudawar, 2002, Phillips, 1988 and Sarangi et al., 2009.

Assumption 2: The referred to conventional or classical relationships for fluid flow and heat transfer will be considered of sufficient accuracy for the micro–channel model. The thermodynamic properties of water such as thermal conductivity and viscosity accounting for variation with temperature are included through curve–fitting data over the temperature range of 0.01 to 200 ^{0}C.

The polynomial correlations obtained from the curve–fitting exercise are used to capture the boiling front and complete necessary calculations involved over different temperature operating conditions over the length for the micro–channel. Similar modeling approaches have accounted for the strong temperature and pressure dependent properties of water where the under–relaxation methods have been employed for convergence of numerical solutions [Koo et al. – 2002]. This assumption is also supported in the modeling work by Sarangi et al., 2009.

Assumption 3: The channel will be evaluated under adiabatic conditions and the base temperature will be considered uniform along the length of the channel. The high conductivity of the micro–channel material enables the assumption to be valid. The use of uniform heating conditions has been implemented by past researchers that included papers from Prasher et al., 2005 and Patterson et al., 2004.

Assumption 4: The liquid coolant flow will be considered to be incompressible as well as to operate under steady laminar flow conditions. The flow of the coolant is usually laminar due to the small hydraulic diameters of the micro–channels [Radmehr and Patankar – 2004]. A similar assumption was

incorporated by Phillips, 1988 with the justification that the coolants were incompressible since pressure drop across the channel would be limited to a few atmospheres.

The low water velocities within the micro–channels enable further support for the steady state laminar condition [Chang et al. – 2005]. Therefore the velocity and mass flow rates of the fluid utilized are considered constant over the length of the micro–channel. The fluid conditions in the micro–channel are considered to operate under fully developed hydrodynamic flow [Singhal et al. – 2003].

Assumption 5: The heat flux is assumed to vary only in the axial or z–direction along the channel. This assumption is supported by Koo et al., 2002 and Sarangi et al., 2009 where the heat flux is assumed to vary only in the z–direction with fluid flow.

3.2 – 2 Single Phase Flow Model – Pressure Drop

The single phase pressure drop equation can be completed from the following Bernoulli Equation [3.1]. Negating the effects of kinetic energy [$\Delta u^2/2$], potential energy [$g\Delta z$] as well as shaft work [$\dot{W}_s$], due to constant flow velocity, no shaft and very little impact of gravity forces. Friction losses are represented by $\hat{F}$, which accounts for minor and major friction losses in the system enabling the pressure drop to be expressed as that of Equation [3.2].

$$\frac{\Delta p}{\rho_L} + \frac{\Delta u^2}{2} + g\Delta z + \hat{F} = \frac{-\dot{W}_s}{\dot{m}} \qquad [3.1]$$

$$\Delta p_{SP} = \rho_L \left[f_{SP} \frac{z_L}{D_h} \frac{u^2}{2} + \frac{Ku^2}{2} \right] \qquad [3.2]$$

The loss coefficient can be approximated through expansion and contraction terms in the single phase region that are expected to occur in the micro–channel environment. The value of 1 for the friction loss coefficient [K] corresponds to an estimation to include the condition of sudden contraction and expansion that are expected to occur for fluid flow in and out of a channel. More precise equations to determine friction loss coefficients are available in Phillips, 1988 and Geankoplis, 1993. However, it is noted that the pressure drop for the inlet and outlet manifolds are estimated to be less than 0.06% of the total measured pressure drop and are thus not usually included [Harirchian and Garimella – 2012].

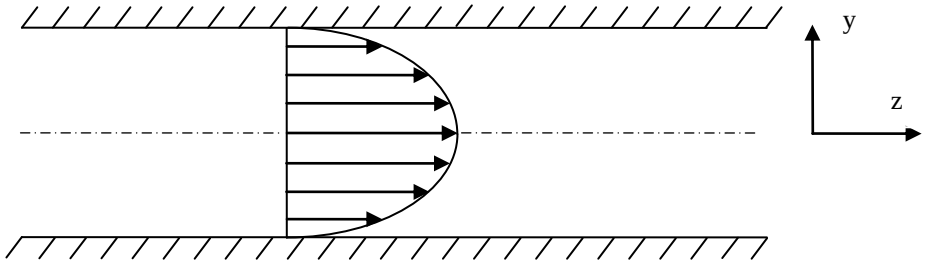

Figure 3.3 – Illustration of Velocity Profile for Laminar Flow in a Pipe [Adapted From: Geankoplis – 1993]

Figure 3.3 illustrates the fully developed flow condition as the flow is not modified by entrance effects and that the velocity profile does not change along the axis of flow which in this case is the z–direction [Geankoplis – 1993]. This condition enables losses to be represented by the Darcy or Moody friction factor described in the Equation [3.3] for the conditions of laminar flow [Geankoplis – 1993]. Since the length of the micro–channel is small the fully developed flow condition assumption neglects the entrance effects for the operating environment.

$$f = \frac{64}{\mathrm{Re}} \qquad [3.3]$$

Reynolds number [Re] is defined as the dimensionless relation that illustrates the transition observed for flow in pipes, tubes or channels to be a function of velocity, density, viscosity of the fluid as well as diameter.

$$\mathrm{Re} = \frac{D_h u \rho_L}{\mu_L} \qquad [3.4]$$

Hydraulic diameter is implemented as the ratio of the cross–sectional area of the channel to that of the wetted perimeter. However for non–circular channels, Equation [3.5] is incorporated to represent an equivalent diameter for the model approach developed. Equation [3.5] is defined as four times the cross–sectional area for flow divided by the total wetted perimeter [Ashrae – 2007]. This hydraulic diameter relationship will be viewed to be of sufficient accuracy for the smaller dimensions encountered regarding micro–channels which will enable flexibility to be applied to non–circular geometries.

$$D_h = \frac{4A_{CH}}{P_{CH}} \qquad [3.5]$$

3.2 – 3 Single Phase Flow Model – Heat Transfer

Conducting a heat balance on the single channel illustrated in Figure 3.2 can provide the temperature profile along the length of the channel for the single phase. Further details concerning the completed heat balance for the single phase region through a circular channel is outlined in Collier and Thome, 1994.

The following expressions below can be illustrated through the consideration of Equation [3.5] that will provide an equivalent diameter for the rectangular channel. Additionally if the rectangular channel is viewed as a circular channel where the area of the channel is calculated through the represented equivalent diameter then the heat balance can be expressed as Equation [3.6].

$$q''\pi D_h z = \dot{m} C_P \left[T_L(z) - T_{IN} \right] \qquad [3.6]$$

$$\frac{q}{\pi D_h L} \bullet \pi D_h z = \dot{m} C_P T_L(z) - \dot{m} C_P T_{IN} \qquad [3.7]$$

$$T_L(z) = T_{IN} + \frac{qz}{\dot{m} C_P L} \qquad [3.8]$$

Equation [3.8] can be utilized in calculating the boiling front which outlines the location along the length of the channel where flow boiling is expected to start. The intersection between the single phase and the two–phase temperature profile to identify the corresponding boiling front is illustrated in the paper by Sarangi et al., 2009. The approach is viewed to be an effective method that will be elaborated on in later sections.

3.2 – 4 Homogeneous Flow Model – Pressure Drop

Two–phase applications typically require knowledge of their single phase characteristics to develop expressions that could be applicable to different flow regimes which generally occur after the onset of boiling [Webb – 2003]. The incorporation of the homogeneous flow model does not confine the approach to a particular assumption regarding flow pattern and thus views both liquid as well as vapour more as a mixture that seems representatively justified since in chemistry books gas is defined as a fluid substance. The model is expected to be valid for the bubbly and wispy annular flow patterns particularly at high linear velocities and pressures [Collier and Thome – 1994]. However the model has often been applied indiscriminately to problems in which other flow patterns would be expected [Collier and Thome – 1994].

The homogeneous approach encountered challenging perspectives of not being applicable to higher surface tension fluids such as water from the work of Qu and Mudawar in 2002. Initial support had been provided to the homogeneous model, for low surface tension property fluids such as methanol, isobutane, and fluoro–chemical refrigerants [Kelkar et al. – 2005]. The work of Sarangi et al., 2009 had illustrated that the homogeneous model would be effective for higher surface tension fluids such as water. To handle the various phases that are observed in the flow boiling phase that include onset of nucleate boiling, bubbly, slug, churn as well as annular flow patterns the homogeneous and annular flow models will be brought together through a weighted approach.

The weighted model approach to calculate the pressure drop for the homogeneous and annular flow procedures is incorporated after the critical length of the single phase flow region is identified which outlines the start of two–phase flow region. The weighted approach method is seen to be an extension of the homogeneous and annular flow regime assumptions to enable a more complete flow model to account for the large changes in flow characteristics over the length of the micro–channel. The procedure for the analysis of a single micro–channel constitutes the infrastructure for determining the practical performance of micro–channel heat sinks involving multiple micro–channels [Kelkar et al. – 2005].

In addition to the initial arguments provided for the single phase flow assumptions, the first three statements provided are inherent to the homogeneous model.

Assumption 1: Both the liquid and vapour components will have equal velocities. [Collier and Thome – 1994].

Assumption 2: There will be the attainment of thermodynamic equilibrium between the phases [Collier and Thome – 1994].

Assumption 3: The homogeneous flow will have a suitable defined single phase friction factor for two–phase flow [Collier and Thome – 1994].

Assumption 4: Negligible effects of gravity, subcooled boiling and surface tension as well as other body forces will be incorporated [Sarangi et al. – 2009].

The homogeneous model is developed from the three governing equations that include the conservation of mass [continuity equation], conservation of momentum [momentum equation], and conservation of energy [energy equation]. The complete development of the conservation equations are thoroughly provided in Convective Boiling and Condensation – 3rd Edition by Collier and Thome 1994, however some of the important features will be illustrated in the following section. The mass conservation equation is outlined in Equation [3.9] to represent the assumption that the mass flow rate is considered steady. The homogeneous density term is determined for the liquid and gas components with consideration to the vapour quality.

$$\frac{\partial m}{\partial t} = \rho_H u_H A \qquad [3.9]$$

The conservation of momentum also referred to as a force balance illustrates that the rate of change of momentum for a mass is proportional to the net force acting on it. [Rate of accumulation of momentum inside the control volume] + [Rate of momentum out of the control volume] – [Rate of momentum into the control volume] = [Sum of forces on the mass inside the control volume].

Equation [3.10] summarizes the rate of accumulation [where δz represents a small distance apart] plus the rate of inflow of phase k momentum directed along the axis which simplifies to expression [3.11] as outlined in Collier and Thome, 1994. The mass flow rate can be expressed as Equation [3.12] which could be utilized to bring about other forms of representation where the mass flow rate of phase k could be presented in terms of the area, void fraction, density and velocity of the fluid [Collier and Thome – 1994].

$$\frac{\partial(\dot{m}_k \delta z)}{\partial t} + \left[(\dot{m}_k u_k) + \delta z \frac{\partial}{\partial z}(\dot{m}_k u_k) \right] - \dot{m}_k u_k \qquad [3.10]$$

$$\frac{\partial(\dot{m}_k \delta z)}{\partial t} + \delta z \frac{\partial}{\partial z}(\dot{m}_k u_k) \qquad [3.11]$$

$$\dot{m}_k = A \alpha_k \rho_k u_k \qquad [3.12]$$

Incorporating the expression [3.12] for mass flow rate, an overview of the sum of forces in the axial direction along with the momentum generation term associated with mass transfer is performed on the control element produces Equation [3.13] as illustrated in Collier and Thome, 1994.

$$\begin{aligned} &\left[A\alpha_k p - \left(A\alpha_k p + \delta z \frac{\partial}{\partial z}(A\alpha_k p) \right) - \left(p\left(-\delta z \frac{\partial}{\partial z}(A\alpha_k) \right) \right) \right] \\ &- A\alpha_k \rho_k \delta z g \sin\theta - \tau_{kW} P_{kW} \delta z + \sum_1^n \tau_{knz} P_{kn} \delta z + u_k \Gamma_k \end{aligned} \qquad [3.13]$$

The entire first square bracket term in Equation [3.13] represents the pressure forces experienced on the fluid element. The second term is allocated for gravitational forces and the third term [τ_{kW}] illustrates the wall shear stress between the phase k and the channel wall while P_{kW} outlines the contact perimeter between the wall and phase k [Collier and Thome – 1994]. The term [τ_{knz}] represents the interfacial shear stress between phase k, as well as n. P_{kn} is defined as the contact perimeter between phase k and n. The final term includes the rate of generation of momentum associated with phase k due to mass transfer under the assumption that the mass transferred across the interface is accelerated to

the mean velocity of the receiving phase [Collier and Thome – 1994]. It is important to note that either P_{kW} or P_{kn} could be zero depending on the disposition of the phases [Collier and Thome – 1994].

Bringing the sum of forces together with the rate of creation of momentum for that phase provides the following Equation [3.14] as outlined in Collier and Thome, 1994.

$$\begin{aligned}&\frac{\partial p}{\partial z}\left(-A\alpha_k\right)\delta z - A\alpha_k\rho_k\delta z g\sin\theta - \tau_{kW}P_{kW}\delta z + \sum_1^n \tau_{knz}P_{kn}\delta z + u_k\Gamma_k \\ &= \frac{\partial\left(\dot{m}_k\delta z\right)}{\partial t} + \delta z\frac{\partial}{\partial z}\left(\dot{m}_k u_k\right)\end{aligned} \qquad [3.14]$$

To illustrate a steady–state two–phase liquid [L]/gas [G] flow condition for a channel of constant area provides the following Equations [3.15] and [3.16].

$$-A_L\partial p - \tau_{LW}P_{LW}dz + \Sigma\tau_{LG}P_{LG}dz - A_L\rho_L dz g\sin\theta + u_L\Gamma_L = \dot{m}_L du_L \qquad [3.15]$$

$$-A_G\partial p - \tau_{GW}P_{GW}dz + \Sigma\tau_{GL}P_{GL}dz - A_G\rho_G dz g\sin\theta + u_G\Gamma_G = \dot{m}_G du_G \qquad [3.16]$$

$$\tau_{LG}P_{LG}dz + u_L\Gamma_L = \tau_{GL}P_{GL}dz + u_G\Gamma_G \qquad [3.17]$$

The conservation of momentum across the interface is represented in Equation [3.17]. Equation [3.15] and [3.16] can be added together while accounting for Equation [3.17] to provide expression [3.18]. The equations above represent the basic differential momentum equation for the simplified one–dimensional homogeneous approach [Collier and Thome – 1994]. The interfacial shear terms [τ_{knz}] and momentum exchange for mass transfer [Γ] sum to zero and are thus not included in the expression [3.18] as outlined in Collier and Thome, 1994.

$$\begin{aligned}&-\left(A_L + A_G\right)\partial p - \tau_{LW}P_{LW}dz - \tau_{GW}P_{GW}dz - g\sin\theta\left[A_L\rho_L + A_G\rho_G\right] \\ &= d\left(\dot{m}_L u_L + \dot{m}_G u_G\right)\end{aligned} \qquad [3.18]$$

Further understanding of the representation in Equation [3.18] would enable the net frictional force corresponding to each phase to be expressed in the following terms.

$$\left(\partial F_G + S\right) = -\tau_{GW} P_{GW} dz - \tau_{GL} P_{GL} dz = -A_G \left(\frac{dp}{dz} F_G\right) dz \qquad [3.19]$$

$$\left(\partial F_L - S\right) = -\tau_{LW} P_{LW} dz + \tau_{GL} P_{GL} dz = -A_L \left(\frac{dp}{dz} F_L\right) dz \qquad [3.20]$$

$$\left(\partial F_L + \partial F_G\right) = -\tau_{LW} P_{LW} dz - \tau_{GW} P_{GW} dz = -A \left(\frac{dp}{dz} F\right) dz \qquad [3.21]$$

Putting expressions [3.19] to [3.21] into Equation [3.18] and through rearrangement can produce the abbreviation of the momentum equation provided in Equation [3.22] as outlined in Collier and Thome, 1994.

$$\left(\frac{dp}{dz}\right) = \left(\frac{dp}{dz} F\right) + \left(\frac{dp}{dz} a\right) + \left(\frac{dp}{dz} z\right) \qquad [3.22]$$

Equation [3.22] outlines the pressure drop in terms of contributions due to friction, acceleration and gravity. Further derivations of the corresponding elements are provided below from Collier and Thome, 1994. Equation [3.23] outlines the total wall shear force and expression [3.24] provides the wall shear stress acting over the inside area of the channel with friction factor term f_{TP} [Collier and Thome – 1994].

$$F_W = \tau_W P_{CH} dz \qquad [3.23]$$

$$\tau_W = f_{TP} \left(\frac{\rho_H u_H{}^2}{2}\right) \qquad [3.24]$$

$$-\left(\frac{dp}{dz} F\right) = \frac{1}{A} \frac{dF_W}{dz} = \frac{\tau_W P_{CH}}{A} = \frac{f_{TP} P_{CH}}{A} \left(\frac{\rho_H u_H{}^2}{2}\right) \qquad [3.25]$$

$$-\left(\frac{dp}{dz}F\right)=\frac{2f_{TP}G^2v_H}{D_h} \qquad [3.26]$$

The term P_{CH}/A_{CH} = $4/D_h$, for a circular tube in expression [3.25] to Equation [3.26] is the final representation of the frictional pressure drop where. The acceleration pressure drop contribution is outlined in Equation [3.27] and the effects of compressibility are illustrated in Equation [3.28]. In the model developed the effects of compressibility will not be included for the vapour component since the operating conditions remain within relatively low pressure.

$$-\left(\frac{dp}{dz}a\right)=G\frac{d(u_H)}{dz}=G^2\frac{d(v_H)}{dz} \qquad [3.27]$$

$$\frac{d(v_H)}{dz}=v_{LG}\frac{dx_v}{dz}+x_v\frac{dv_G}{dp}\left(\frac{dp}{dz}\right) \qquad [3.28]$$

The gravitational pressure drop term contribution is outlined in Equation [3.29] which will not be included since the flow applications to be investigated are horizontal in nature.

$$-\left(\frac{dp}{dz}z\right)=\rho_H g\sin\theta=\frac{g\sin\theta}{v_H} \qquad [3.29]$$

Combining the expressions [3.26], [3.28] and [3.29] the total pressure drop for the homogeneous model can be represented as that of Equation [3.30] as provided in Collier and Thome, 1994. Further simplification enables the homogeneous model to be expressed as that of Equation [3.31].

$$-\frac{dp}{dz}=\frac{\dfrac{2f_{TP}G^2v_L\left[1+x_v\dfrac{v_{LG}}{v_L}\right]}{D_h}+G^2v_L\left[\dfrac{v_{LG}}{v_L}\right]\dfrac{dx_v}{dz}+\dfrac{g\sin\theta}{v_L+x_vv_{LG}}}{1+G^2x_v\dfrac{dv_G}{dp}} \qquad [3.30]$$

$$-\frac{dp}{dz} = \frac{2 f_{TP} G^2 v_L \left[1 + x_v \frac{v_{LG}}{v_L}\right]}{D_h} + G^2 v_L \left[\frac{v_{LG}}{v_L}\right] \frac{dx_v}{dz} \qquad [3.31]$$

Introducing the change in vapour quality in the z–direction [axial direction] and integrating Equation [3.31] the final expression for pressure drop regarding the homogeneous flow model is outlined in Equation [3.32].

$$\Delta P = -\left[\frac{2 f_{TP} G^2}{D_h}\left(v_L + qz \frac{v_{LG}}{AG^2 h_{LG}}\right) + G^2 v_{LG} \frac{q}{AG^2 h_{LG}}\right] z \qquad [3.32]$$

The homogeneous model simplifies the two–phase flow to a single phase expression using averaged fluid properties. However, under such assumptions it is not able to take into account the very detailed interaction between the vapour and liquid [Sarangi et al. – 2009]. The two–phase friction factor incorporated into the homogeneous model can be estimated between the values of 0.0029 and 0.005 which have been provided from experimental data of steam [Collier and Thome – 1994].

$$f_{TP} = 0.0029 - 0.005 \qquad [3.33]$$

The density of the homogeneous model is calculated with consideration to the vapour quality [x_v] as expressed in the Equation [3.34]. Moreover the Cicchitti et al. relation for viscosity of the fluid mixture is expressed as follows from Hewitt and Taylor, 1970 in Equation [3.35].

$$\frac{1}{\rho_H} = \frac{x_v}{\rho_G} + \frac{\left[1 - x_v\right]}{\rho_L} \qquad [3.34]$$

$$\mu_H = x_v \mu_G + \left[1 - x_v\right] \mu_L \qquad [3.35]$$

Although, Equation [3.35] has not been incorporated into the development of this particular model, it was deemed important to include in this section as other forms of the homogeneous approach implement the relationship for calculations concerning the two–phase friction factor.

3.2 – 5 Homogeneous Flow Model – Heat Transfer

The heat transfer relationship for the two–phase flow region is outlined in the following section. In the paper by Sarangi et al., 2009 the Clausius–Clapeyron expression illustrated in Equation [3.36] was utilized to determine the temperature distribution along the channel. The Antoine Equation outlined in expression [3.37] could also be incorporated to calculate the pressure and temperature profile for fluids over a specified operating range. It is noted in the case of water that constants are provided for the Antoine Equation regarding temperatures ranging from 0^0C to 60 ^{0}C and 60^0C to 150 ^{0}C. The Antoine constants to be applied for the temperature range of 60^0C to 150 ^{0}C regarding Equation [3.37] include an A1 value of 7.96681, B as 1668.210 and C as 228. The aforementioned constant values are employed since the single channel does not remain below 60^0C for long periods. There is a small difference noted in the calculated saturation values below 60^0C with the Antoine constants employed for the temperature range of 60^0C to 150 ^{0}C instead of 0^0C to 60 ^{0}C. Equation [3.37] can be rearranged to determine the temperature of the fluid provided the corresponding saturation pressure is known.

$$\ln p_{Sat} = -\frac{h_{LG}}{RT} + E \qquad [3.36]$$

$$\log_{10} p_{Sat} = A1 - \frac{B}{T + C} \qquad [3.37]$$

Equation [3.38] illustrates the Kandlikar heat transfer coefficient correlation that has been incorporated for the flow boiling region. The Kandlikar expression has been correlated over a vast amount of experimental data and demonstrated good general prediction corresponding to results within a 20% error interval [Kandlikar – 1990].

$$h_{conv} = h_L \left(C_1 C_o{}^{C_2} \left(25 Fr_{lo} \right)^{C_5} + C_3 Bo^{C_4} F_{fl} \right) \qquad [3.38]$$

The Kandlikar correlation provides constants for both the convective and nucleate boiling region as outlined in Table 3.2. The constant C_5 = 0 for vertical tubes and horizontal tubes with Froude number [Fr_{lo}] > 0.04. Equation [3.38] has been employed in the homogeneous model to represent the heat transfer coefficient by Koo et al., 2002 and Sarangi et al., 2009 as well as a number of other researchers.

Table 3.1 – Constants for Correlation [Adapted From: Kandlikar – 1990]

Constant	Convective Region Co < 0.65	Nucleate Boiling Region Co > 0.65
C_1	1.1360	0.6683
C_2	- 0.9	- 0.2
C_3	667.2	1058.0
C_4	0.7	0.7
C_5	0.3	0.3

Expanding on the characteristics of the Kandlikar correlation presented in Equation [3.38], expression [3.39] is employed to evaluate the heat transfer coefficient for the single phase region. Equation [3.39] is utilized for the turbulent region of single phase flow and is deemed suitable since the mixture experienced in the two–phase region is estimated to be comparable [Kandlikar – 1990].

$$h_L = 0.023 \mathrm{Re}_L^{0.8} \mathrm{Pr}^{0.4} \left[\frac{k_L}{D_h} \right] \qquad [3.39]$$

$$\mathrm{Pr} = \frac{C_P u_L}{k_L} \qquad [3.40]$$

The Reynolds number described in Equation [3.4] and the Prandtl number represented in [3.40] provides correlation to the shear component of diffusivity for momentum $\left[\mu_l / \rho \right]$ to the diffusivity for heat $\left[k_l / \rho c_p \right]$ [Geankoplis – 1993]. These expressions physically relate the relative thickness of the hydrodynamic layer and the thermal boundary layer [Geankoplis – 1993].

The boiling number expression includes the heat flux based on the wetted perimeter of the micro–channel divided by the mass flux and latent heat of vaporization as outlined in Equation [3.41]. The Froude number [Fr_{lo}] outlined in Equation [3.42] considers the influence of inertia effects of flow of the fluid.

$$Bo = \frac{q''}{Gh_{LG}} \qquad [3.41]$$

$$Fr_{lo} = \frac{G^2}{gD_h\rho_L{}^2} \qquad [3.42]$$

Table 3.2 illustrates the various fluid dependent parameters that are incorporated into the Kandlikar heat transfer coefficient correlation. It is noted that for fluids not presented in Table 3.2 further details for calculating the fluid dependent parameter are available in the paper by Kandlikar, 1990.

Table 3.2 – Fluid Dependent Parameter F_{fl} in Kandlikar Correlation [Adapted From: Kandlikar – 1990]

Fluid	F_{fl}
Water	1.00
R–11	1.30
R–12	1.50
R–1381	1.31
R–22	2.20
R–113	1.30
R–114	1.24
R–152a	1.10
Nitrogen	4.70
Neon	3.50

The energy equations for the control volume for a single channel outlined in Figure 3.2 are presented to account for the fluid property variations experienced over the length of the channel. Equations [3.43] and [3.44] represent the change in the heat of the fluid over the length of the channel. Additionally the heat transfer coefficient for the two–phase region and fin efficiency are incorporated in Equation [3.43] to account for the energy exchanged between the channel wall and the fluid.

Equations [3.43] and [3.44] have been incorporated in the homogeneous models of Koo et al., 2002 and Sarangi et al., 2009. The first term in expression [3.45] accounts for heat conduction along the channel wall [Koo et al. – 2002]. The second term outlines the convection heat transfer rate, while the third component accounts for heat loss to the environment through the associated resistance. The radiation heat loss is also neglected in the homogeneous model developed which has been incorporated by Koo et al., 2002.

$$\dot{m}C_P T_{L|z} = \dot{m}C_P T_{L|z+\Delta z} + \eta h_{conv} P_{CH} \Delta z \left[T_W - T_L\right] \qquad [3.43]$$

$$\dot{m}\frac{\partial h_L}{\partial z} - \eta h_{conv} P_{CH}\left[T_W - T_L\right] = 0 \qquad [3.44]$$

$$\frac{\partial}{\partial z}\left[k_W A_W \frac{\partial T_W}{\partial z}\right] - \eta h_{conv} P_{CH}\left[T_W - T_L\right] - \frac{w\left[T_W - T_L\right]}{\left[\frac{1}{h_{conv} L\left[2\eta d + w\right]}\right]} + q'' w = 0 \qquad [3.45]$$

$$T_W = T_L + \frac{q}{h_{conv}\left[wL + 2dL\eta\right]} \qquad [3.46]$$

Equation [3.46] provides the relationship between the channel wall and fluid temperature over the length of the channel [Sarangi et al. – 2009].

3.2 – 6 Annular Flow Model – Pressure Drop

The annular flow model considers the vapour phase flowing through the center of the channel while the liquid flows as a thin film along the channel wall [Sarangi et al. – 2009]. The following annular flow approach is outlined in further detail in Sarangi et al., 2009, however it is important to note that the solution procedure has been modified which is outlined later in this chapter. The conservation of mass [continuity equation] can be described through the following terms outlined in Equation [3.47] to [3.49]. Equation [3.47] illustrates the liquid effluent fraction and Equation [3.48] outlines the corresponding vapor quality that sum to a total value of one as presented in expression [3.49].

$$e = \frac{\dot{m}_{LL}}{\dot{m}} \qquad [3.47]$$

$$x_v = \frac{\dot{m}_G}{\dot{m}} \qquad [3.48]$$

$$e + x_v = 1 \qquad [3.49]$$

Taking into account the mass transfer corresponding to evaporation regarding the heat supplied to the micro–channel can be outlined as Equation [3.50].

$$\Gamma_{LG} = \frac{q}{Lh_{LG}} \qquad [3.50]$$

The conservation of momentum is given in two parts that include the liquid film and the vapour core. The liquid film control volume is illustrated in Figure 3.4 as a rectangular shape in the stream wise direction. The inner boundary of the control volume stretches to the surface layer between the liquid film and the vapour core as well the outer boundary is located a distance y from the channel wall as illustrated in Sarangi et al., 2009.

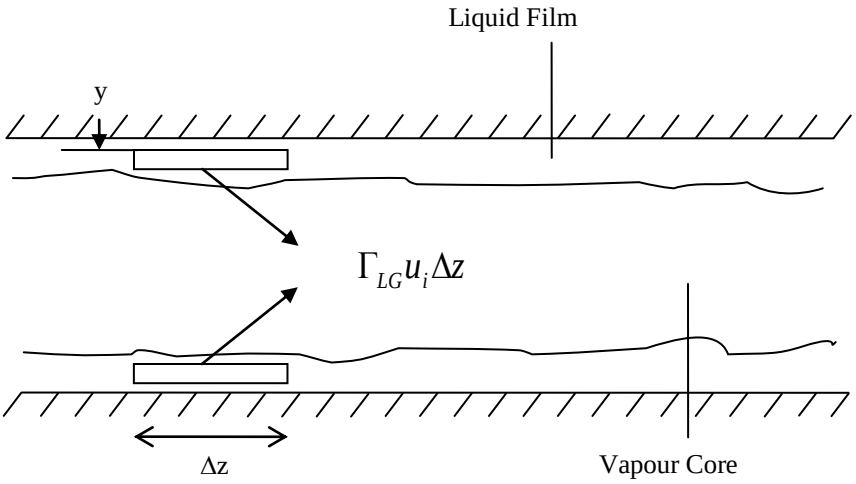

Figure 3.4 – Schematic of Momentum Interactions [Adapted From: Sarangi et al. – 2009]

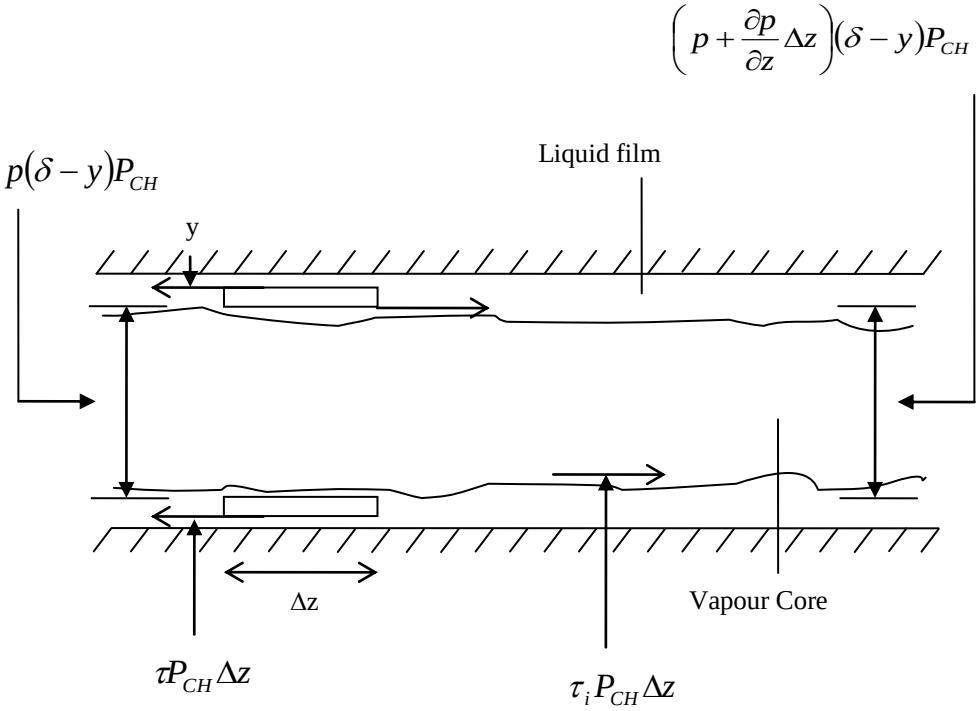

Figure 3.5 – Schematic of Control Volume of Forces Acting on Liquid Film [Adapted From: Sarangi et al. – 2009]

The momentum exchange along the liquid film interface where the net force balance illustrates the evaporation effect as outlined in Figure 3.4 [Sarangi et al. – 2009]. To simplify further development, the interfacial velocity u_i is set equal to twice the mean liquid velocity as seen in Equation [3.51] as employed in Qu and Mudawar, 2003 as well as Sarangi et al., 2009. Equation [3.52] outlines the liquid film velocity which is related to the film mass flow rate divided by the density of the fluid multiplied by the difference between the cross–sectional area of the channel and of the vapour core.

$$u_i = 2u_{LL} \qquad [3.51]$$

$$u_{LL} = \frac{\dot{m}_{LL}}{\rho_L\left[A_{CH} - A_C\right]} \qquad [3.52]$$

From Figure 3.5 the forces acting on the same control volume in the stream wise direction are illustrated. Assuming a small film thickness the sum of forces in the z–direction can expressed as that of Equation [3.53] as outlined in Sarangi et al., 2009.

$$p(\delta - y)P_{CH} - \left(p + \frac{\partial p}{\partial z}\Delta z\right)(\delta - y)P_{CH} - \tau P_{CH}\Delta z + \tau_i P_{CH}\Delta z \qquad [3.53]$$

The first and second terms in this Equation [3.53] are pressure forces, while the third and fourth terms are shear forces [Sarangi et al. – 2009]. Employing momentum conversation where the sum of all the forces acting on the control volume in the z–direction is equal to the net balance which provides Equation [3.54].

$$\tau = (\delta - y)\left(-\frac{\partial p}{\partial z}\right) + \tau_i - \frac{1}{P_{CH}}\Gamma_{LG}u_i \qquad [3.54]$$

$$\tau = \mu_L \frac{\partial u_{LL}}{\partial y} \qquad [3.55]$$

The shear stress in the laminar film is related to the local velocity gradient by Equation [3.54]. With the substitution of Equation [3.54] and [3.55] outlines the expression [3.56] as provided in Sarangi et al., 2009.

$$\frac{\partial u_{LL}}{\partial y} = \frac{1}{u_L}(\delta - y)\left(-\frac{\partial p}{\partial z}\right) + \frac{1}{u_L}\tau_i - \frac{1}{u_L P_{CH}}\Gamma_{LG} u_i \qquad [3.56]$$

The local velocity in the liquid film can be obtained by integrating Equation [3.56] through the no slip condition outlined as u_{LL}= 0 at y = 0 to obtain Equation [3.57] as illustrated in Sarangi et al., 2009.

$$u_{LL} = \frac{1}{u_L}\left(\delta y - \frac{y^2}{2}\right)\left(-\frac{\partial p}{\partial z}\right) + \frac{y}{u_L}\tau_i - \frac{y}{u_L P_{CH}}\Gamma_{LG} u_i \qquad [3.57]$$

Further integration of the velocity over the film thickness enables the determination of the liquid mass flow rate which is demonstrated in the expression [3.58] provided in Sarangi et al., 2009.

$$\dot{m}_{LL} = \rho_L P_{CH} \int_0^{\delta} u_{LL} \partial y \qquad [3.58]$$

Arrangement of Equation [3.57] and [3.58] produce the pressure drop expression for the annular flow regime in Equation [3.59].

$$\left(-\frac{\partial p}{\partial z}\right) = \frac{3\mu_L}{P_{CH}\rho_L\delta^3}\dot{m}_{LL} - \frac{3}{2\delta}\tau_i + \frac{3}{2\delta P_{CH}}\Gamma_{LG} u_i \qquad [3.59]$$

Figures 3.6 and 3.7 illustrate the control volume of length Δz for the vapour core and extending to the liquid film interface. The control volume outlined in Figure 3.6 for the net momentum is expressed as Equation [3.60]. The first two terms represent the momentum change due to core acceleration while the third term accounts for the interfacial evaporation [Sarangi et al. – 2009].

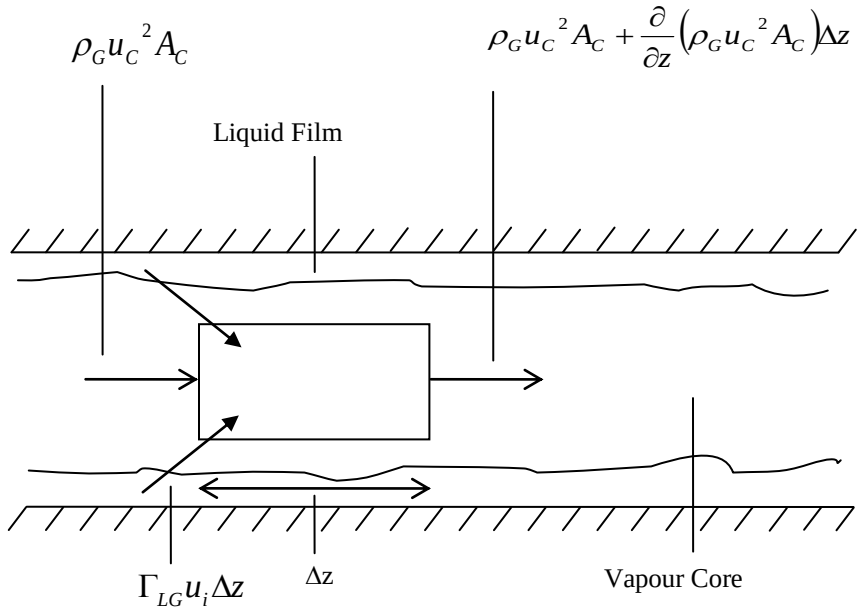

Figure 3.6 – Schematic of Control Volume of Momentum Interactions for Vapour Core [Adapted From: Sarangi et al. – 2009]

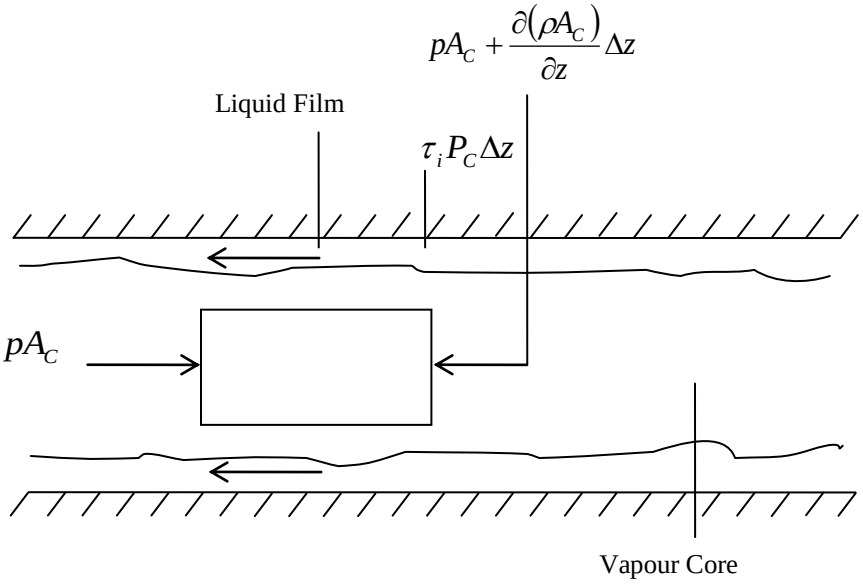

Figure 3.7 – Schematic of Control Volume Schematic of Forces Acting on Vapour Core [Adapted From: Sarangi et al. – 2009]

$$\left[\rho_G u_C^2 A_C + \frac{\partial}{\partial z}\left(\rho_G u_C^2 A_C\right)\Delta z\right] - \rho_G u_C^2 A_C - \Gamma_{LG} u_i \Delta z \qquad [3.60]$$

Figure 3.7 illustrates the forces acting on the control volume in the axial direction to provide Equation [3.61]. Equations [3.60] and [3.61] can be rearranged to produce the expression [3.62] which represents the interfacial shear stress term.

$$pA_C - \left[pA_C + \frac{\partial\left(pA_C\right)}{\partial z}\Delta z\right] - \tau_i P_{CH} \Delta z \qquad [3.61]$$

$$\tau_i = \frac{1}{P_{CH}}\left[A_C\left(-\frac{\partial p}{\partial z}\right) - p\left(\frac{\partial A_C}{\partial z}\right)\right] - \frac{1}{P_{CH}}\frac{\partial}{\partial z}\left(\rho_G u_c^2 A_C\right) + \frac{1}{P_{CH}}\Gamma_{LG} u_i \qquad [3.62]$$

The interfacial friction factor can be defined as expression [3.63] as well as the representation provided based on aspect ratio of the vapour core as illustrated in Equation [3.64]. The vapour core aspect ratio is defined in Equation [3.65] and the Reynolds number is outlined in expression [3.66].

$$f_i = \frac{\tau_i}{\frac{1}{2}\rho_G\left(u_C - u_i\right)^2} \qquad [3.63]$$

$$f_i \,\mathrm{Re}_c = 24\begin{pmatrix} 1 - 1.3553\beta_C + 1.9467\beta_C{}^2 - 1.7012\beta_C{}^3 \\ + 0.9564\beta_C{}^4 - 0.2537\beta_C{}^5 \end{pmatrix} \qquad [3.64]$$

$$\beta_C = \frac{w - 2\delta}{d - 2\delta} \qquad [3.65]$$

$$\mathrm{Re}_C = \frac{\rho_G\left(u_C - u_i\right)D_{h,C}}{\mu_G} \qquad [3.66]$$

$$\tau_i = f_i\left[\frac{1}{2}\rho_G\left(u_C - u_i\right)^2\right] - \frac{\Gamma_{LG}}{2P_{CH}}\left(u_C - u_i\right) \quad [3.67]$$

It is stated that the mass transfer experienced at the interface could have a significant influence on the interfacial friction which has been accounted for regarding the interfacial shear stress that is provided in Equation [3.67] from Sarangi et al., 2009.

The area of a rectangular channel is defined in expression [3.68]. The attributes for the annular flow model include the definition of the vapour core cross–sectional area outlined in Equation [3.69] and the hydraulic diameter defined in expression [3.70]. The rectangular micro–channel vapour core perimeter that accounts for the film thickness is illustrated in Equation [3.71] as provided in Sarangi et al., 2009.

$$A_{CH} = wd \quad [3.68]$$

$$A_C = \left[w - 2\delta\right]\left[d - 2\delta\right] \quad [3.69]$$

$$D_{h,C} = \frac{4A_C}{P_C} \quad [3.70]$$

$$P_C = 2\left[\left(w - 2\delta\right) + \left(d - 2\delta\right)\right] \quad [3.71]$$

Equations [3.68] to [3.71] outline the definitions employed for the analysis of the vapour core component of the annular flow model. The above expressions illustrate the significant relationship that film thickness has to the equivalent vapor core flow area and perimeter. Upon analyzing the mechanism of the annular flow method it is illustrated that the vapour core travels through the center of the channel at increased speeds apparently due to the reduced vapour core flow area.

3.2 – 7 Alternate Annular Flow Approach

Upon further inspection of the development of the annular flow method by Sarangi et al., 2009 and review of Qu and Mudawar, 2003. A new approach is presented for the annular method to predict the pressure drop. In the work of Qu and Mudawar, 2003 the annular flow vapour core region had been approximated through the assumption of a homogeneous phase for the core component of the model. The flow characteristics of the annular region are marked by an estimated higher flow velocity of the vapour phase associated with a reduced core flow area that travels through the center of the channel.

It was viewed that the flow assumption for the annular flow model could be incorporated through the homogeneous approach. It is suggested that the flow area be approximated from the cross–sectional area calculated from the hydraulic diameter estimation of the channel. The calculated cross–sectional area would provide a good approximation to facilitate the reduced flow area of the vapour phase described by the annular flow model. Implementing this assumption would enable an expected higher velocity of the two–phase fluid through means of a smaller estimation of the flow area for the channel. This assumption would reduce computational expense by having no need for iterations of the film thickness to satisfy any equations.

Moreover this approach would enable the new annular flow method to be applied to non–rectangular geometries to evaluate pressure drop results. Equation [3.72] to [3.73] outlines how the assumption of estimating the flow area from the hydraulic diameter of the micro–channel increases the mass flux which enables the expression to satisfy a modified annular flow approach. Incorporating Equation [3.73] into the homogeneous model expression instead of Equation [3.72] enables an increased homogeneous vapour velocity and a reduced flow area estimate for pressure drop calculations from Equation [3.31].

$$G = \frac{\dot{m}}{A_{CH}} \qquad [3.72]$$

$$G = \frac{\dot{m}}{A_{D_h}} \qquad [3.73]$$

3.3 Methodology

Pressure drop predictions using regime based models are very sensitive to the length of different flow regimes in the micro–channels and thus regime maps capable of accurately determining the transition points should be used [Harirchian and Garimella – 2012]. Therefore great care should be exercised in determining the boiling front of the micro–channel of interest should such maps not be available. Figure 3.8 illustrates that the boiling front is identified by the intersection between the single and two–phase temperatures determined through the thermodynamic equilibrium saturation condition.

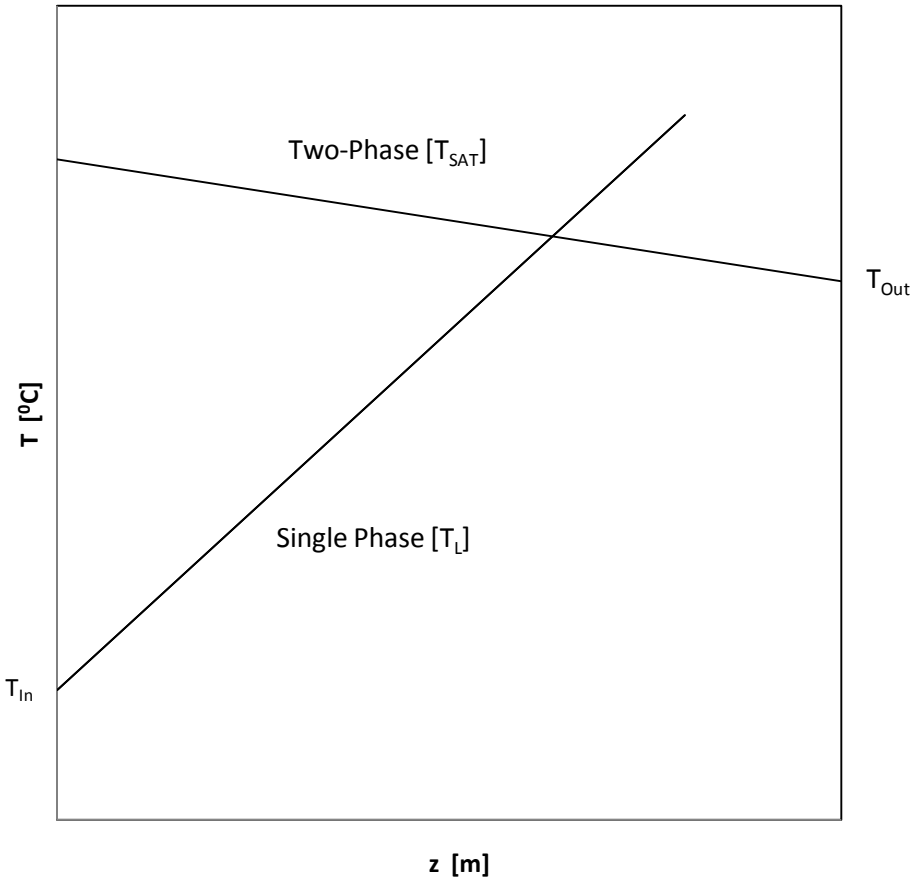

Figure 3.8 – Prediction of Boiling Front [Adapted From: Sarangi et al. – 2009]

There are a number of elements that are factored into the measurement of the onset of nucleate boiling that include inlet conditions, contact angle, velocity, subcooling effects, pressure and micro–channel

dimensions [Bertsch et al. – 2008]. It has been stated that after the onset of nucleate boiling all boiling curves collapse onto a single curve irrespective of the inlet conditions further outlining the dominance of nucleate boiling [Liu and Garimella – 2007]. The aforementioned arguments are seen to provide further support to the careful identification of the onset of nucleate boiling condition or the boiling front. Once the boiling front is identified through the intersection produced from the pressure saturation condition for the single and two–phase region as well as incorporating the thermo–physical property variations for temperature that include density, latent heat of evaporation, specific heat and viscosity. The appropriate single phase and two–phase calculations associated with the fluid of choice which in this case is water for each phase can be more accurately accounted for along the length of the channel.

The complete flow chart [Figure 3.10] for the developed model process is provided to refer to at the end of the chapter. Due to very high pressure drops across the micro–channel especially in the two–phase region the thermo–physical properties of the fluid undergo appreciable changes as noted by Koo et al., 2002. It is acknowledged in the literature that saturated flow boiling in micro–channels and the associated heat transfer mechanisms are not as well understood as the fluid dynamics and heat transfer characteristics of single phase flow [Bertsch et al. – 2008]. Further considering the various challenges associated with retrieving reliable experimental data as reflected in the work of Bertsch et al., 2008 which mentions that due to the small channel size, in situ pressure measurements are difficult. The determination of fluid temperature at any given point, should it not be measured directly, rely on assumptions regarding the pressure fluctuation along the micro–channel [Bertsch et al. – 2008]. Thus the experimental data sets should be handled with care and be provided the necessary error margins such results may require.

Incorporating water as the working fluid, curve fitting can be conducted to obtain appropriate relations that can be used to determine these properties as function of pressure and/or saturation temperature. Data over 0.01 to 200^{0}C had been implemented from the Ashrae Handbook in 1997 to cover an accurate data range for operating conditions. Included below are the polynomial expressions developed over the range of 0.01 to 200^{0}C for liquid density, viscosity, thermal conductivity, specific heat capacity and the change in enthalpy between liquid and vapour as outlined in Equations [3.74] to [3.78]. It is important to note that these correlations are expressed with temperature defined in degrees Celsius [^{0}C].

Density $\left[\frac{kg}{m^3}\right]$ =

$$-1.52939E-12\left[T\left(^0C\right)\right]^6 + 1.10840E-09\left[T\left(^0C\right)\right]^5 - 3.41444E-07\left[T\left(^0C\right)\right]^4 + 5.84420E-05\left[T\left(^0C\right)\right]^3 - 8.13088E-03\left[T\left(^0C\right)\right]^2 + 6.04217E-02\left[T\left(^0C\right)\right] + 9.99813E+02 \quad [3.74]$$

Viscosity $\left[\frac{kg}{m \bullet s}\right]$ =

$$4.0220E-16\left[T\left(^0C\right)\right]^6 - 2.8755E-13\left[T\left(^0C\right)\right]^5 + 8.2940E-11\left[T\left(^0C\right)\right]^4 - 1.2501E-08\left[T\left(^0C\right)\right]^3 + 1.0791E-06\left[T\left(^0C\right)\right]^2 - 5.6116E-05\left[T\left(^0C\right)\right] + 1.7815E-03 \quad [3.75]$$

Thermal Conductivity $\left[\frac{W}{m \bullet {}^0C}\right]$ =

$$-1.15E-12\left[T\left(^0C\right)\right]^5 + 5.71E-10\left[T\left(^0C\right)\right]^4 - 8.23E-08\left[T\left(^0C\right)\right]^3 - 4.80E-06\left[T\left(^0C\right)\right]^2 + 2.04E-03\left[T\left(^0C\right)\right] + 5.60E-01 \quad [3.76]$$

Specific Heat Capacity $\left[\frac{J}{kg \bullet {}^0C}\right]$ =

$$1.0242E-10\left[T\left(^0C\right)\right]^6 - 6.3535E-08\left[T\left(^0C\right)\right]^5 + 1.5297E-05\left[T\left(^0C\right)\right]^4 - 1.7836E-03\left[T\left(^0C\right)\right]^3 + 1.1390E-01\left[T\left(^0C\right)\right]^2 - 3.5743E+00\left[T\left(^0C\right)\right] + 4.2210E+03 \quad [3.77]$$

Change in Enthaphy $\left[\frac{J}{kg}\right]$ =

$$-0.0143\left[T\left(^0C\right)\right]^3 + 0.8543\left[T\left(^0C\right)\right]^2 - 2382.2453\left[T\left(^0C\right)\right] + 2\,500\,656.9340 \quad [3.78]$$

3.4 Computational Method and Iterative Procedure

Since closed–formed solutions may not be available in some cases a numerical approach may be needed for the solution [Singhal et al. – 2003]. The finite difference method is the numerical solution used to solve the equations while incorporating thermo–physical property variations. The finite difference method has been used in papers by Qu and Mudawar, 2002, Webb, 2003, and Sarangi et al., 2009 to solve developed systems of equations. The finite difference method was among the first methods applied to the numerical solution of differential equations. It was first utilized by Euler around 1768 [Blazek – 2001]. The method itself is directly applied to the differential form of the governing equations. The principle is to employ a Taylor series expansion for the discretisation of the derivatives of the flow variables. An important advantage of the finite difference methodology is its simplicity as well as ease in obtaining higher order approximations which enables higher order accuracy of spatial discretisation [Blazek – 2001]. The method requires a structured grid which thus makes the application restricted. Furthermore, the finite difference method cannot be directly applied in body–fitted [curvilinear] coordinates. The governing equations have to be first transformed into a Cartesian coordinate system, or expressed in other words from the physical to the computational space [Blazek – 2001]. Figure 3.9 illustrates the 50 node layout involved in the structured grid for the finite difference method which implements the non–linear equations involving thermo–physical property variations as functions of temperature.

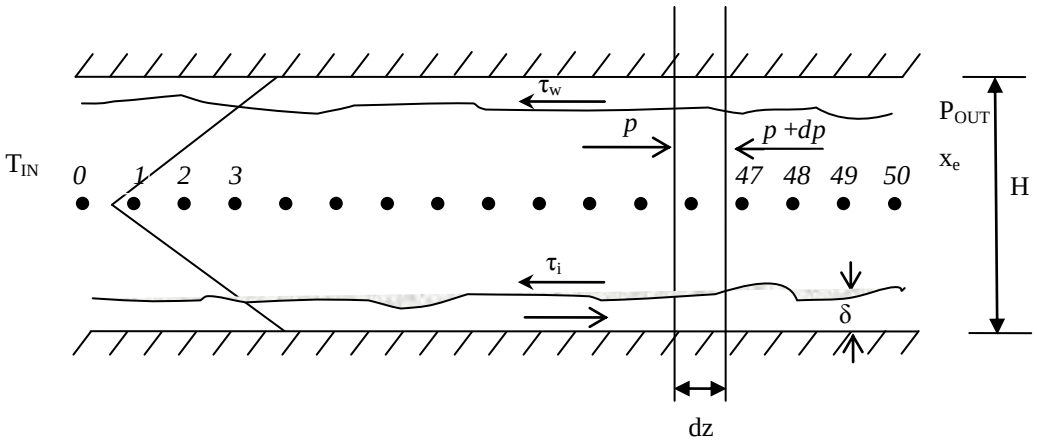

Figure 3.9 – Illustration of Finite Difference Layout

The procedure to solve the annular model is outlined below where it is noted that modifications have been made to simplify the calculation method compared to the work of Sarangi et al., 2009. The procedure to solve the homogeneous model is well illustrated in Figure 3.10.

1. The location of the onset of annular flow is determined first through the identification of the saturation condition between the single and presumed initiation of two–phase flow. The one–dimensional grid with 50 cells is incorporated along the entire length of the channel to cover both the single phase, homogeneous and annular flow region separately. The solution initiated for the homogeneous and annular flow region occurs at the end node since the vapour quality can be determined independently at the pressure outlet [P_{OUT}].
2. The mass flow rates of the vapour core and liquid film can be effectively determined through multiplying the quality determined in step 1 to the total mass flow rate. T_{out} can be found from P_{out} and the fluid properties at the upstream adjacent node are calculated based the exit pressure conditions.
3. A value for the film thickness [δ] is initially guessed at the end node. This value should be in the fractional range of the hydraulic diameter expressed usually while trying to consider the surface roughness of the channel. The film thickness [δ] value is iterated until a convergence of approximately 0.15% of Equation [3.79] is achieved. Γ_{LG} can also be calculated.
4. A_C and P_C can be calculated using the value of δ. The terms u_i and u_C are obtained knowing the mass flow rates and the geometrical parameters. The interfacial shear stress is then evaluated.
5. Equation [3.59] Is solved to obtain –dp/dz
6. The pressure gradient obtained is then substituted to evaluate the mass flow rate of the liquid film through completion of the integral for u_{LL} across the film thickness which corresponds to the below expression [3.79]. Knowing the value of $\dot{m}_{LL}$ from the mass conservation outlined in Equation [3.47]. The obtained value should be similar to that of the known initial value within sufficient accuracy for the solution to be complete at the end node.

   If not the calculations must be repeated from step 3 by guessing a new value of δ. The process has been augmented by assuming that a near linear relationship exists from the exit to inlet for a value of δ. The film thickness increases from outlet to inlet by a steady slope of the initial value of δ. The linear variation implemented enables the calculations to step upstream more efficiently to satisfy the equations at each node within a reasonable error tolerance.

7. The solution procedure is slightly modified compared to the outlined methods in Sarangi et al., 2009, Harirchian and Garimella, 2012, as well as Qu and Mudawar, 2002. The remaining upstream node calculations can be completed through incorporating an appropriated slope regarding the film thickness to acquire the required accuracy of mass flow rate liquid film at each node. The slope is changed until there is a difference of approximately 0.80 to 1.0% from the value of Equation [3.79] noted at the boiling front to maintain consistent results. This procedure is then repeated by each step upstream to finally obtain a local solution for all the nodes in the annular region.

$$\dot{m}_{LL} = \frac{P_{CH}\rho_L\delta^3}{3\mu_L}\left(-\frac{\partial p}{\partial z}\right) + \frac{P_{CH}\rho_L\delta^2}{2\mu_L}\tau_i - \frac{\rho_L\delta^2}{2\mu_L}\Gamma_{LG}u_i \qquad [3.79]$$

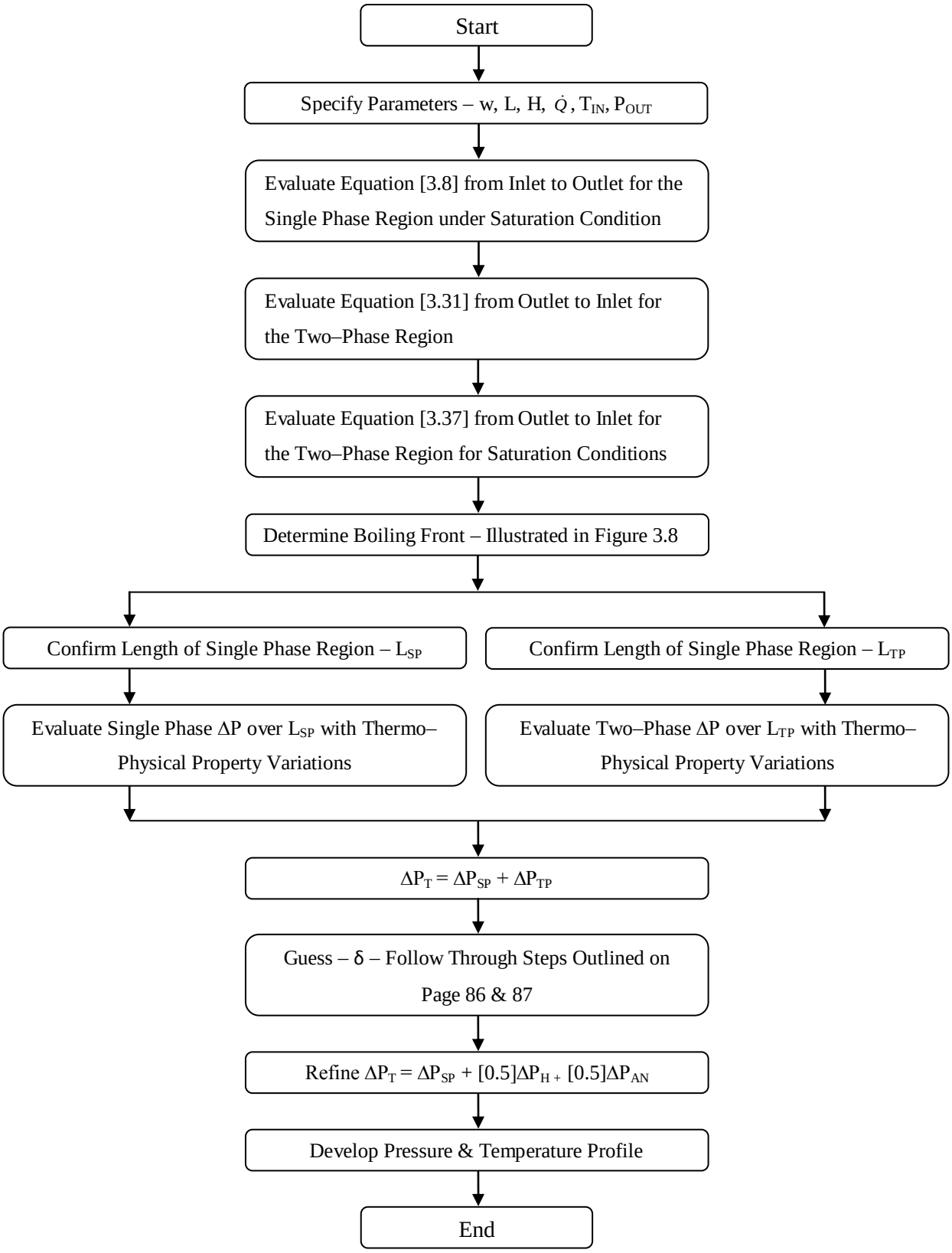

Figure 3.10 – Flowchart of Model Process

3.5 Chapter 3 – Summary

An identified need is presented in the micro–channel research literature to provide an accurate model that can predict pressure drop and heat transfer coefficients for broader experimental data sets. The model also needs to capture the physical phenomena of various flow patterns that upon the onset of nucleation boiling are noted occur in the [two–phase] region. The model approach developed intends to be evaluated for the purpose of facilitating an efficient design instrument for micro–channels to predict the pressure drop and heat transfer coefficient related to heat input for the single phase through to the boiling [two–phase] region. The model components for both the single and two–phase flow have been developed from conventional correlations for [macro] channels to describe the nature of the phenomena expected to occur in [micro] channels. The single phase and two–phase flow region assumptions employed enable less computationally rigorous equations to be utilized.

The model uses the homogeneous approach as a basis with the assumption that it is able to adequately represent the bubble and wavy annular regions. The homogeneous model had been emphasized to produce reasonable results for pressure drop calculations over a number of different experimental data sets. However, it has been stated that the homogeneous approach has often been applied to other flow patterns that may not be best suited to all the underlying assumptions. The annular flow model is developed as a single regime approach that is able to cover the annular flow and wavy annular flow regions. It had been noted that neighboring flow regimes of the flow pattern modeled can be predicted with some accuracy. The simplified homogeneous model is intended to provide a lower bound for pressure drop estimates and the weighted annular–homogeneous model produces upper bound values. Input parameters include the thermo–physical properties of the respected coolant, micro–channel dimensions, fluid flow rate, inlet temperature, and outlet pressure. Polynomial correlations for water are obtained from curve–fitting data available from the 1997 Ashrae Handbook over the temperature range of 0.01 to 200 ^{0}C for the thermodynamic properties that include liquid density, viscosity, thermal conductivity, specific heat capacity and change of enthalpy [latent heat of vapourization]. One–dimensional analysis is supported in other papers to be of reasonable accuracy to estimate necessary operating parameters. A 50 node grid is employed along the length of the channel to facilitate the finite difference method. The equations for the homogeneous and annular flow models have been analyzed through the implementation of the conservation of mass, momentum and energy. The two–phase flow components of the models are solved through the finite difference method from the exit to inlet nodes.

CHAPTER 4
RESULTS & DISCUSSION

The following chapter provides the predictions obtained for the homogeneous and annular models compared to the simulated study by Sarangi et al., 2009 that is included to evaluate values under ideal conditions before investigating experimental data sets. The homogeneous and weighted annular–homogeneous model results are compared to four independent experimental data sets conducted under different operating conditions. A detailed discussion of the experimental and model results are provided for each data set. The present thesis hypothesizes that the weighted annular–homogeneous model approach provides an additional benefit to pressure drop calculations than compared to the homogeneous method alone is evaluated.

The homogeneous and annular flow models have been consistently incorporated in the research literature for evaluating the pressure drop and heat transfer aspects concerning the two–phase flow regions for experimental data sets. The contributions of the model developed in this work include sifting through much research literature to determine the true effectiveness of the homogeneous method as well as the evaluation of employing simplifying assumptions to describe broader experimental data sets. It is important to state that there are alternative assumptions that can accompany the homogeneous models utilized in the literature. Variations in friction factors, definitions of homogeneous density and viscosity are applied to the homogeneous model. There exist different assumptions for how the annular flow regime can be described as well, as an example the vapour core region has been estimated as a homogeneous vapour flow by Qu and Mudawar, 2003 or as a pure vapour core as outlined in Sarangi et al., 2009. Incorporating the homogeneous and weighted annular–homogeneous models is considered to provide the attribute of flexibility to the designer to accurately capture the identified key features of pressure drop and heat transfer coefficient for a single channel. Heat transfer coefficient calculations are carried out using the Kandlikar correlation and the Kandlikar enhancement factor method that are discussed in further detail in the following sections. The model assumptions were simplified to reduce computational expense as well as to facilitate the design applications should flow pattern maps not be readily available.

The purpose of the modeling approach developed in the present thesis is to provide clarity to the much confounded research literature related to determining the preferred modeling method for two–phase flow in micro–channels. The current methods receiving attention are efforts proposing to adapt model calculations to each particular two–phase flow regime. Since the pressure drop and heat transfer coefficient values are influenced by the flow patterns it is likely that such parameters are to vary over the two–phase region of the micro–channel. It is important to note that a single channel is evaluated for all data sets. The present model illustrates many areas for design considerations that include an approximation of the boiling front, pressure drop, two–phase heat transfer coefficient, as well as wall temperature profile over various operating conditions. The small hydraulic diameters of micro–channels can lead to inceased pressure drop whicds to higher power consumption which is not a desirable attribute for electronic systems [Lee and Mudawar – 2005]. Clearly, an understanding of the relationship between pressure drop, flow rate and heat flux is of paramount importance to micro–channel heat sink design [Lee and Mudawar – 2005].

4.1 Simulated Results for Sarangi et al. – 2009

The following section provides a comparison to the homogeneous and annular model components separately to the simulated results presented by Sarangi et al. 2009. The simulated values are considered under ideal conditions which will illustrate the general fluid [water] behavior expected to occur for each approach.

4.1 – 1 Homogeneous & Annular Model for Micro–Channel [Width 50µm & Depth 70µm]

Figures 4.1 and 4.2 provide comparison to the homogeneous model predictions to that of the simulated values presented by Sarangi et al., 2009. To initiate confidence in the ability of the homogeneous model to predict flow boiling behavior the identification of the boiling front is an important aspect to evaluate. The flow boiling regime outlined in the simulated study of Sarangi et al., 2009 is illustrated through ideal conditions where no heat loss to the environment is presumed. The literature data had been obtained by numerating or digitizing values from figures provided in the paper by Sarangi et al., 2009. It is important to state that although effort to minimize error had been employed in obtaining the numerical values, their will exist some small difference from the results presented in the literature.

The boiling front is considered to illustrate the location along the length of the channel where the important transition from single phase flow to two–phase flow is expected to occur. Figure 4.1 demonstrates the boiling front expectations in concern to the heat input for the current homogeneous model component that is compared to the independent homogeneous model approach developed by Sarangi et al., 2009. The homogeneous model component employed three empirical friction factors that include 0.003, 0.004 and 0.005, since these cover the identified value range obtained from experimental data for steam as outlined in Collier and Thome, 1994. The developed homogeneous model illustrates good agreement with the boiling front trend for the simulated values presented by Sarangi et al., 2009. Figure 4.1 illustrates that the boiling front expectations associated with the friction factor value of 0.003 provides a slightly larger error margin to that of the values of 0.004 and 0.005 when compared to the simulated values of Sarangi et al., 2009. The boiling front is observed to occur sooner as more heat is added to the channel. The presented single micro–channel of the Sarangi et al., 2009 incorporates a length of 2 cm, width of 50 µm, depth of 75 µm and a calculated hydraulic diameter of 60 µm. The inlet

temperature is 25^{0}C with a fluid flow rate of 0.1 mL/min and outlet pressure of 1 atmosphere [1.01325 bar] are outlined for the operating conditions. The simulated values illustrate that the boiling front ranges from about 1.3 to 0.65 cm for heat input of 1 to 3 W.

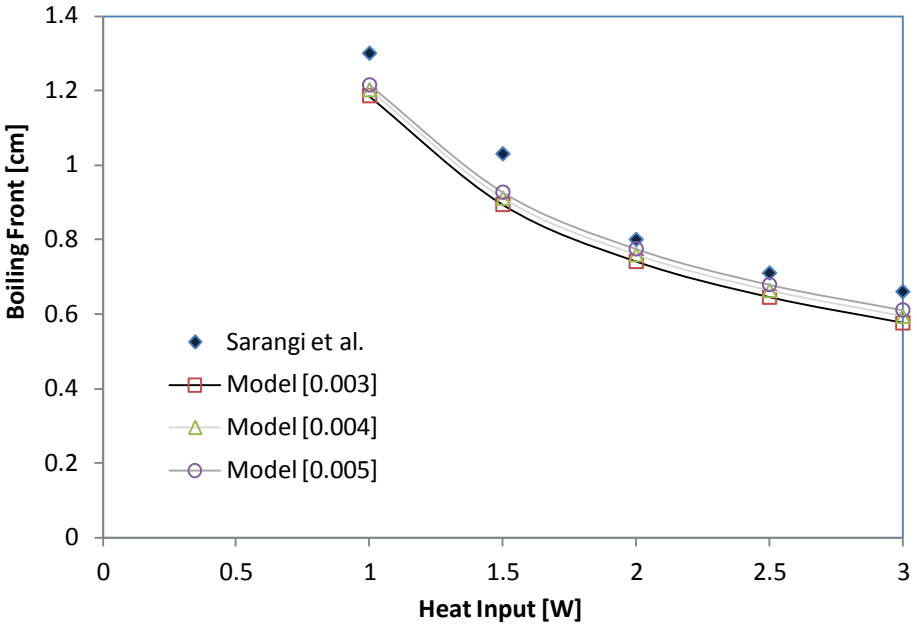

Figure 4.1 – Simulated Data: L = 2 cm, w = 50 µm, d = 75 µm, D_h = 60 µm, T_{IN} = 25^{0}C, P_{OUT} = 1.01325 bar, $\dot{Q}$ = 0.1 mL/min [Adapted From: Sarangi et al. – 2009]

Incorporating the mean absolute error method presented in Equation [4.1] estimated the boiling front predictions to be within about 10% of the simulated values of Sarangi et al, 2009 for the homogeneous model that employed a friction factor of 0.003. The homogeneous model results with 0.004 for the friction factor corresponded to an 8.2% difference. Lastly the homogeneous model that implemented the empirical friction factor value of 0.005 estimated the boiling front to be within 6.3% of the simulated values of Sarangi et al, 2009.

$$MAE = \frac{1}{N}\left|\frac{\Delta p_{PRED} - \Delta p_{EXP}}{\Delta p_{EXP}}\right| x100\% \qquad [4.1]$$

Figure 4.2 illustrates the pressure drop expectations for the operating characteristics outlined by Sarangi et al., 2009 that include ideal conditions with no presumed heat loss from the micro–channel to the environment. The operating conditions include a fluid flow rate 0.1 mL/min, inlet temperature of 25^{0}C and outlet pressure of 1 atmosphere [1.01325 bar]. Figure 4.2 illustrates that as the heat input is increased the pressure drop becomes steadily greater. The homogeneous model pressure drop values presented by Sarangi et al., 2009 ranged approximately from 0.5 to 3 bar over heat inputs of 0.5 to 3 W.

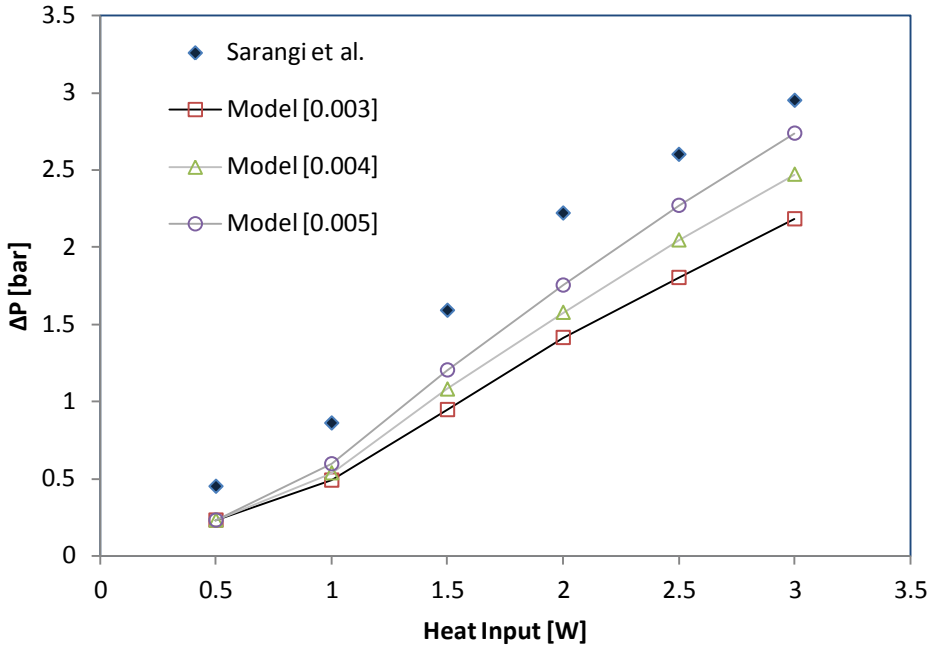

Figure 4.2 – Simulated Data: L = 2 cm, w = 50 µm, d = 75 µm, D_h = 60 µm, T_{IN} = 25^{0}C, P_{OUT} = 1.01325 bar, $\dot{Q}$ = 0.1 mL/min [Adapted From: Sarangi et al. – 2009]

The homogeneous approach illustrates good agreement in concern to the trend displayed by the simulated values of Sarangi et al., 2009. The employed empirical friction factor of 0.003 for the homogeneous model corresponded to pressure drop results which are associated with a 38% mean absolute error calculated from Equation [4.1]. The mean absolute error associated with the empirical friction factor of 0.004 was 31% and 24% for 0.005. The empirical friction factor of 0.003 has been used by Bhide et al., 2009 and 0.005 had been incorporated by Qu and Mudawar, 2002 for the homogeneous model method. The empirical friction factor value of 0.004 is implemented for the homogeneous model going forward to provide an effective lower bound estimate for pressure drop results.

The annular flow model simulated values of Sarangi et al., 2009 illustrated in Figure 4.3 outlines the boiling front to be approximately 1.3 to 0.65 cm for heat inputs over the range of 1 to 3 W. The annular flow model calculated by the approach outlined in Section 3.4 is identified as [Method 1] in Figure 4.3. The annular flow model completed through the alternate approach outlined in 3.2 – 7 is labeled as [Method 2]. The two methods are compared to the simulated values presented for the annular flow model developed by Sarangi et al., 2009. The annular flow model [Method 1] is similar to the approach developed by Sarangi et al., 2009, where there are a few important changes to the calculation procedure which have been incorporated. A different convergence criteria and iterative procedure to reduce computation expense are further outlined in section 3.4.

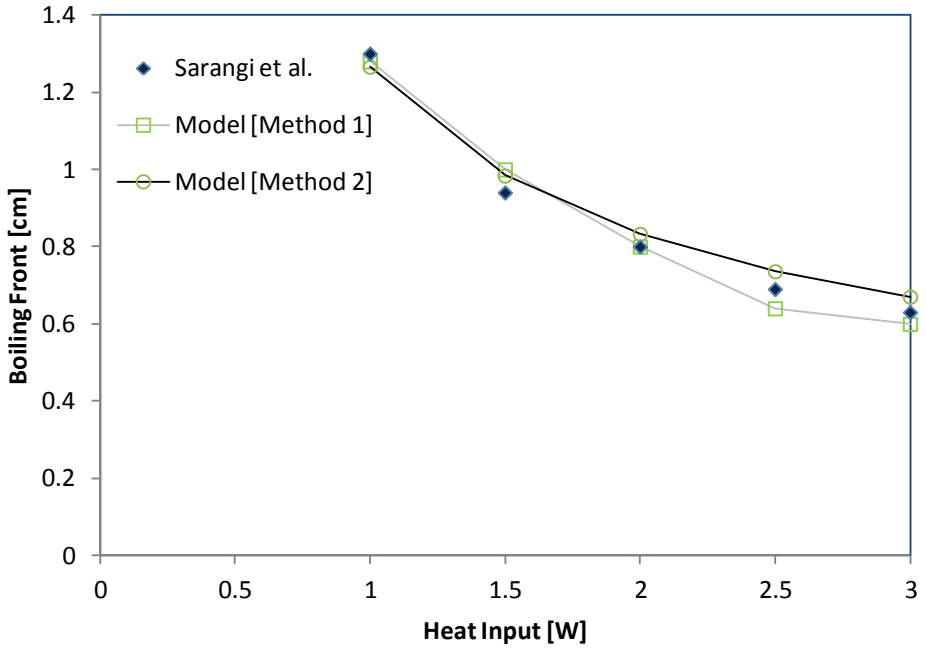

Figure 4.3 – Simulated Data: L = 2 cm, w = 50 µm, d = 75 µm, D_h = 60 µm, T_{IN} = 25^{0}C, P_{OUT} = 1.01325 bar, $\dot{Q}$ = 0.1 mL/min [Adapted From: Sarangi et al. – 2009]

It is noticed that similar expectations in the boiling front are expected for the annular flow model results compared to the homogeneous model values provided in Figure 4.1. As the heat input increases, the boiling front is expected to occur sooner along the length of the channel corresponding to a greater portion of the micro–channel involved in two–phase flow activity. Figure 4.3 illustrates that the boiling front estimation from the annular model procedure identified as [Method 1] are within 4% difference of

the simulated values of Sarangi et al., 2009 through the utilization of Equation [4.1]. Method 2 estimated the boiling front within a 4.6% mean absolute error. It is important to note that the results completed by method 2 for the annular flow model are calculated through modifying the expected flow area of the derived homogeneous model. The cross–sectional channel area is estimated via the hydraulic diameter as outlined in section 3.2 – 7. The empirical friction factor of 0.005 is implemented for the annular flow approach calculated by method 2 to enable a higher pressure drop estimate associated with that flow regime.

The operating conditions for the annular flow simulated values presented in Figure 4.4 include a inlet temperature of 25^0C followed with a fluid flow rate of 0.1 mL/min and outlet pressure of 1 atmosphere [1.01325 bar]. The micro–channel dimensions include a length of 2 cm, width of 50 µm, depth of 75 µm. Figure 4.4 illustrates the annular flow simulated pressure drop values of Sarangi et al., 2009 that are greater than the corresponding homogeneous model pressure drop values presented in Figure 4.2.

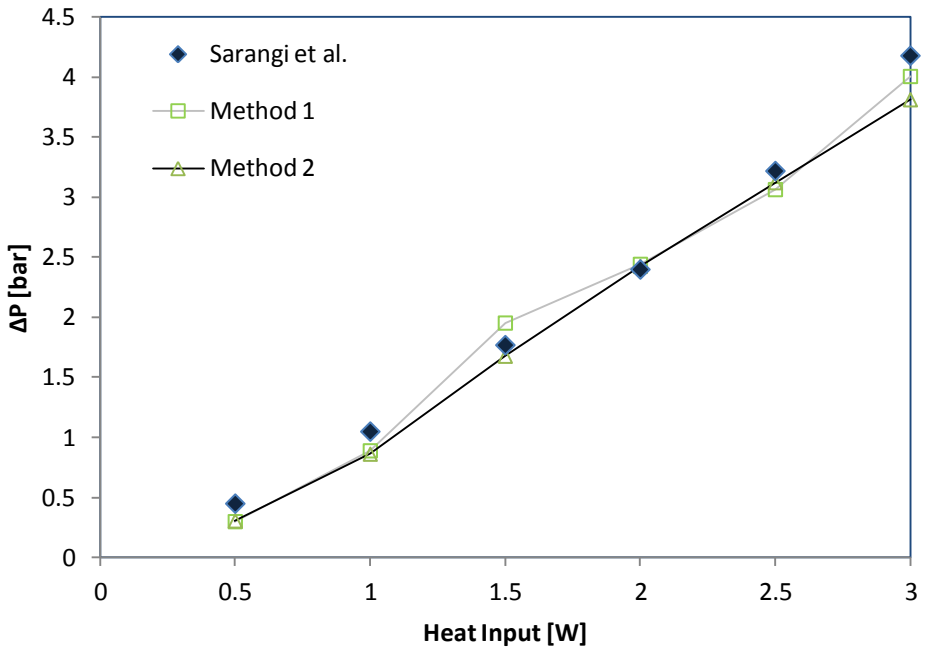

Figure 4.4 – Simulated Data: L = 2 cm, w = 50 µm, d = 75 µm, D_h = 60 µm, T_{IN} = 25^0C, P_{OUT} = 1.01325 bar, $\dot{Q}$ = 0.1 mL/min [Adapted From: Sarangi et al. – 2009]

Figure 4.4 illustrates the annular flow pressure drop values of Sarangi et al., 2009 to range approximately from 0.5 to over 4 bar for corresponding heat inputs of 0.5 to 3 W. It is noted from Figure 4.3 that as a greater portion of the channel is involved with two–phase flow activity through having the boiling front occur sooner along the length of the micro–channel which directly relates to higher pressure drop values. Evaluating the annular flow model calculated through method 1 results in values that ranged within a 11% mean absolute error to the simulated values of Sarangi et al., 2009. The annular flow model calculated by method 2 were determined to have a 12% mean absolute error compared to the values presented by Sarangi et al., 2009.

4.1 – 2 Homogeneous & Annular Model for Micro–Channel [Width 150µm & Depth 225µm]

The boiling fronts for the larger channel dimensions provided by Sarangi et al., for a width of 150 µm and depth of 225 µm are evaluated. The homogeneous and annular components of the model developed here with friction factor of 0.003, 0.004 and 0.005 illustrate the capacity to provide reasonable results under ideal conditions with no heat loss from the system. Additionally it is observed that the friction factor had little influence on the determination of expected boiling front calculations for the homogeneous approach for larger channels as illustrated in Figure 4.5.

From the model results presented in Figure 4.5 compared with Figure 4.1 demonstrate that the boiling front is expected to occur sooner in the larger channels for similar heat inputs. A possible explanation for the aforementioned results could be that the flow velocity is higher in smaller channels that in turn reduces the amount of heat absorption by the fluid along the length of the channel. A similar trend as outlined in Figure 4.1 of a decreasing boiling front from approximately 1 to 0.35 cm with increased heat inputs over the range of 1 to 3 W are illustrated in Figure 4.5. A mean absolute error calculation illustrates a 6% difference to the values of Sarangi et al., 2009 for all three cases.

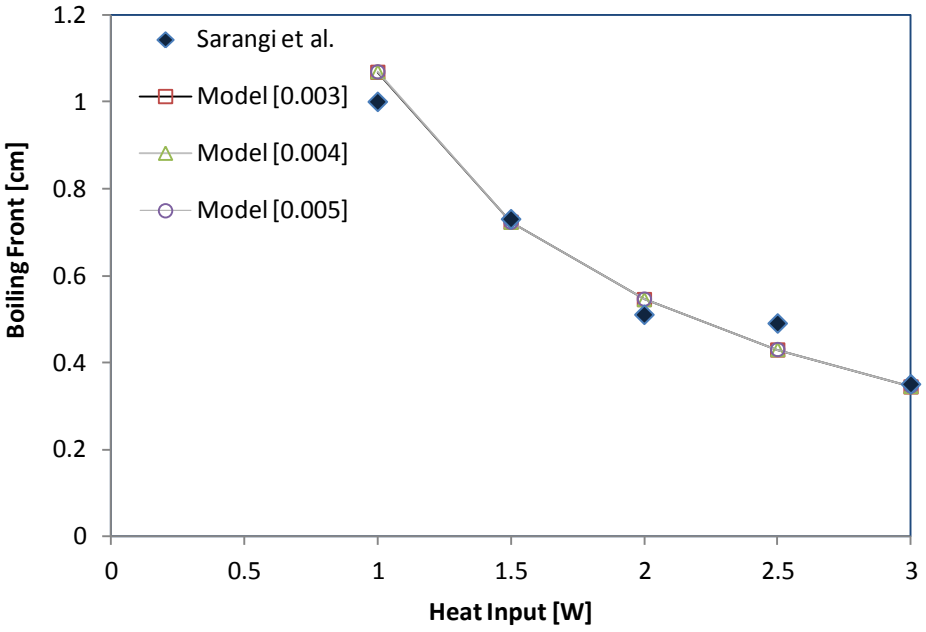

Figure 4.5 – Simulated Data: L = 2 cm, w = 150 µm, d = 225 µm, D_h = 180 µm, T_{IN} = 25^{0}C, P_{OUT} = 1.01325 bar, $\dot{Q}$ = 0.1 mL/min [Adapted From: Sarangi et al. – 2009]

Figure 4.6 illustrate similar boiling front expectations for the annular flow values compared to the results regarding the homogeneous model presented in Figure 4.5. Figure 4.6 illustrates a decreasing boiling front with values ranging from approximately 1.1 to 0.35 cm for heat inputs of 1 to 3 W. The annular flow results calculated by method 1 and 2 illustrated in Figure 4.6 provide close agreement to the simulated values presented by Sarangi et al., 2009. The trend of decreasing boiling front with increased heat input illustrates that more of the channel is experiencing two–phase flow activity.

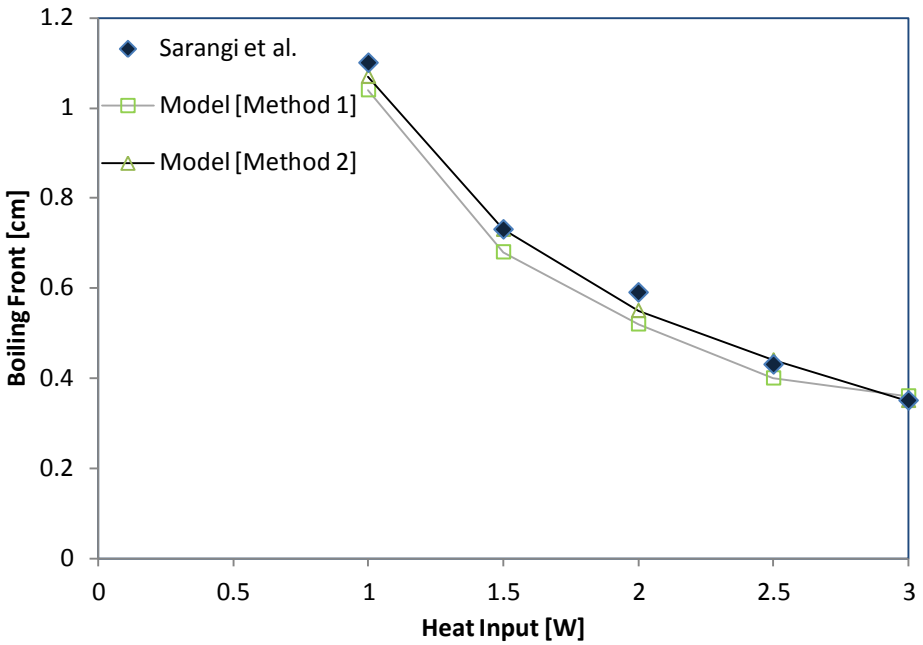

Figure 4.6 – Simulated Data: L = 2 cm, w = 150 µm, d = 225 µm, D_h = 180 µm, T_{IN} = 25^{0}C, P_{OUT} = 1.01325 bar, $\dot{Q}$ = 0.1 mL/min [Adapted From: Sarangi et al. – 2009]

The results illustrate the mean absolute error of 7% for the annular flow model calculated by method 1 and 2.4% for the boiling front determined by method 2. Therefore the separate homogeneous and annular models have illustrated the ability to capture the simulated values presented by Sarangi et al., 2009 for ideal conditions with reasonable accuracy.

4.2 Experimental Evaluation of Model Results

Experimental data from four different reseachers that include Zhang et al., 2002, Bhide et al., 2009, Qu and Mudawar, 2003 along with Galvis and Culham, 2012, will be modeled to evaluate the accuracy of the assumptions utilized in the development of the homogeneous and weighted annular–homogeneous model methods. Details concerning the experimental set up are provided in sections 2.6 – 1 and 2.6 – 4.

Insight into some of the experiment operating conditions are restated to outline important attributes that are considered in the modeling approach. The micro–channel dimensions of width, depth length, estimated hydraulic diameter, temperature inlet along with fluid flow rate are illustrated in figure captions to provide a reference to the main operating conditions accounted for in the model. Model assumptions are outlined in Chapter 3, however it is important to restate to the reader that such discussion of homogeneous model can involve different forms of mathematical relationships for friction factors, weighted average of density as well as viscosity. Therefore the assumptions employed should be closely considered for each individual model. The homogeneous and weighted annular–homogeneous model is evaluated with channel dimensions ranging from 50 µm to 713 µm. The independent experimental data sets were numerically reproduced from figures presented in the research literature to adequately capture the pressure drop, heat transfer coefficient, wall temperature profile, and vapour quality relationships. Mean absolute error analysis is completed to provide a measure of accuracy regarding the model approach to experimental data.

4.2 – 1 Experimental Data of Zhang et al. – 2002

The first experimental data set to be modeled is the work of Zhang et al., 2002 which incorporated water as the working fluid in a single micro–channel. More specific information pertaining to the experimental set up are provided in section 2.6 – 1. To cover some details of the experiment in concern to the parameter inputs considered in the model. The length of the flow region for the micro–channel is stated to be 2 cm in Zhang et al., 2002. The heated region is outlined to be 1.6 cm corresponding to the dimensions of the incorporated resistor that functions as the respected heat source. The micro–channel dimensions include a width of 50 µm, depth of 70 µm to produce a calculated hydraulic diameter of 58.3 µm. The flow rate of water was 0.1 mL/min and the inlet temperature was referenced to be 20 ^{0}C with an outlet pressure of 1.17 bar. Figure 4.7 illustrates the homogeneous model which incorporated a friction factor of 0.004 to produce conservative values for the experimental pressure drop data. The weighted annular–homogeneous model calculated through utilizing the new annular model approach along with the homogeneous model envelopes a good portion of the experimental data.

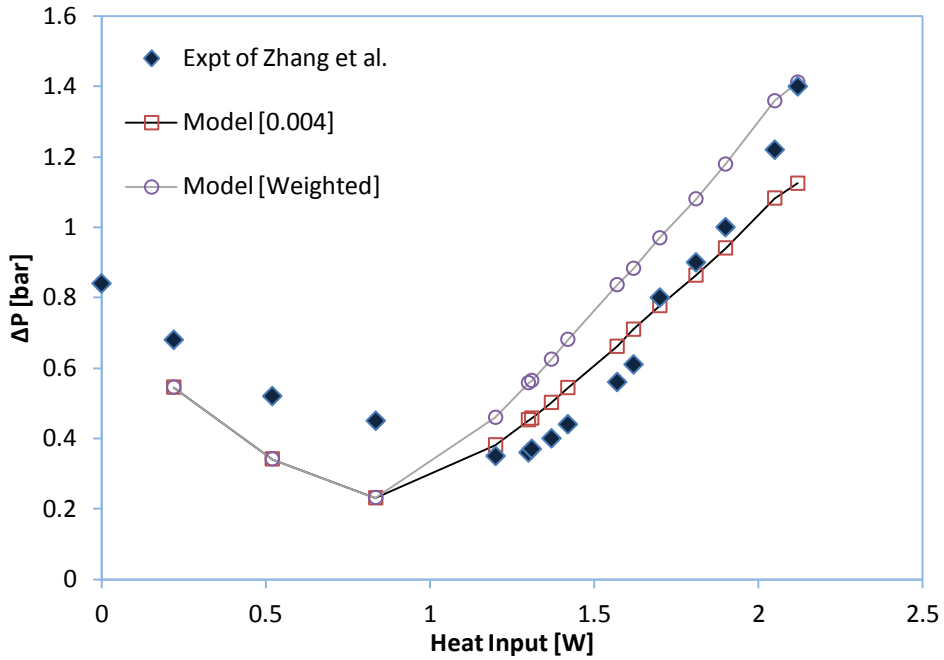

Figure 4.7 – Experimental Data: L = 2 cm, w = 50 µm, d = 70 µm, D_h = 58.3 µm, T_{IN} = 20^{0}C, P_{OUT} = 1.17 bar, $\dot{Q}$ = 0.1 mL/min [Adapted From: Zhang et al. – 2002]

The experimental data set outlined by the diamond shaped data points in Figure 4.7 illustrates an initial decrease in pressure drop mostly due to the influence of changes in viscosity with respect to temperature. At approximately 1.3 W the experimental pressure drop data values start to increase as more heat is added. The transition point noted around 1.3 W is considered to be where the fluid enters the two–phase region. This increase from the advent of two–phase flow illustrates the higher pressure drop associated with such two–phase [boiling] conditions. The heat loss from the micro–channel is established to be 26% with 12% to preheating [Zhang et al. – 2002]. To account for the heat loss component a simplfying assumption had been employed, where the model considered that for every watt provided to the system only 74% is viewed to be received by the fluid for this experiment conducted by Zhang et al., 2002. Figure 4.7 illustrated a slightly earlier transition to the boiling region captured by the model than outlined by the experimental data set of Zhang et al., 2002. The possible reason for an earlier anticiated transition region could be related to a higher estimated slope in concern to the calculated temperature rise in the single phase region.

While in the Zhang et al., 2002 paper their homogeneous model provided a better fit to the experimental data, it is to noted that the model incorporated a two–phase friction factor that was stated to be well suited to their results. The homogeneous and weighted annular–homogeneous model incorporated simplifying assumptions that include the loss coefficient of the single phase and the friction loss coefficient for the two–phase region. The values used may not best represent the experimental operating conditions over the length of the micro–channel which thus produced some differences in pressure drop calculations. However, conducting the mean absolute error analysis outlined in Equation [4.1] for the average results between the homogeneous and weighted annular–homogeneous model predictions in Figure 4.8, a difference of 25% is determined. Two points that have the highest error are noted to be from the single phase region. Incorporating experimental data uncertainty could slightly lower the calculated error. The importance of the model results outline what will be referred to as an operational range of pressure drop expectations for the experimental conditions. Two–phase flow experiments available in the literature have stated to observe oscillations regarding pressure and temperature readings from the sensors used. Although the mention of fluctuations in electrical signals was observed in the work of Zhang et al., 2002, the paper stated such distrubances to provide a good indication that boiling is occurring. However, the average resistance measurements were noted to be more difficult to interpret. The homogeneous and weighted annular–homogeneous model results are significant as they have been completed through simplifying

assumptions which employed the finite difference method containing only 50 nodes to represent the entire length of the micro–channel where past theoretical models have used far more involved mathematical systems to complete their calculations.

Figure 4.8 is included to outine the experimental data from Zhang et al., 2002 with consideration to employing the micro–channel flow length of 1.6 cm instead of 2 cm. Sarangi et al., 2009 used the homogeneous model to estimate the micro–channel length to be 1.6 cm for the work of Zhang et al., 2002. The justification for the actual length of the micro–channel to be considered 1.6 cm is related to the actual length of the heated resistor component instead of the entire 2 cm length of the micro–channel. Therefore it is viewed that only 1.6 cm of the micro–channel is in contact with the heat source. The homogeneous approach with friction factor of 0.004 illustrates less increase in pressure drop in comparison to the experimental results outlined in Figure 4.8. An mean absolute error analysis between the average of the homogeneous and weighted annular–homogeneous model results provides an approximate 23% difference in values to the experimental data of Zhang et al., 2002.

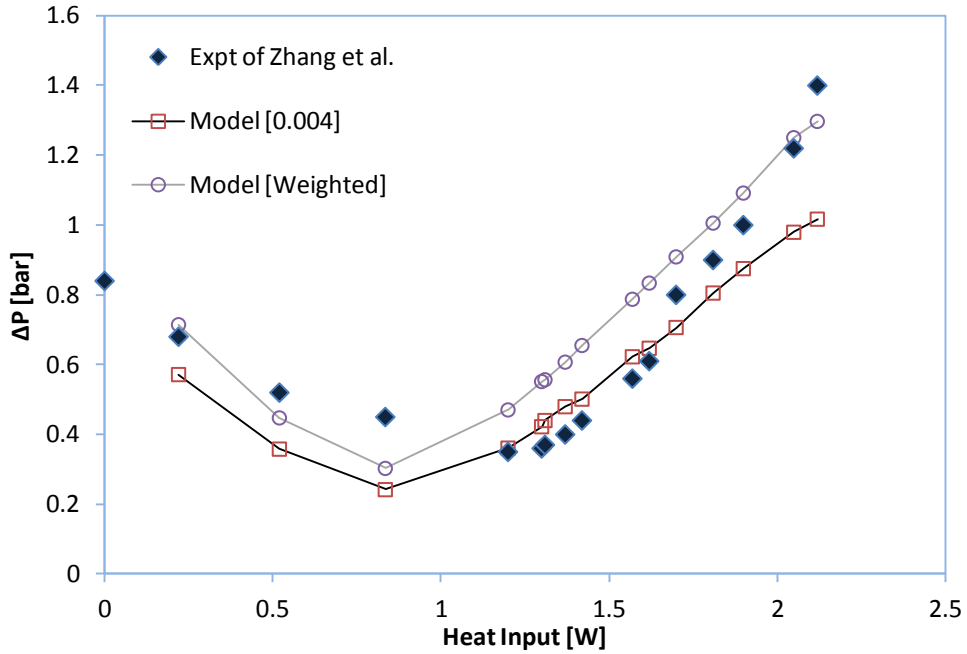

Figure 4.8 – Experimental Data: L = 1.6 cm, w = 50 µm, d = 70 µm, D_h = 58.3 µm, T_{IN} = 20^0C, P_{OUT} = 1.17 bar, $\dot{Q}$ = 0.1 mL/min [Adapted From: Zhang et al. – 2002]

Figure 4.9 illustrates the heat input of experimental data for the corresponding wall temperatures provided in Zhang et al., 2002 for 1.32 W and 2.12 W compared to the developed model temperature profile based on the homogeneous approach. To illustrate the variation along the length of the channel for the respected heat input, the length of 1.6 cm which corresponds to the length of the heated resistor is accounted for in the model calculations. Equation [3.46] is incorporated to account for the wall temperature variations along the length of the channel. It is noted that as the heat input is increased from 1.32 to 2.12 W higher wall temperature values are experienced . It is observed that the greater heat input of 2.12 W cause the wall temperatures to rise sooner in the channel compared to the 1.32 W wall temperature profile. The modeled results illustrate that for 2.12 W of heat input the highest temperature region is expected to occur around 0.8 cm along the channel. This approximation is currently perceived to be early which is contributing to some of the differences in pressure drop expectations outlined in Figure 4.8. The modeled results for the wall temperatures along the length of the micro–channel are completed under the assumption that the fluid temperature corresponds to the saturation pressure value as well as accounting for the effects of heat input, channel dimension, single phase and two–phase heat transfer coefficients. Completing a mean absolute error analysis illustrate the predictions to be within a difference of 6% to the experimental data of Zhang et al., 2002.

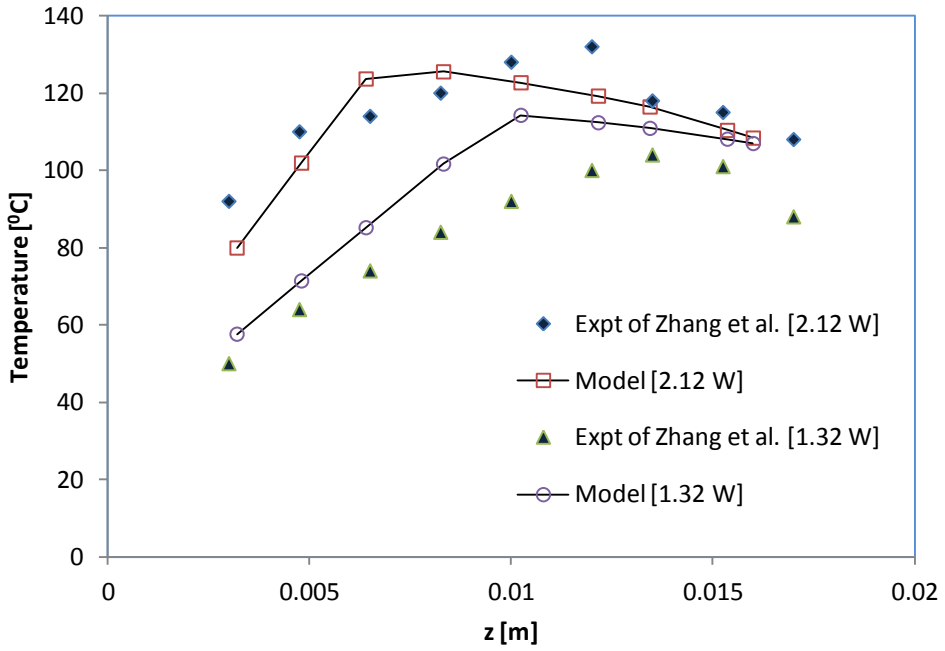

Figure 4.9 – Experimental Data: L = 1.6 cm, w = 50 µm, d = 70 µm, D_h = 60 µm, T_{IN} = 20^{0}C, P_{OUT} = 1.17 bar, $\dot{Q}$ = 0.1 mL/min [Adapted From: Zhang et al. – 2002]

The heat transfer coefficient results were not presented in the paper by Zhang et al., 2002, however two different versions of the Kandlikar correlation are employed to provide the heat transfer coefficient expectations for the experimental conditions conducted. The original Kandlikar correlation is restated in Equation [4.2] where further aspects regarding the method are presented in more detail in section 3.2 – 5. The Kandlikar enhancement factor expression is outlined in Equation [4.4] that account for the effects of vapour quality which has been used in the paper by Kelkar et al., 2005.

.

$$h_{conv} = h_L\left(C_1 C_o{}^{C_2}\left(25Fr_{lo}\right)^{C_5} + C_3 Bo^{C_4} F_{fl}\right) \quad [4.2]$$

$$h_{TP} = h_{SP,L}\max\left[h^E{}_{NBD}, h^E{}_{CBD}\right] \quad [4.3]$$

$$h^E{}_{NBD} = \left[0.6683 C_o{}^{-0.2} + 1058 Bo^{0.7} F_{fl}\right]\left[1 - x_v\right]^{0.8} \quad [4.4]$$

The average of the two Kandlikar correlation methods produced heat transfer coefficient results in the area of 110 000 W/m^2 K corresponding to the highest vapour quality of 0.20 for the operating conditions that include a heat flux of 2.12 W, fluid flow rate of 0.1 mL/min, temperature inlet 20^{0}C and outlet pressure of 1.17 bar. The estimated values were calculated for an approximate heat flux of 50 W/cm^2 based on the wetted perimeter for channel dimensions of width of 50 µm, depth of 70 µm and length of 2 cm. The heat transfer coefficient values were calculated from the 1.64 cm location of the entire 2 cm in length micro–channel.

The Kandlikar heat transfer coefficient correlation predictions were completed to provide a measure of comparsion to the values outlined in Bhide et al., 2009 that will be provided in the following section. It is important to note that the estimated values would be around 1 500 W/m^2 K higher if the channel length had only been 1.6 cm and the corresponding heat transfer coefficient values were calculated for the exit node. The two–phase estimates are significantly higher than the heat transfer coefficients for single phase flow which produced values around 5 000 W/m^2 K based on Equation [3.39].

However, it is also possible to estimate the liquid heat transfer coefficient through Equation [4.5] which accounts for aspect ratios greater than 1 for a channel. The estimates for the heat transfer coefficients regarding single phase flow from Equation [4.6] produce values around 30 000 W/m^2 K. Equation [4.6] has been incorporated into the work of Galvis and Culham, 2010 for heat transfer coefficient estimations corresponding to laminar single phase flow. Equation [4.6] had been incorporated into the calculations for wall temperature estimations in the single phase region.

$$h = \frac{Nu}{D_h} \qquad [4.5]$$

$$Nu = 7.541\left(1 - 2.61\beta^{-1} + 4.97\beta^{-2} - 5.119\beta^{-3} + 2.702\beta^{-4} - 0.548\beta^{-5}\right) \qquad [4.6]$$

The vapour quality is incorporated into the calculation of the Kandlikar heat transfer coefficient correlations. It is important to note that the exit vapour quality presented in Equation [4.7] can be solved for a different saturation temperature to that of 100^{0}C for water. The intersection saturation temperature between the single and two–phase region usually occurs at higher temperatures as illustrated in Figure 3.8 can be incorporated. The saturation temperature is considered to vary along the length of the channel corresponding to various experimental operating parameters. This particular element can become more important as the heat input is increased which can lead to differences regarding the required amount of heat to produce the corresponding vapour quality. The location along the length of the micro–channel that the heat transfer coefficient is calculated will have different estimates for vapour qualities that should also be considered. The exit vapour quality outlined in Equation [4.7] is calculated based on the wetted perimeter of the channel which only includes three of the four sides of the rectangular channel and neglects the top surface component.

$$x_e = \frac{1}{h_{LG}}\left[\frac{q'' P_{CH} L}{\dot{m}} - C_p\left[T_{SAT} - T_{IN}\right]\right] \qquad [4.7]$$

4.2 – 2 Experimental Data of Bhide et al. – 2009

The work of Bhide et al., 2009 was included for the experimental section as it had a comparable hydraulic diameter of 65 µm to 58.3 µm from the work of Zhang et al., 2002. Similar flow conditions were employed that enables some comparable discussion points. Section 2.6 – 2 discusses in more detail some of the experimental set up conditions involved for the work of Bhide et al., 2009. It is important to mention that the following micro–channel is one of a trapezoidal geometry where the channel dimensions are outlined in Table 4.1. Figure 4.10 provides a cross–sectional view of the channel to illustrate the calculations involved in expression [4.8]. The length of the micro–channel slant had not been noted in the paper and therefore was calculated based on the Pythagorean Theorem. The parameters of the experiment include a micro–channel length of 2 cm with a top width of 137 µm, bottom width of 62 µm and depth of 53 µm to produce a calculated slant length of 64.9 µm. The flow rate of water was 0.1 mL/min and the maximum inlet temperature was referenced to be 30 ^{0}C with an outlet pressure of 1.01325 bar since the experiment was opened to the atmosphere.

Table 4.1 – Trapezoidal Micro–Channel Dimensions [Adapted From: Bhide et al. – 2009]

	w_{Top} [µm]	w_{Bottom} [µm]	d [µm]	D_h [µm]
Channel	137	62	53	65

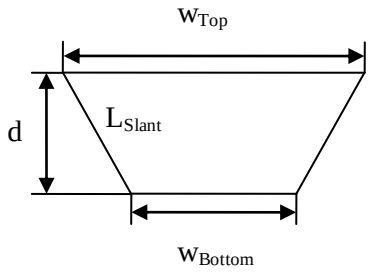

Figure 4.10 – Illustration of Trapezoidal Micro–Channel [Adapted From: Bhide et al. – 2009]

Equation [4.8] provides the definition for the heated perimeter of the channel where expression [4.9] provides the cross–sectional area for the trapezoidal geometry. Equation [4.8] had been used to establish the heat input in terms of Watts from the labeled W/m^2 expressions in presented in the figures by Bhide et al., 2009 in section 2.6 – 2.

$$A_P = (2L_{Slant} + w_{Bottom})L \quad [4.8]$$

$$A_{TZ} = 0.5(w_{Top} + w_{Bottom})d \quad [4.9]$$

It is presented in Bhide et al., 2009 that a direct linear relationship exists between the power loss and the temperature of the micro–channel surface. Additionally Bhide et al., 2009 corrected for the heat losses to air which occurred for the fluid before entering the micro–channel. The experimental data illustrated in the figures of section 2.6 – 2 account for the heat loss components. Thus the heat flux presented in their research paper is the amount of heat that is viewed to have reached the working fluid for the micro–channel under adadiatic conditions. It is important to note that the experimental pressure drop data was carried out over a mass flux of 442 kg/m^2 s.

Figure 4.11 illustrates the values for the homogeneous model approach that incorporated a friction factor of 0.004 to produce conservative pressure drop values compared to the experimental data. The weighted annular–homogeneous model calculated through utilizing the new outlined annular method along with the homogeneous model slightly envelopes the experimental data. The experimental results outlined by the diamond shaped data points in Figure 4.11 from Bhide et al., 2009 illustrates an initial decrease in pressure drop most notably from the changes in viscosity of water with respect to temperature. However, at approximately 0.6 W the experimental pressure drop data values start to increase as more heat is added and is where the boiling region is considered to start.

Completing the mean absolute error analysis expressed in Equation [4.1] for the average between the homogeneous and weighted annular–homogeneous model predictions illustrated in Figure 4.11 produced an error of 20%. It is important to note that the experimental data set for pressure drop are not exact and have a upper and lower degree of variation associated with pressure drop fluctuations that occur upon the onset of boiling within the single micro–channel.

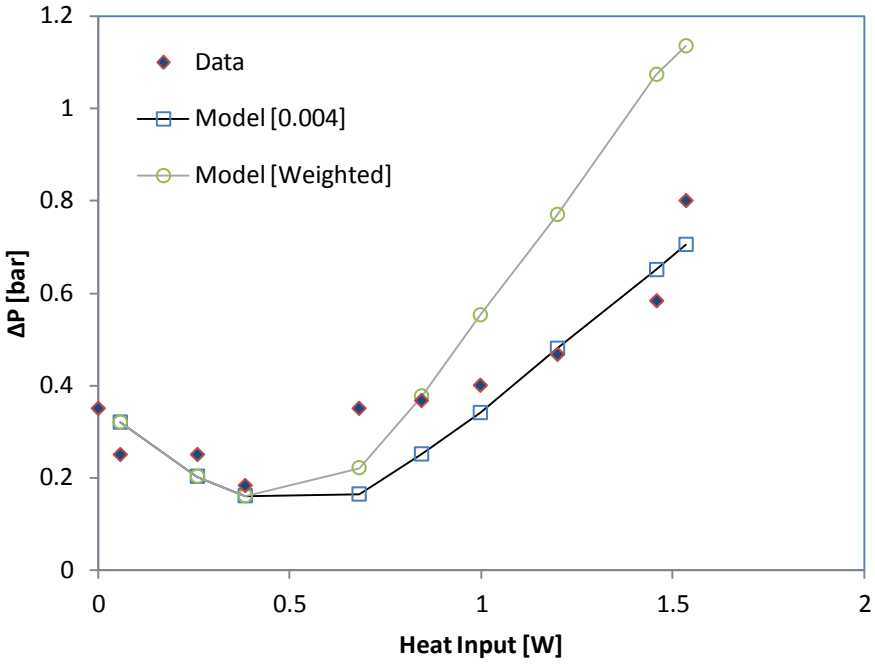

Figure 4.11 – Experimental Data: L = 2 cm, w_{TOP} = 137 µm, w_{BOTTOM} = 62 µm, z = 53 µm, D_h = 65 µm, T_{IN} = 30^{0}C, P_{OUT} = 1 bar, $\dot{Q}$ = 0.10 mL/min [Adapted From: Bhide et al. – 2009]

The variation in the experimental pressure drop data points in Figure 4.11 illustrates to some degree the effects of oscillations that are observed in various micro–channel experiments upon the onset of boiling. The fluctuations were greater than 0.2 bar over measured pressure drop data at higher heat fluxes which is outlined in more detail in the paper by Bhide et al., 2009. It was stated that such oscillation behavior was related to a buildup of pressure that would eventually displace a bubble formation involved with blocking the flow in the channel [Bhide et al. – 2009].

Completing the mean absolute error analysis for the model predictions in Figure 4.12 provides an estimated difference of 22%. Additional adjustments were made to account for the trapezoidal nature of the micro–channel to capture the heated perimeter and appropriate cross–sectional area. The model approach illustrates the capability to handle different geometries and the trends associated with the pressure drop over the course of various heat input conditions.

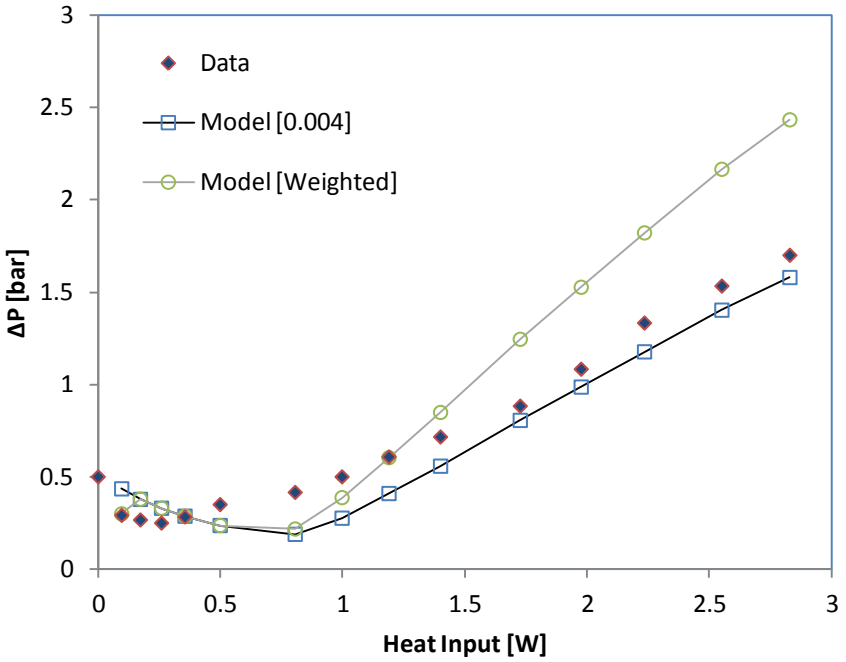

Figure 4.12 – Experimental Data: L = 2 cm, w_{TOP} = 137 µm, w_{BOTTOM} = 62 µm, z = 53 µm, D_h = 65 µm, P_{OUT} = 1 bar, T_{IN} = 30^{0}C, $\dot{Q}$ = 0.14 mL/min [Adapted From: Bhide et al. – 2009]

The heat transfer coefficient measurements were presented in the paper by Bhide et al., 2009 and are outlined by the diamond shaped data points in Figure 4.13. The values were measured at 1.65 cm location of the 2 cm in length micro–channel and under a mass flux of 448 kg/m^2 s for heat fluxes greater than 75 W/cm^2. The original Kandlikar correlation and the Kandlikar modification factor method that incorporates a correction term related to the vapour quality for the expected micro–channel operating conditions were evaluated.

The modeled heat transfer coefficient values were calculated from the 1.64 cm location of the 2 cm in length micro–channel compared to the measured results in work of Bhide et al., 2009. Figure 4.13 demonstrates a decreasing trend of the heat transfer coefficient from 80 000 to 60 000 W/m^2 K over vapour qualities of 0.10 to 0.46 [Bhide et al. – 2009].

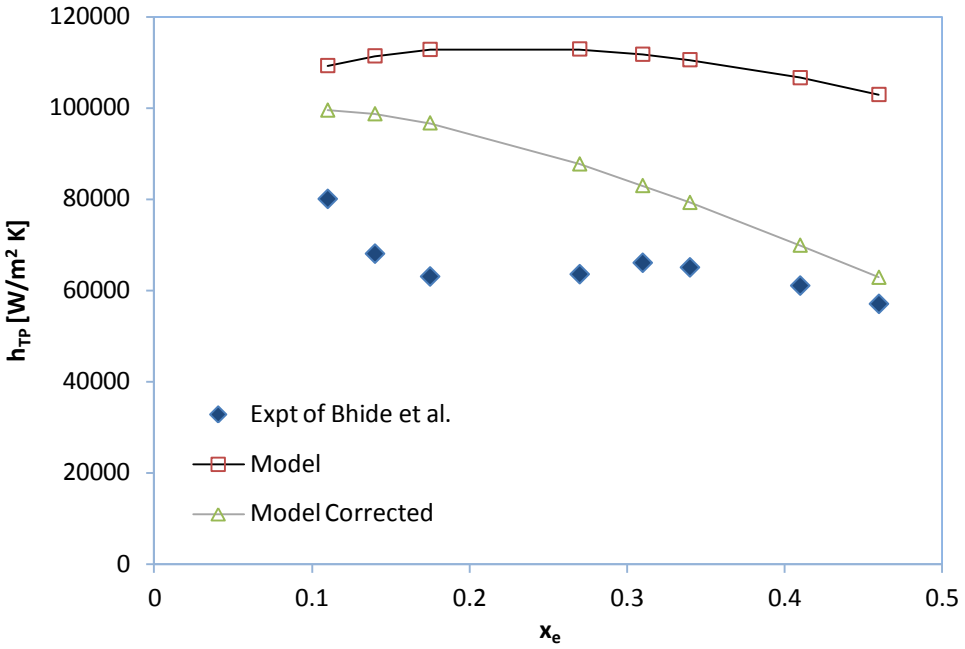

Figure 4.13 – Experimental Data: L = 2 cm, w_{TOP} = 137 µm, w_{BOTTOM} = 62 µm, z = 53 µm, D_h = 65 µm, P_{OUT} = 1 bar, T_{IN} = 30^{0}C, $\dot{Q}$ = 0.1424 mL/min [Adapted From: Bhide et al. – 2009]

The modeled results were based on the homogeneous flow approach with a friction factor of 0.004 that provided the necessary calculations for the fluid saturation temperature involved with determining the thermo–physical property variations along the length of the micro–channel associated with heat input. The heat transfer coefficient values are different at each location along the length of the channel. The vapour quality calculations were completed based on a constant thermodynamic equilibrium condition associated with a saturation temperature of 100^{0}C.

Figure 4.13 illustrates that the original Kandlikar correlation labeled as [Model] produced heat transfer coefficients that ranged from 100 000 to 110 000 W/m^2 K which did not capture the decreasing trend as pronounced as the Kandlikar enhancement term procedure identified as [Model Corrected]. The

Kandlikar enhancement term effectively captured the decreasing trend associated with the experimental data for the heat transfer coefficients values that ranged approximately from 100 000 W/m^2 K to 63 000 W/m^2 K. Completing a mean absolute error analysis for the original Kandlikar correlation produced a difference of 69% while the Kandlikar enhancement term method provided an estimated error of 29%.

To draw some comparisons to the modeled results for the experimental conditions carried out in Zhang et al., 2002 discussed in the previous section. The averaged heat transfer coefficients between the two Kandlikar correlation methods were estimated to be approximately 110 000 W/m^2 K, however these occurred for mass fluxes of approximately 475 kg/m^2 s. The heat transfer coefficient values were calculated at an estimated heat flux of 50 W/cm^2 for channel dimensions with width of 50 µm, depth of 70 µm and a hydraulic diameter of 58.3 µm for maximum vapour qualities of 0.2. A look into the Bhide et al., 2009 predictions for a vapour quality of 0.2 from the correlations presented in Figure 4.13 illustrate an average estimate of the Kandlikar correlations around 105 000 W/m^2 K. The experimental conditions associated with Bhide et al., 2009 include a hydraulic diameter of 65 µm for a mass flux of 448 W/m^2 K. Therefore the modeled heat transfer coefficient results are comparable to Zhang et al., 2002 where further increases in the mass flux from 448 to 475 W/m^2 K are expected to produce slightly greater calculated values for the work of Bhide et al., 2009. However the experimental data point from the work of Bhide et al., 2009 for the vapour quality of 0.2 regarding the heat transfer coefficient is about 60 000 W/m^2 K which illustrates that the Kandlikar correlation strongly overpredicts the result corresponding to that specific point.

4.2 – 3 Experimental Data of Qu and Mudawar – 2003

Section 2.6 – 3 outlines specific information concerning the experimental set up provided for the work of Qu and Mudawar, 2003. Figure 4.14 illustrates a single channel that is reproduced from Lee and Qu, 2006 to provide a conceptual understanding into the calculations completed for the heat transfer coefficient. Figure 4.14 outline the heat flux supplied to the bottom of the planform for the micro–channel heat sink [q''_{eff}], while the heat flux supplied to the heated perimeter of the channel is labeled as [q''_{p}].

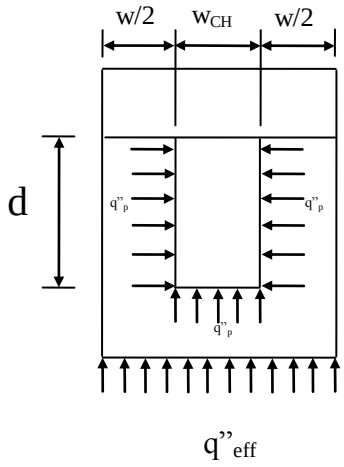

Figure 4.14 – Illustration of Heat Applied to a Single Channel [Adapted From: Lee and Qu – 2006]

The dimensions of the channel in the experiment by Qu and Mudawar, 2003 include a width of 231 µm a depth of 713 µm and a length of 4.48 cm. The inlet temperature was 60^0C and outlet pressure was maintained at 1.17 bar. The hydraulic diameter is calculated to be 349 µm and the mass flux had been 255 kg/m^2 s. The experimental results illustrate heat transfer coefficients that remained rather steady or slightly above 30 000 W/m^2 K over a vapour quality range of 0 to 0.20.

Equation [4.10] outlines the calculation for the effective heat flux based on the planform area that is utilized in the heat transfer coefficient results of Qu and Mudawar, 2003. Equation [4.11] provides the method to calculate the heat flux based on the wetted perimeter of the channel to determine the heat transfer coefficent. The heat flux value is incorporated into the Kandlikar correlation through the boiling number expression which impacts the calculated heat transfer coefficient.

$$q''_{eff} = \frac{P_{Supp}}{\left(2\frac{w}{2} + w_{CH}\right)L} \quad [4.10]$$

$$q''_{P} = \frac{P_{Supp}}{(2d + w_{CH})L} \quad [4.11]$$

Incorporating the heat flux associated with the planform area [q"$_{eff}$] will lead to the first model results to be discussed in Figure 4.15. The original Kandlikar correlation and the enhancement factor correlation are identified in Figure 4.15 as – Model [xe] and Model Corrected [xe] where the exit vapour quality had been based on the intersection thermodynamic equilibrium temperature which is generally greater than 100^{0}C for water. The vapour quality based on the saturation temperature of 100^{0}C for the original Kandlikar correlation and the enhancement factor version are identified as – Model [Tsat] and Model Corrected [Tsat]. The intersection temperature is identified between the single and two–phase regions which changes with operating conditions and usually occurs at higher temperatures to that of 100^{0}C for the saturation temperature of water at one atmosphere. However, It is seen from the results that there are very little difference between the calculated values corresponding to either method incorporating the intersection thermodynamic equilibrium temperature or the saturation temperature of 100^{0}C for water regarding this particular experimental case. It is important to mention that the heat transfer coefficient values were calculated from the 4.44 cm location of the channel.

The heat flux calculated from the planform area [q"$_{eff}$] is presented in Figure 4.15. The original Kandlikar correlation method provides values of 32 000 to 52 000 W/m^2 K over the vapour qualities range of 0 to 0.2 based on the intersection thermodynamic equilibrium temperature with a 500 to 1 500 W/m^2 K increased value compared to when calculated via the saturation temperature of 100^{0}C. The corrected method of the Kandlikar correlation provides slightly lower values of 31 000 to 50 000 W/m^2 K based on the intersection thermodynamic equilibrium temperature with about 1 000 W/m^2 K higher value

compared to when calculated via the saturation temperature of 100^0C. Completing the mean absolute error analysis on the orginial Kandlikar correlation and the Kandlikar enhancement term expression produces a range of 30% and 23% difference for the calculation based on the planform area concerning the estimated heat flux.

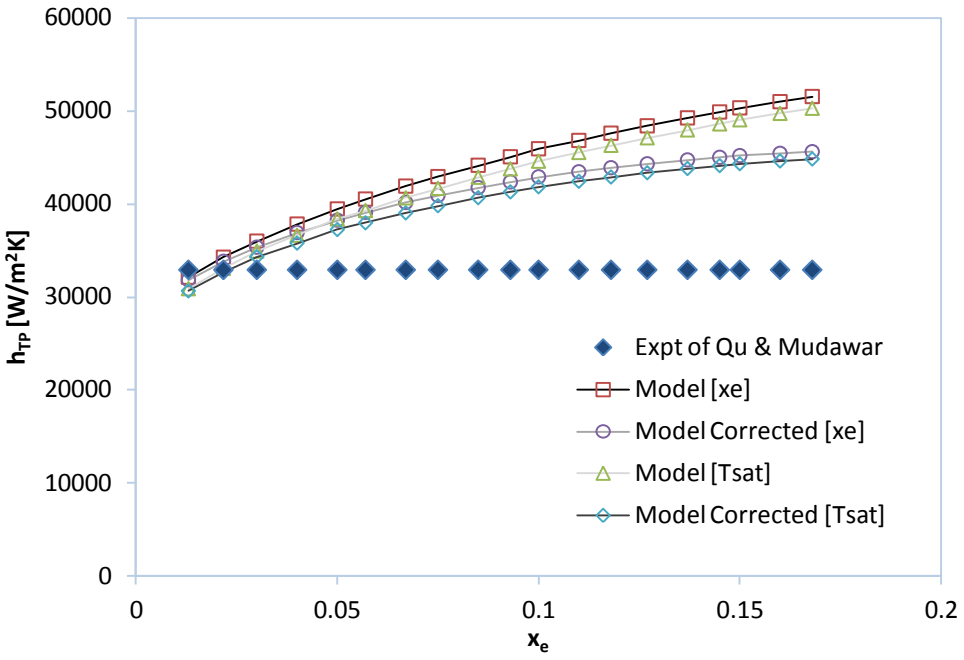

Figure 4.15 – Experimental Data: L = 4.48 cm, w = 231 µm, d = 713 µm, D_h = 349 µm, T_{IN} = 60^0C, P_{OUT} = 1.17 bar, $\dot{Q}$ = 2.56 mL/min [Adapted From: Qu and Mudawar – 2003]

Evaluating the heat flux based on the wetted perimeter area [q''_p] instead of the planform area [q''_{eff}] is outlined in Figure 4.16. The original Kandlikar correlation method provides values of 21 000 to 32 000 W/m^2 K over vapour qualities of 0 to 0.2 based on the intersection thermodynamic equilibrium temperature with about 400 to 1 000 W/m^2 K increased value difference compared to when calculated via the saturation temperature of 100^0C for water. The corrected method of the Kandlikar correlation provides slightly lower values of 21 000 to 29 000 W/m^2 K for the based on the intersection thermodynamic equilibrium temperature with about 300 to 600 W/m^2 K higher difference compared to when calculated via the saturation temperature of 100^0C for water. The model results illustrates a consistent increase for heat transfer coefficient values with greater vapour qualities. Higher heat transfer coefficient predictions are obtained when the heat flux is based on the planform area instead of

being calculated for the wetted perimeter of the channel. The mean absolute error analysis on the orginial Kandlikar correlation and the enhancement term expression produces a difference of 17% and 20% to experimental data for the calculation based on the saturation temperature of 100^0C for water over the length of the channel. A maximum error difference of about 2% lower is achieved for the heat transfer coefficient results that are calculated based on the intersection temperature.

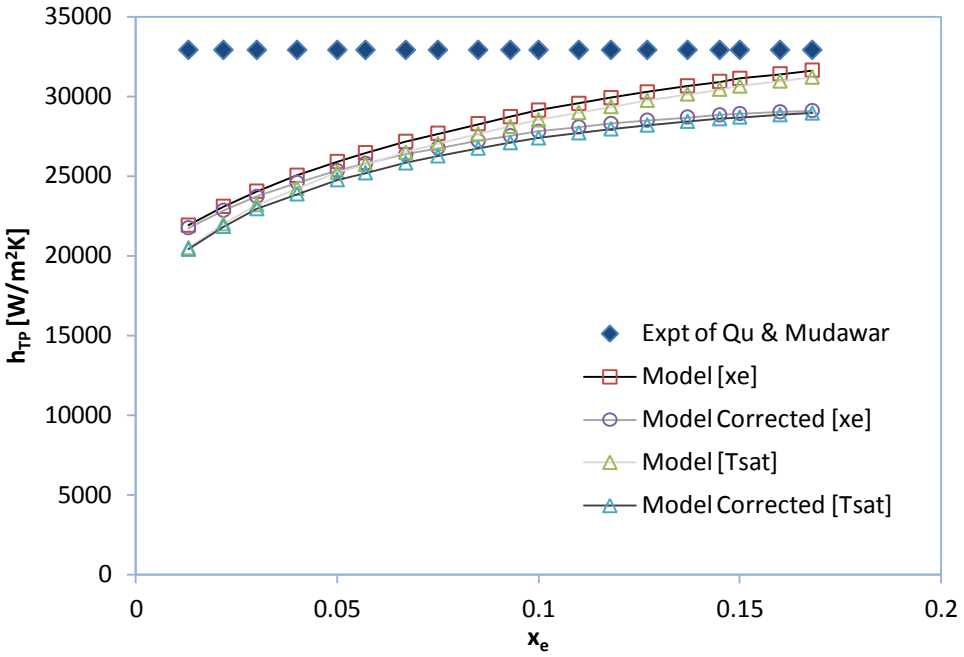

Figure 4.16 – Experimental Data: L = 4.48 cm, w = 231 µm, d = 713 µm, D_h = 349 µm, T_{IN} = 60^0C, P_{OUT} = 1.17 bar, $\dot{Q}$ = 2.56 mL/min [Adapted From: Qu and Mudawar – 2003]

The heat flux calculated via the wetted perimeter of the channel is generally employed to complete the heat transfer coefficient results as illustrated in Figure 4.16. The trend of the heat transfer coefficient experimental data begins to slightly decrease over an increase in vapour quality. If the model results are extrapolated past a vapour quality of 0.25 it is noted that the heat transfer coefficients start to follow the decreasing trend with further increases in vapour quality. The heat transfer coefficient results are more accurate for the operating area of interest regarding the two–phase flow region where the vapour qualities are usually greater than 0.05.

4.2 – 4 Experimental Data of Galvis and Culham – 2012

Section 2.6 – 4 outlines more detailed information in concern to the experimental set up conducted by Galvis and Culham, 2012. Figure 4.17 illustrates the available experimental heat transfer coefficient data for a single channel with dimensions that include a width of 471 µm, depth of 378 µm and length of 2.19 cm. The hydraulic diameter is calculated to be 419 µm where the inlet temperature is 50^0C with an outlet pressure of 1 bar and a fluid flow rate of 4 mL/min or mass flux of 364 kg/m^2 s. It is important to restate that the experiment was completed with no mechanisms to regulate the oscillating flow of vapour upon onset of nucleate boiling. Thus the channel experienced dryout and rewetting cycles which could have some effects on the heat transfer coefficient values.

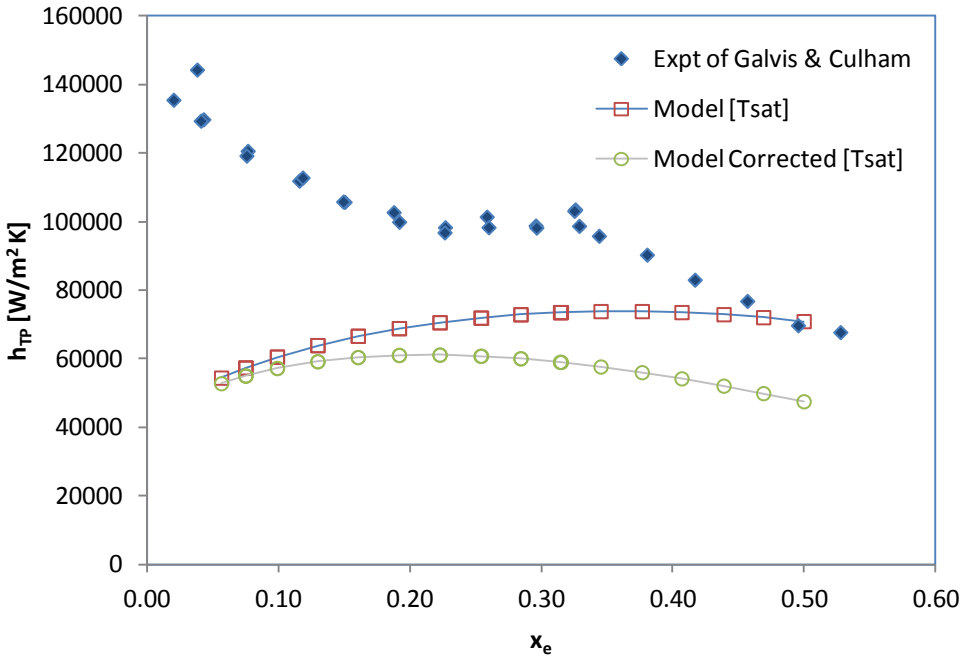

Figure 4.17 – Experimental Data: L = 2.19 cm, w = 471 µm, d = 378 µm, D_h = 419 µm, T_{IN} = 50^0C, P_{OUT} = 1 bar, $\dot{Q}$ = 4 mL/min [Adapted From: Galvis and Culham – 2012]

In Figure 4.17 it is observed that the heat transfer coefficient values follow a decreasing trend from vapour quality values close to 0.01 to 0.50. The heat transfer coefficients start at approximately 140 000 W/m^2 K and move towards values close to 70 000 W/m^2 K. It is the understanding that the heat transfer

coefficient values were determined at the exit length of the channel. The values were calculated by measurements based on the heat input that reached the fluid after accounting for heat losses divided by the difference between the wall temperature and the saturation temperature. The homogeneous model calculates the heat transfer coefficient via the original Kandlikar correlation and Kandlikar enhancement factor method where the heat flux term is based upon the wetted perimeter of the channel as previously discussed in section 4.2 – 3. The exit vapour quality is based on the saturation temperature of 100^0C for the original Kandlikar correlation and the Kandlikar enhancement factor method which are identified as – Model [Tsat] and Model Corrected [Tsat] in Figure 4.17.

The model calculated the heat transfer coefficient at the 2.19 cm location of the channel. It is observed that the Kandlikar correlation underpredicts the experimental heat transfer values especially at the very low vapour qualities and starts to converge towards the experimental data set at higher vapour qualities. Similiarly, the Kandlikar enhancement factor method underpredicts the values throughout the entire vapour quality range, however upon closer observation it is viewed that the corrected correlation does follow the decreasing heat transfer coefficient trend with increases in vapour quality. It is important to mention that there are sources of error in the experiment that included the temperature of the inlet steadily increasing with greater heat input. The experimental data outlined in Figure 4.17 had been completed with vapour quality calculations incorporating the saturation temperature of water to be below 100^0C.

A mean absolute error analysis from Equation [4.1] produces an error for the Kandlikar correlation of 31% and 42% for the Kandlikar enhancement factor method compared to the experimental data of Galvis and Culham, 2012. Incorporating some experimental uncertainty in the calculations will reduce the error margin, however the results are seen to be good since the operating conditions employed are much different than previous experimental data sets evaluated. It is important to mention that a decreasing trend in heat transfer coefficients is presented in Bhide et al., 2009. The work of Qu and Mudawar, 2003 did not experience as high of heat transfer coefficient values for similar channel dimensions, however the experiment had been completed under very different operating conditions. The heat fluxes completed in the single channel for Figure 4.17 were up to 300 W/cm^2.

Figure 4.18 illustrates pressure drop data for channel dimensions with width of 471 μm, depth of 378 μm and length of 2.19 cm. The inlet temperature is 50^0C with an outlet pressure of 1 bar and the fluid

flow rate is 4 mL/min. It is important to mention that the results outlined in Figure 4.18 are not available in the research literature and thus were not included in section 2.6 – 4. The experimental results illustrate similar behaviour to that expected for two–phase experiments where a sharper increase in pressure drop occurs after the onset of nucleate boiling. The experimental data for the single phase region seems to have a much higher pressure drop than compared to the modeled results. A possible explanation could be attributed to the channel being in developing flow which is not accounted for in the model as it had incorporated the fully developed laminar flow condition for single phase pressure drop calculations. Moreover oscillations in the experiment vary pressure drop values between an approximate difference of plus or minus 20 to 40%. Completing the mean absolute error calculation without accounting for the oscillations over the average between the homogeneous and weighted annular–homogeneous model produces a difference of 50%. However, if the oscillations are accounted for in the mean absolute error analysis for the average results of the homogeneous and weighted annular–homogeneous models a difference of approximately 30% is calculated.

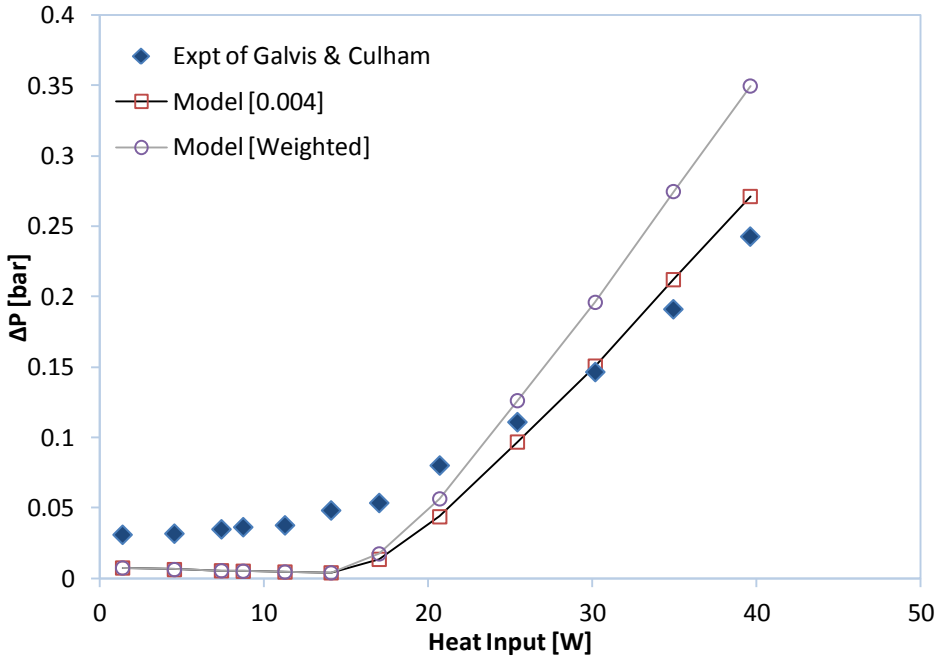

Figure 4.18 – Experimental Data: L = 2.19 cm, w = 471 µm, d = 378 µm, D_h = 419 µm, T_{IN} = 50^{0}C, P_{OUT} = 1 bar, $\dot{Q}$ = 4 mL/min [Adapted From: Galvis and Culham – 2012]

Figure 4.19 evaluates the heat transfer coefficients carried out in the experiment under the conditions of a fluid flow rate of 8 mL/min which is equivalent to a mass flux of 730 kg/m^2 s for the similar channel dimensions with width of 471 µm, depth of 378 µm and length of 2.19 cm. The inlet temperature is 50^{0}C and the outlet pressure is 1 bar. The heat transfer coefficient is calculated incorporating the saturation temperature to be 100^{0}C for determining the corresponding vapour quality of water. The Kandlikar correlation initially underpredicts the experimental heat transfer results at low vapour quality values and then starts to steadily rise to overpredict the heat transfer coefficient data. The Kandlikar enhancement correlation illustrates similar behaviour, however it is noticed that the model results start to follow the experimental data more closely than the original Kandlikar correlation. If the model is extrapolated past vapor qualities of 0.25 the Kandlikar enhancement factor correlation starts to follow the decreasing heat transfer coefficient trend which illustrates the relevance of correcting for vapor quality.

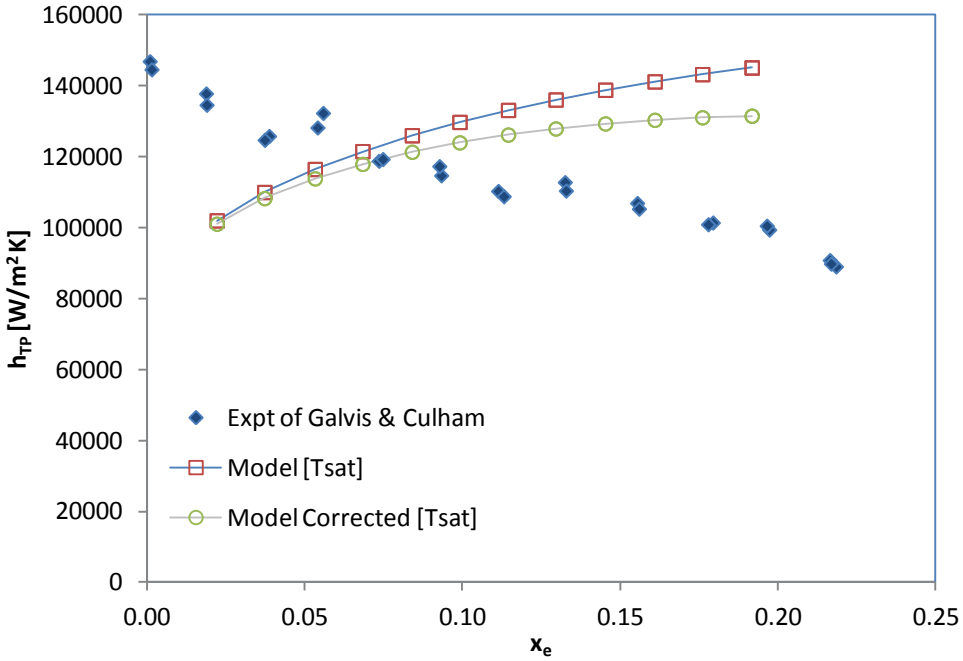

Figure 4.19 – Experimental Data: L = 2.19 cm, w = 471 µm, d = 378 µm, D_h = 419 µm, T_{IN} = 50^{0}C, P_{OUT} = 1 bar, $\dot{Q}$ = 8 mL/min [Adapted From: Galvis and Culham – 2012]

Completing an mean absolute error analysis will produce an approximate difference of 26% for the original Kandlikar correlation and 21% for the Kandlikar enhancement factor procedure.

4.3 Chapter 4 – Summary

Experimental data from four different reseachers that include Zhang et al., 2002, Bhide et al., 2009, Qu and Mudawar, 2003 along with Galvis and Culham, 2012 that ranged in channel dimensions of 50 µm to 713 µm were modeled to evaluate the accuracy of the assumptions utilized in the development of the homogeneous and weighted annular–homogeneous models. Details concerning these experimental set up are provided in sections 2.6 – 1 and 2.6 – 4 along with the certain operating condtions employed. The heat input calculations from the heat flux reported are based on the heated wetted area of the channel and not the base area of the heated chip as has been used in some of the published literature [Bertsch et al. – 2008]. Pressure drop, heat transfer coefficient, vapour qualities and wall temperature profile are calculated by the model for independent experimental data sets under various operating conditions. The model approximates the pressure drop and heat transfer coefficient results within a reasonable error of approximately 30%. The results are significant due to the fact that simplified assumptions were able to effectively capture different experimental data sets for various geometries and operating conditions. The model had been developed in Excel using 50 nodes over the length of the channels to faciliate the numerical calculations based on the finitie difference method. It further demonstrates that the homogeneous model is a good base, however the weighted annular–homogeneous model provides an effective upper bound estimate for the pressure drop calculations.

The presented relationship between the vapour quality and the heat transfer coefficient illustrate some similar results and trends compared to experimental data sets. The experimental heat transfer coefficient results were in the range of 80 000 to 60 000 W/m^2 K for the trapezoidal micro–channel experiment by Bhide et al., 2009. Values for heat transfer coefficients included 30 000 W/m^2 K for the work of Qu and Mudawar, 2003 as well as 140 000 W/m^2 K to 70 000 W/m^2 K for the experiments by Galvis and Culham, 2012. Not all details were readily provided in the literature for some of the experimental and model results completed. Pressure oscillations were noted to occur in all experimental data sets for the single channel investigated after the onset of boiling. The heat transfer coefficient values calculated by Kandlikar's two correlations for the two–phase region exceeded 110 000 W/cm^2 K. Experimental data sets and model results had been completed for heat fluxes ranging from 50 W/cm^2 to values up to 300 W/cm^2.

CHAPTER 5
CONCLUSIONS & RECOMMENDATIONS

Model results are evaluated over four independent experimental data sets available in the research literature which demonstrated sufficient accuracy for channel dimensions ranging from 50 μm to 713 μm. The independent experimental data sets were numerically reproduced from figures presented in the literature. The simplified homogeneous model that employed the empirical friction factor of 0.004 provided effective lower bound pressure drop results and the weighted annular–homogeneous model produced reasonable upper bound values. The values between the homogeneous and weighted annular–homogeneous model results regarding pressure drop calculations were averaged to determine the mean absolute error calculations of the predictions compared to experimental data sets. The modeled pressure drop results for a single channel were within a 30% mean absolute error over the four experimental data sets evaluated for heat fluxes ranging from 50 W/cm^2 up to 300 W/cm^2.

The pressure drop model calculations effectively demonstrated the decreasing trend in the single phase region due to the viscosity changes of water with temperature. Increases in pressure drop values associated with the two–phase region were captured by the homogeneous and weighted annular–homogeneous models. Pressure fluctuations were noted to occur in all experimental data sets for a single channel after the onset of boiling. The one–dimensional application of the finite difference method that included 50 nodes to describe the length of a channel had demonstrated to be an effective approach towards calculating the heat transfer coefficient and pressure drop in the micro–channel flow boiling [two–phase] region over a wide range of operating conditions. A wall temperature profile had been compared to the experimental work of Zhang et al., 2002 and provided a mean absolute error of 6%.

Heat transfer coefficient calculations were made via the original Kandlikar correlation and the Kandlikar enhancement term method which is corrected for vapour quality. The heat transfer coefficient values calculated by the two methods produced a mean absolute error of approximately 30% for all experimental data investigated. The Kandlikar enhancement correlation method better captured the heat transfer coefficient trend for the majority of the experimental data sets. The heat transfer

coefficient predicted values calculated for the work of Zhang et al., 2002 were comparable to the modeled results of Bhide et al., 2009 for a single micro–channel of similar dimensions and operating conditions. Calculated two–phase heat transfer coefficients reached values greater than 110 000 W/cm^2 K which are much greater than values achieved by single phase flow.

The modeled heat transfer coefficient calculations completed for the experimental work of Qu and Mudawar, 2003 were determined by incorporating two different values for the heat flux. The heat flux values implemented in the heat transfer coefficient calculations were completed from two methods that included one based on the planform area of the channel and the other derived from the wetted perimeter. It was found that the heat transfer coefficients calculated via the wetted perimeter produced better results with a lower error margin. Heat transfer coefficient and vapour qualities values calculated based on the intersection temperature which is usually greater than 100^{0}C for water along with predictions with the saturation temperature of 100^{0}C corresponding to water at one atmosphere were illustrated to provide similar results.

In conclusion the significance of the model in the present thesis illustrates that simplified assumptions are capable of handling various operating conditions and providing results with a mean absolute error margin of 30% for pressure drop and heat transfer coefficient calculations. Therefore it is recommended that should two–phase flow pattern maps not be readily available that the homogeneous model be employed with the empirical friction factor of 0.004 to provide a lower bound estimate for pressure drop calculations. An upper bound pressure drop result can be obtained by the weighted annular–homogeneous model which is considered important as fluctuations are noted to occur in the flow boiling [two–phase] region that can lead to higher pressure drop values. Additionally, great care should be exercised for the mathematical relationships applied to calculate pressure drop and heat transfer coefficient results.

Micro–channel technology is already being incorporated into industrial applications such as video cards. It has been stated that once the micro–channel technology has been employed, it is expected to last for approximately 20 years thereafter [Venere – 2005]. Micro–channel heat sink designs employing two–phase flow are capable of effectively addressing heat fluxes well over 150 W/cm^2. Micro–channels incorporating two–phase flow could be expected to be incorporated into various design applications in the next 1 to 3 years.

Recommendations for future work include the following:

1) The model could be expanded to incorporate the non–uniform heat flux condition to better predict additional operating environments.

2) The number of nodes utilized for the numerical analysis could be increased to further the accuracy of the pressure drop and heat transfer coefficient calculations.

3) Optimization techniques that include the reduction of entropy could be employed to better serve micro–channel designs.

4) The model could be further developed to estimate pressure drop and heat transfer coefficients for multi micro–channel designs.

5) Completing experimental data for heat flux applications in the range of 100 – 300 W/cm^2 or greater would provide more results to validate models to higher heat flux operating conditions.

6) Different heat transfer coefficient correlations could be evaluated over experimental data sets to determine the most accurate method.

REFERENCES

[1] Agarwal A., Garimella S. [2006] Modeling of Pressure Drop During Condensation in Circular and Non-Circular Micro–Channels. Proceedings of IMECE 2006 – ASME International Mechanical Engineering Congress and Exposition, November 5 – 10, Chicago, Illinois, USA

[2] Agostini B., Fabbri M., Park, J. E., Wojtan L., Thome, J. R., Michel B. [2007] State of the Art of High Heat Flux Cooling Technologies. Heat Transfer Engineering – Vol 28 [4], PP 258 – 281

[3] Asako Y., Hong C., Miwa J, Faghri M. [2006] Performance of Gaseous Parallel–Flow Micro–Exchangers. Proceedings of IMECE 2006 – ASME International Mechanical Engineering Congress and Exposition, November 5 – 10, Chicago, Illinois, USA

[4] Ashrae Handbook – Fundamentals – SI Edition [1997] American Society of Heating, Refrigerating and Air–Conditioning Engineers Inc, Atlanta, USA, PP 1.1 – 4.16

[5] Bahrami M., Yovanovich M. M., Culham J. R. [2006] A Novel Solution for Pressure Drop in Singly Connected Micro–channels of Arbitrary Cross–Section. International Journal of Heat and Mass Transfer – Vol 50 [13–14], PP 2492 – 2502

[6] Bejan A., Kraus A. D. [2003] Heat Transfer Handbook. New Jersey – John Wiley and Sons, Inc

[7] Bergles A. E., Lienhard V J. H., Kendall G. E., Griffith P. [2003] Boiling and Evapouration in Small Diameter Channels. Heat Transfer Engineering 24 [1], PP 18 – 40

[8] Bertsch S. S., E. A. Groll, S. V. Garimella [2008] Review and Comparative Analysis of Studies on Saturated Flow Boiling in Small Channels. Nanoscale and Microscale Thermophysical Engineering – Vol 12 [3], PP 187 – 227

[9] Bhide R. R., Singh S. G., Sridharan A., Duttagupta S. P., Agrawal A. [2009] Pressure Drop and Heat Transfer Characteristics of Boiling Water in Sub–Hundred Micron Channel. Experimental Thermal and Fluid Science – Vol 33, PP 963 – 975

[10] Billo E. J. [2007] Excel – for Scientists and Engineers. New Jersey – John Wiley and Sons, Inc

[11] Bird R. B., Stewart W. E., Lightfoot E. N. [2002] Transport Phenomena – Second Edition. New York – John Wiley and Sons, Inc

[12] Blazek J. [2001] Computational Fluid Dynamics: Principles and Applications New York – Elsevier

[13] Bowers M. B., Mudawar I. [1994] High Flux Boiling in Low Flow Rate, Low Pressure Drop Mini–Channel and Micro–Channel Heat Sinks. International Journal of Heat and Mass Transfer – Vol 37 [2], PP 321 – 332

[14] Cabral P. S., Lam T. T. [2003] Boundary Effect on Temperature Gradients in Micro–Channels. Proceedings of IPACK03 – International Electronic Packaging Technical Conference and Exhibition, July 6 – 11, Maui, Hawaii, USA

[15] Chang J–Y., Prasher R., Chau D., Myers A., Dirner J., Prstic S., He D. [2005] Convective Performance of Package Based Single Phase Micro – Channel Heat Exchanger. Proceedings of IPACK 2005 – ASME InterPack'05, July 17 – 22, San Francisco, California, USA

[16] Chein R., Huang G. [2005] Analysis of Micro–channel Heat Sink Performance Using Nanofluids. Applied Thermal Engineering – Vol 25, PP 3104 – 3114

[17] Chen Q., Xin M., Amano R. S. [2004] Experimental Study of R134A Condensation Heat Transfer Inside the Horizontal Micro – Fin Tubes. Thermal and Thermomechanical Phenomena in Electronic Systems 2004, ITHERM'04. The Ninth Intersociety Conference, June 1 – 4, Las Vegas, NV, Vol 2, PP 40 – 46

[18] Chen T., Garimella S. V. [2005] Flow Boiling Heat Transfer to a Dielectric Coolant in a Micro–Channel Heat Sink. Proceedings of IPACK 2005 – ASME InterPack'05, July 17 – 22, San Francisco, California, USA

[19] Collier J. G., Thome J. R. [1994] Convective Boiling and Condensation – 3rd Edition. New York – Oxford University Press Inc

[20] Collado F. J., Monné C., Pascau A., Fuster D., Medrano A. [2005] Thermodynamics of Void Fraction in Saturated Flow Boiling. Journal of Heat Transfer – Vol 128 [6], PP 611 – 615. Retrieved From Link – http://www.lmm.jussieu.fr/~fuster/ASME-J.HeatTransfer%2005.pdf

[21] David M. P., Steinbrenner J. E., Miler J., Goodson K. E. [2011] Adiabatic and Diabatic Two–Phase Venting Flow in a Micro–Channel. International Journal of Multiphase Flow – Vol 37, PP 1135 – 1146

[22] Dickey J. T., Lam T. T. [2003] Heat Transfer in Triangular Micro–Channels. Proceedings of IPACK03 – International Electronic Packaging Technical Conference and Exhibition, July 6 – 11, Maui, Hawaii, USA

[23] Dong M., Chatzis I. [2004] An Experimental Investigation of Retention of Liquids in Corners of a Square Capillary. Journal of Colloid and Interface Science – Vol 273, PP 306 – 312

[24] Felder R. M., Rousseau R. W. [2000] Elementary Principles of Chemical Processes New York – John Wiley and Sons, Inc

[25] Fushinobu K., Tokushige M., Nakata M., Okazaki K. [2004] Novel Flow Control Concepts in Micro–Channels. Thermal and Thermomechanical Phenomena in Electronic Systems 2004, ITHERM'04. The Ninth Intersociety Conference, June 1 – 4, Las Vegas, NV,

[26] Galvis E., Culham J. R. [2010]. Lower Entropy Generation in Micro–Channels with Laminar Single Phase Flow. Proceedings of the 8th International Conference on Nano–Channels, Micro–Channels and Mini–Channels. ICNMM2010 – August 1 – 5, Montreal, Canada

[27] Galvis E., Culham J. R. [2012] Measurement and Flow Pattern Visualizations of Two–Phase Flow Boiling in Single Channel Microevaporators. International Journal of Multiphase Flow – Vol 42, PP 52 – 61

[28] Geankoplis C. J. [1993] Transport Processes and Unit Operations – Second Edition. Massachusetts – Allyn and Bacon Inc

[29] Goldstein R. J., Eckert E. R. G., Ibele W. E., Patankar S. V., Simon T. W., Kuehn T. H., Strykowski P. J., Tamma K. K., Bar–Cohen A., Heberlein J. V. R., Davidson J. H., Bischof J., Kulacki F. A., Kortshagen U., Garrick S., Srinivasan V. [2005] Heat transfer – A Review of 2002 Literature. International Journal of Heat and Mass Transfer – Vol 48, PP 819 – 927

[30] Gottfried B. S. [2003] Spreadsheet Tools for Engineers Using Excel. New York – McGraw–Hill

[31] Harirchian T, and Garimella S V. [2012] Flow Regime–Based Modeling of Heat Transfer and Pressure Drop in Micro–Channel Flow Boiling, International Journal of Heat and Mass Transfer – Vol 55, PP 1246 – 1260

[32] Herescu A., Allen J. S. [2006] Compressibility Effects in the Gas Phase for Unsteady Annular Two –Phase Flow in a Micro–Channel. Proceedings of IMECE 2006 – ASME International Mechanical Engineering Congress and Exposition, November 5 – 10, Chicago, Illinois, USA

[33] Hernandez J. E., Allen J. S. [2006] Spontaneous Liquid–Liquid Slug Flow in Micro–Channels. Proceedings of IMECE 2006 – ASME International Mechanical Engineering Congress and Exposition, November 5 – 10, Chicago, Illinois, USA

[34] Herwig H., Mahulikar S. P. [2006] Variable Property Effects in Single–Phase Incompressible Flows Through Micro–Channels. International Journal of Thermal Sciences Vol – 45, PP 977–979

[35] Hewitt G. F., Hall–Taylor N. S. [1970] Annular Two–Phase Flow. Oxford – Pergamon Press

[36] Hrnjak P., Tu X. [2007] Single Phase Pressure Drop in Micro–Channels. International Journal of Heat and Fluid Flow – Vol 28 [1], PP 2 – 14

[37] Ishii M., Hibiki T. [2006] Thermo–Fluid Dynamics of Two–Phase Flow – Volume I and Volume II. New York – Springer

[38] Iyengar M., Garimella S. [2006] Design and Optimization of Micro–Channel Cooling Systems. Thermal and Thermomechanical Phenomena in Electronics Systems, ITHERM'06. The Tenth Intersociety Conference, May 30 – June 2, San Diego, California, PP 54 – 62

[39] Jang S. P., Kim S. J. [2003] Fluid Flow and Thermal Characteristics for a Micro–Channel Heat Sink Subject to an Impinging Jet. Proceedings of IPACK03 – International Electronic Packaging Technical Conference and Exhibition, July 6 – 11, Maui, Hawaii, USA

[40] Jensen M. K., Peles Y., Kosar A, Kuo C–J. [2006] Methods and Preliminary Results on Enhanced Boiling Heat Transfer in Second Generation Micro–channels. Microfluid Nanofluid – Vol 2, PP 387 – 397

[41] Jones W. K., Zampino M., Kappagantula S. [2005] Jet Impingment Cooling Using Micro–Channel in Low Temperature Cofire Ceramic [LTCC] Substrates. Proceedings of IPACK 2005 – ASME InterPack'05, July 17 – 22, San Francisco, California, USA

[42] Kandlikar S. G. [1990] A General Correlation for Saturated Two – Phase Flow Boiling Heat Transfer Inside Horizontal and Vertical Tubes. Journal of Heat Transfer – Vol 112, PP 219 – 228

[43] Kandlikar S. G. [2004] Heat Transfer Mechanisms During Flow Boiling in Micro–Channels. Journal of Heat Transfer – Vol 126, PP 8 – 16

[44] Kandlikar S. G. [2005] High Flux Heat Removal with Micro–Channels – A Roadmap of Challenges and Opportunities. Proceedings of ICMM2005 – 3rd International Conference on Micro–Channels and Mini–Channels, June 13 – 15, Toronto, Ontario, Canada

[45] Kandlikar S., Garimella S., Li D., Colin S., King M. R. [2006] Heat Transfer and Fluid Flow in Mini–Channels and Micro–Channels. The Boulevard, Langford Lane Kidlington, Oxford – Elsevier Ltd

[46] Kandlikar S. G., Grande W. J. [2003] Evolution of Micro–channel Flow Passages – Thermohydraulic Performance and Fabrication Technology. Heat Transfer Engineering Vol 24 [1], PP 3 – 17

[47] Kelkar K. M., Patankar S. V., Kang S. [2005] Computational Method for Characterization of a Micro–Channel Heat Sink Involving Two–Phase Flow. Proceedings of IPACK 2005 – ASME InterPack'05, July 17 – 22, San Francisco, California, USA

[48] Kelkar K. M., Patankar S. V., Kang S. [2006] Computational Method for Characterization of a Micro–Channel Heat Sink With Multiple Channels Involving Two–Phase Flow. Thermal and Thermomechanical Phenomena in Electronics Systems, ITHERM'06. The Tenth Intersociety Conference, May 30 – June 2, San Diego, California, PP 33 – 44

[49] Khan W. A., Yovanovich, M. M. [2008] Analytical Modeling of Fluid Flow and Heat Transfer in Micro–Channel/Nano–Channel Heat Sinks. Journal of Thermophysics and Heat Transfer – Vol 22 [3], PP 352 – 359

[50] Koo J–M., Im S., Jiang L., Goodson K. E. [2005] Integrated Micro–Channel Cooling for Three–Dimensional Electronic Circuit Architectures. Journal of Heat Transfer – Vol 127, PP 49 – 58

[51] Koo J–M., Jiang L., Bari A., Zhang L., Wang E., Kenny T. W., Santiago J. G., Goodson K. E. [2002] Convective Boiling in Micro–Channel Heat Sinks with Spatially–Varying Heat Generation. Thermal and Thermomechanical Phenomena in Electronics Systems, ITHERM'06. The Eighth Intersociety Conference, May 30 – June 2, San Diego, California, PP 341 – 346

[52] Koo J–M., Jiang L., Zhang L., Zhou P., Banerjee S., Kenny T. W., Santiago J. G., Goodson K. E. [2001] Modeling of Two–Phase Micro–Channel Heat Sinks for VIS1 Chips. Proceedings 14th IEEE Conference on MEMS, Interlaken, Switzerland, Jan 21 – 25, PP 422 – 426

[53] Kreith F. [2000] The CRC Handbook of Thermal Engineering. Boca Raton – CRC Press LLC

[54] Kundu R. K., Cohen I. M. [2002] Fluid Mechanics – Second Edition. San Diego, USA – Academic Press

[55] Lai W. M., Rubin D., Krempl E. [2002] Introduction to Continuum Mechanics – Third Edition. Butterworth – Heinemann Ltd, Burlington, Massachusetts, USA

[56] Lasance C. J. M., Simons R. E. [2005] Advances in High Performance Cooling for Electronics. Retrieved November 23, 2010 – From Link – http://www.electronics-cooling.com/2005/11/advances-in-high-performance-cooling- for-electronics/

[57] Lee J., Mudawar I. [2005] Two–Phase Flow in High–Heat–Flux Micro–Channel Heat Sinks for Refrigeration Cooling Applications: Part I – Pressure Drop Characteristics. International Journal of Heat and Mass Transfer – Vol 48, PP 928 – 940

[58] Lee J., Mudawar I. [2005] Two–Phase Flow in High–Heat–Flux Micro–Channel Heat Sinks for Refrigeration Cooling Applications: Part II – Heat Transfer Characteristics. International Journal of Heat and Mass Transfer – Vol 48, PP 941 – 955

[59] Lee P–S., Garimella S. V., Liu D [2005] Investigation of Heat Transfer in Rectangular Micro–Channels. International Journal of Heat and Mass Transfer – Vol 48, PP 1688 – 1704

[60] Lee S., Qu W. [2006] Thermal Design Methodology for Low Flow Rate Single–Phase and Two–Phase Micro–Channel Heat Sinks. Thermal and Thermomechanical Phenomena in Electronic Systems 2006, ITHERM'06. The Tenth Intersociety Conference, May 30 – June 2, San Diego, CA, PP 19 – 32

[61] Liu C. W., Gau C., Ko H. S., Yang C. S., Dai B.T. [2006] Fabrication Challenges for a Complicated Micro–Flow Channel System at Low Temperature Process. TRANDUCERS'05 – The 13th International Conference on Solid–State Sensors and Actuators and Microsystems. June 5 – 9, Seoul, Korea – Vol 130 – 131, PP 575 – 582

[62] Liu D., Garimella S. V. [2003] Analysis and Optimization of the Thermal Performance of Micro–Channel Heat Sinks. Proceedings of IPACK03 – International Electronic Packaging Technical Conference and Exhibition, July 6 – 11, Maui, Hawaii, USA

[63] Liu D., Garimella S. V. [2007] Flow Boiling Heat Transfer in Micro–Channels. Journal of Heat Transfer – Vol 129, PP 1321 – 1332

[64] Liu J–T, Peng X–F, Yan W–M [2007] Numerical Study of Fluid Flow and Heat Transfer in Micro–channel Cooling Passages. International Journal of Heat and Mass Transfer – Vol 50, PP 1855 – 1864

[65] Marghitu D. B. [2001] Mechanical Engineer's Handbook. Academic Press – San Diego, USA

[66] Mayer P. M., Ram R. J. [2006] Optimization of Heat Sink Limited Thermoelectric Generators. Nanoscale and Microscale Thermophysical Engineering 10, PP 143 – 156

[67] Michel B., Glatz W., Smith B. [2009] Mini – and Micro–channels in Thermal Interfaces: Spatial, Temporal, Material and Practical Significance. Electronics Cooling – IBM Zurich Research Laboratory. Retrieved From Link – http://www.electronics-cooling.com/2009/02/mini-and-microchannels-in-thermal-interfaces-spatial-temporal-material-and-practical-significance/

[68] Miller C. A., Neogi P [1985] Interfacial Phenomena – Equilibrium and Dynamic Effects, Surfactant Science Series. Marcel Dekker: New York

[69] Mo H. L., Prattipati R., Lin C. X. [2005] Experimental Study of Liquid Flow and Heat Transfer in Micro–Channels with In – Line Array of Cubes. Proceedings of HT2005 – ASME Summer Heat Transfer Conference, July 17 – 22, San Francisco, California, USA

[70] Moreno R. M., Tao Y–X [2006] Thermal and Flow Performance of a Microconvective Heat Sink with Three–Dimensional Constructal Channel Configuration. Journal of Heat Transfer – Vol 128, PP 740 – 752

[71] Mudawar I. [2001] Assessment of High – Heat – Flux Thermal Management Schemes. IEEE Transactions on Components and Packaging Technologies – Vol 24 [2], PP 122 – 141

[72] Mukherjee S., Mudawar I. [2002] Smart, Low–Cost, Pumpless Loop for Micro–Channel Electronic Cooling Using Flat and Enhanced Surfaces. 2002 Inter Society Conference on Thermal Phenomena, PP 360 – 370

[73] Mukherjee S., Mudawar I. [2003] Pumpless Loop for Narrow Channel and Micro–Channel Boiling. ASME Journal of Electronic Packaging – Vol 125, PP 431 – 441

[74] Müller N., Fréchette L. G. [2002] Optimization and Design Guidelines for High Flux Micro–Channel Heat Sinks for liquid and Gaseous Single–Phase Flow. 2002 Inter Society Conference on Thermal Phenomena, PP 449 – 456

[75] Nakayama W. [2006] Heat Sinks – Exploring the Limits of Air Cooling. Electronics Cooling Magazine. Retrieved December 2, 2012 From – http://staging.electronics-cooling.com/2006/08/exploring-the-limits-of-air-cooling/

[76] Nextreme Thermal Solutions Inc. [2006] Cooling Hot Spots on High Performance CMOS ICs. Retrieved November 29, 2012 From – http://www.nextremethermal.com/media/pdf/nextreme_cooling_hotspots.pdf

[77] Nickerson J. L., Cerza M., Garcia S. M. F. [2007] Modeling Bubble Growth in Micro–Channel Cooling Systems. Proceedings of IMECE 2007 – ASME International Mechanical Engineering Congress and Exposition, November 11 – 15, Seattle, Washington, USA

[78] Ohadi, M. M. [2007] A Self-Contained System for Thermal Management of Next Generation High Heat Flux Electronics. 7th Annual Business and Technology Summit – August 22 – 23, Natrick, MA

[79] Ouderkirk R. [2002] Rigorously Size Relief Valves for Supercritical Fluids, CEP, PP 34 – 43

[80] Palm B. [2001] Review – Heat Transfer in Micro–Channels. Microscale Thermophysical Engineering – Vol 5, PP 155 – 175

[81] Pang A. J., Desmulliez M. P. Y., Leonard M., Dhariwal R. S., Reuben R. L., Holmes A. S., Hong G., Pullen K. R., Waldron F., Slattery O., Rencz M., Emerson D. R., Barber R. W. [2004] Design, Manufacture, and Testing of a Low Cost Micro–Channel Cooling Device. 2004 Electronics Packaging Technology Conference, PP 564 – 568

[82] Park H. S., Punch J. [2008] Friction Factor and Heat Transfer in Multiple Micro–Channels with Uniform Flow Distribution. International Journal of Heat and Mass Transfer – Vol 51 [17–18], PP 4535 – 4543

[83] Pate D. T., Jones R. J., Bhavnani S. H. [2006] Cavity–Induced Two–Phase Heat Transfer in Silicon Micro–Channels. Thermal and Thermomechanical Phenomena in Electronic Systems 2006, ITHERM'06. The Tenth Intersociety Conference, May 30 – June 2, San Diego, CA, PP 71 – 78

[84] Patterson M. K., Wei X., Joshi Y., Prasher R. [2004] Numerical Study of Conjugate Heat Transfer in Stacked Micro–Channels. Thermal and Thermomechanical Phenomena in Electronic Systems 2004, ITHERM'04. The Ninth Intersociety Conference, June 1 – 4, Las Vegas, NV, Vol – 2, PP 372 – 380

[85] Phelan P. E., Chiriac V. A., Lee T–Y. T. [2002] Current and Future Miniature Refrigeration Cooling Technologies for High Power Microelectronics. IEEE Transactions on Components, and Packaging Technology – Vol 25 [3], PP 356 – 365

[86] Phillips R. J. [1988] Forced–Convection, Liquid–Cooled, Micro–channel Heat Sinks – MASc Thesis. Massachusetts Institute of Technology – Lincoln Laboratory – Department of Mechanical Engineering. Retrieved From – http://dspace.mit.edu/handle/1721.1/14921

[87] Prasher R. S., Dirner J., Chang J–Y., Myers A., Chau D., Prstic S., He D. [2005] Effect of Localized Hotspot on the Thermal Performance of Two–Phase Micro–Channel Heat Exchanger. Proceedings of IPACK 2005 – ASME InterPack'05, July 17 – 22, San Francisco, California, USA

[88] Price D. C. [2003] A Review of Selected Thermal Management Solutions for Military Electronic Systems. IEEE Transactions on Components and Packaging Technologies – Vol 26 [1], PP 26 – 39

[89] Qazizade A., Manzari M. T., Hannani S. K. [2006] Thermal Transport in Combined Pressure – Electroosmotically Driven Flow in Micro–Channels. Thermal and Thermomechanical Phenomena in Electronic Systems 2006, ITHERM'06. The Tenth Intersociety Conference, May 30 – June 2, San Diego, CA, PP 63 – 70

[90] Qu W., Mudawar I. [2002] Thermal Design Methodology for High–Heat–Flux Single–Phase and Two–Phase Micro–Channel Heat Sinks. The Eighth Society Conference on Thermal and Thermomechanical Phenomena in Electronic Systems – ITHERM 2002, June 2002, San Diego, CA, PP 347 – 359

[91] Qu W., Mudawar I. [2002] Transport Phenomena in Two–Phase Micro–Channel Heat Sinks. Proceedings of IMECE 2002 – ASME International Mechanical Engineering Congress and Exposition, November 17 – 22, New Orleans, Louisiana, PP 1 – 13

[92] Qu W., Mudawar I. [2003] Flow Boiling Heat Transfer in Two–Phase Micro–Channel Heat Sinks – I. Experimental Investigation and Assessment of Correlation Methods. International Journal of Heat and Mass Transfer – Vol 46, PP 2755 – 2771

[93] Qu W., Mudawar I. [2003] Flow Boiling Heat Transfer in Two–Phase Micro–Channel Heat Sinks – II. Annular Two–Phase Flow Model. International Journal of Heat and Mass Transfer – Vol 46, PP 2773 – 2784

[94] Radmehr A., Patankar S. V. [2004] A Flow Network Analysis of a Liquid Cooling System That Incorporates Micro–Channel Heat Sinks. 2004 Inter Society Conference on Thermal Phenomena, PP 714 – 721

[95] Rahman M. M., Shevade S. S. [2005] Fluid Flow and Heat Transfer in a Composite Trapezoidal Micro–Channel. Proceedings of HT2005 – ASME Summer Heat Transfer Conference, July 17 – 22, San Francisco, California, USA

[96] Rice C. K. [1987] The Effect of Void Fraction Correlation and Heat Flux Assumption on Refrigerant Charge Inventory Predictions. Technical and Symposium Papers – 1987 Winter Meeting in New York – Ashrae Inc – Vol 93 Part I, PP 341– 367

[97] Rij J. V., Ameel T., Harman T. [2006] The Effects of Viscous Dissipation on Two–Dimensional Micro–Channel Heat Transfer. Proceedings of IMECE 2006 – ASME International Mechanical Engineering Congress and Exposition, November 5 – 10, Chicago, Illinois, USA, PP 1 – 9

[98] Roy S. K., Avanic B. L. [1996] A Very High Heat Flux Micro–Channel Heat Exchanger for Cooling of Semiconductor Laser Diode Arrays. IEEE Transactions on Components, Packaging, and Manufacturing Technology – Part B – Advancing Packaging – Vol 19 [2], PP 444 – 451

[99] Sarangi R. K., Bhattacharya A., Prasher R. B. [2009] Numerical Modelling of Boiling Heat Transfer in Micro–Channels. Applied Thermal Engineering – Vol 29, PP 300 – 309

[100] Singh S. G., Kulkarni A., Duttagupta S. P., Puranik B. P., Agrawal A. [2008] Impact of Aspect Ratio on Flow Boiling of Water in Micro–Channels. Experimental Thermal and Fluid Science – Vol 33, PP 153 – 160

[101] Singhal V., Liu D., Garimella S. V. [2003] Analysis of Pumping Requirement for Micro–Channel Cooling Systems. Proceedings of IPACK03 – International Electronic Packaging Technical Conference and Exhibition, July 6 – 11, Maui, Hawaii, USA

[102] Skandakumaran P., Ortega A., Jamal–Eddine T., Vaidyanathan R. [2004] Multi–Layered SiC Micro–Channel Heat Sinks – Modeling and Experiment. 2004 Inter Society Conference on Thermal Phenomena, PP 352 – 360

[103] Steinke M. E., Kandlikar S. G. [2004] An Experimental Investigation of Flow Boiling Characteristics of Water in Parallel Micro–Channels. Transactions of the ASME – Vol 126, PP 518 – 526

[104] Steinke M. E., Kandlikar S. G., Magerlein J. H., Colgan E. G., Raisanen A. D. [2006] Scale Effects on Hydrodynamics and Heat Transfer in Two–Dimensional Mini and Micro–Channels. Heat Transfer Engineering – Vol 27 [4], PP 41–52

[105] Tech ARP. [2012]. Intel CPU Size and Power. Retrieved July 17, 2012 From – http://www.techarp.com/showarticle.aspx?artno=354&pgno=6

[106] Thome J. R. [2004 – 2010] Engineering Data Book III. Wolverine Tube Inc, Lausanne, Switzerland

[107] Thome J. R. [2006] State–of–the–Art Overview of Boiling and Two–Phase Flows in Micro–Channels. Heat Transfer Engineering – Vol 27 [9], PP 4 – 19

[108] Tosun I. [2002] Modeling in Transport Phenomena – A Conceptual Approach. Oxford – Elsevier

[109] Tran Q–K., Reynolds M. [2002] Sizing of Relief Valves for Two–Phase Flow in the Bayer Process. Kaiser Engineers Pty Limited, Western Australia, PP 1 – 11. Retrieved From Link – http://ebookbrowse.com/sizing-relief-valves-1-pdf-d224245058

[110] Tuckerman D. B. and Pease R. F. [1981] High Performance Heat Sinks for VSLI. IEEE Electron Device Letters – Vol 2[5], PP 126 – 129

[111] Upadhye H. R., Kandlikar S. G. [2004] Optimization of Micro–Channel Geometry for Direct Chip Cooling Using Single Phase Heat Transfer, Micro–Channels and Mini–Channels – ICMM2004–2398, June 17 – 19, Rochester, New York, USA, PP 679 – 685

[112] Upadhya G., Munch M., Zhou P., Hom J., Werner D., McMaster M. [2006] Micro–Scale Liquid Cooling System for High Heat Flux Processor Cooling Applications, 22nd IEEE Semi–Conductor Thermal Measurement and Management Symposium, March 14 – 16, Dallas, TX, PP 116 – 119

[113] Vatell Corporation [2002] Thermateq" –nology – Advances Heat Vector Sensor. Newsletter, PO Box 66 Christiansburg, VA 24068 [http://www.vatell.com]

[114] Venere E. [2005] Purdue Miniature Cooling Device Will Have Military, Computer Uses. Purdue University News. Retrieved December 21, 2011 From – http://www.purdue.edu/uns/html4ever/2005/050413.Mudawar.microchannel.htm

[115] Wang X–Q., Mujumdar A., Yap C. [2006] Effect of Bifurcation Angle in Tree–Shaped Micro–Channel Networks. Journal of Applied Physics, Vol – 102 [7], PP 073530 – 073530 – 8

[116] Webb R. L. [2003] Effect of Manifold Design on Flow Distribution in Parallel Micro–Channels. Proceedings of IPACK03 – International Electronic Packaging Technical Conference and Exhibition, July 6 – 11, Maui, Hawaii, USA

[117] Wei X., Joshi Y. [2002] Optimization Study of Stacked Micro–Channel Heat Sinks for Micro–Electronic Cooling, 2002 Inter Society Conference on Thermal Phenomena, San Diego, CA, PP 441–448

[118] Weigl B. H., Williams C. L., Hayenga J. W., Bardell R. L., Schulte T. E. [2005] Pumpless MicroFluidics. United States Patent Application Publication – No – US2005/0045479 A1 Retrieved From Link – http://www.freepatentsonline.com/y2005/0045479.html

[119] Wolverine Tube Inc – Engineering Thermal Innovation [2010] MicroCool General Presentation 2010. Wolverine MicroCool Engineering Thermal Innovation. Retrieved January 22, 2013 From Link – http://www.microcooling.com/technology/technical-articles-case-studies

[120] Wunderle B., Schacht R., Wittler O., Michel B., Reichl H. [2004] Performance and Thermo–Mechanical Reliability of Micro–Channel Coolers – A Parametric Study, Thermal and Thermomechanical Phenomena in Electronic Systems 2004, ITHERM'04. The Ninth Intersociety Conference, June 1 – 4, Las Vegas, NV, PP 11 – 16

[121] Yamaguchi Y., Takagi F., Watari T., Yamashita K., Nakamura H., Shimizu H., Maeda H. [2004] Interface Configuration of the Two Layered Laminar Flow in a Curved Micro–channel. 7th International Conference on Microreaction Technology, September 2003, Lausanne, Switzerland – Chemical Engineering Journal – Netherlands – Vol 101 [1–3], PP 367 – 372

[122] Yarin, L. P., Mosyak A., Hetsroni G. [2009] Fluid Flow, Heat Transfer and Boiling in Micro–Channels. New York – Springer – Verlag Berlin Heidelberg

[123] Yin J. M., Bullard C. W., Hrnjak P. S. [2000] Pressure Drop Measurements in Micro–Channel Heat Exchanger. Department of Mechanical and Industrial Engineering, ACRC CR – 30, University of Illinois

[124] Zhang L., Goodson K. E., Kenny T. W. [2004] Silicon Micro–Channel Heat Sinks – Theories and Phenomena. New York – Springer – Verlag Berlin Heidelberg

[125] Zhang L., Koo J–M., Jiang L., Asheghi M., Goodson K. E., Santiago J. G., Kenny T. H. [2002] Measurements and Modeling of Two–Phase Flow in Micro–Channels With Nearly Constant Heat Flux Boundary Conditions. Journal of Microelectromechanical Systems – Vol 11 [1], PP 12 – 19

[126] Zhang H. Y., Pinjala D. [2005] Flow Boiling Heat Transfer in Micro–Channel Heat Sinks of Different Flow Orientations. Proceedings of IPACK 2005 – ASME InterPack'05, July 17 – 22, San Francisco, California, USA